Supporting Information

Lithium Anthraquinoids as Catalysts in the ROP of Lactide and Caprolactone into Cyclic Polymers

Cristina Ruiz Martínez,[a],1 Juana M. Pérez,[a],1 Francisco M. Arrabal-Campos,[a] Antonio Rodríguez-Diéguez,[b] Duane Choquesillo-Lazarte,[c] Juan A. Martínez-Lao,[a] Manuel A. Ortuño[d] and Ignacio Fernández*[a]

[a] Department of Chemistry and Physics, Research Centre CIAIMBITAL, University of Almería, Ctra. Sacramento, s/n, 04120, Almería, Spain. E-mail: ifernan@ual.es

[b] Departamento de Química Inorgánica, Facultad de Ciencias, Universidad de Granada, Av. Fuentenueva s/n, 18071 Granada, Spain.

[c] Laboratorio de Estudios Cristalográficos, IACT, CSIC-UGR Av. Las Palmeras nº4, 18100 Granada, Spain.

[d] Centro Singular de Investigación en Química Biolóxica e Materiais Moleculares (CIQUS) Universidad de Santiago de Compostela, 15782, Santiago de Compostela, Spain

Table of contents

1. General procedures of laboratory

All experiments involving moisture-sensitive compounds were performed under an inert atmosphere of N_2 using standard Schlenk techniques or a glovebox. Deuterated solvents were degassed and dried over activated molecular sieves prior to use. 1-Chloroanthraquinone and hydrazine hydrate were purchased from Sigma-Aldrich and used as received. Acetone, 2-quinoline carboxaldehyde, salicylaldehyde and benzaldehyde were purchased from Acros and used for the synthesis of **1** without further purification. THF, hexane and diethyl ether used for air sensitive processes were dried and degassed in a Solvent Purification System. LiHMDS was purchased from ABCR and used as received. *L*- and *rac*-lactide were purchased from Acros and recrystallized with toluene three times before used. MALDI-TOF mass spectra were acquired using a mass spectrometer Bruker Autoflex Speed system (Bruker, Germany). Diffusion NMR measurements, average molecular weights, and hydrodynamic radii calculations were performed as previously reported.[1]

NMR spectra were measured in a Bruker Avance III 500 spectrometer. IR (ATR and DRIFT) spectra were recorded in a FT-IR Bruker Alpha spectrometer. Elemental analyses (EA) were performed on an Elementar vario EL cube in the CHN mode. Mass spectra were acquired using a mass spectrometer Orbitrap Thermo Fisher Scientific (ExactiveTM, Thermo Fisher Scientific, Bremen, Germany) using an electrospray interface (ESI) (HESI-II, Thermo Fisher Scientific, San Jose, CA, USA). The ESI parameters for the spectrometric detection, were as follows: spray voltage, 4 kV; sheath gas (N_2, >95%), 35 (adimensional); auxiliary gas (N_2, >95%), 10 (adimensional); skimmer voltage, 18 V; capillary voltage, 35 V; tube lens voltage, 95 V; heater temperature, 305 °C; capillary temperature, 300 °C. The mass spectra were acquired employing two alternating acquisition functions: (1) full MS, ESI+, without fragmentation (the higher collisional dissociation (HCD) collision cell was switched off), mass resolving power = 25 000 full width at half maximum (FWHM); scan time = 0.25 s, (2) full MS, ESI- using the aforementioned settings, (3) all-ions fragmentation (AIF), ESI+, with fragmentation (HCD on, collision energy 30 eV), mass resolving power = 10000 FWHM; scan time = 0.10 s, and (4) AIF, ESI- using the settings explained for (3).

2. General procedures

General procedure for the synthesis of ligands. Ligands **1** were synthesized from 1-hydrazinoanthraquinone, which was prepared following a method previously described in the literature.[28] 1-Hydrazinoanthraquinone (7.2 mmol) was suspended in methanol (250 mL), and the corresponding aldehyde or ketone (8.7 mmol, 1.2 equiv.) was added. The mixture was stirred and refluxed for 3.5 h, after which a red precipitate was observed. The suspension was cooled to room temperature, and the pure product was obtained as a deep red powder by filtration under reduced pressure.

General procedure for the synthesis of Li-complexes 2. Li-complexes were synthesized following a described procedure.[27] LiHMDS (42 mg, 0.238 mmol) was dissolved in THF (10 mL) and added to a suspension of 1 (0.238 mmol, 1.0 equiv.) in THF (10 mL). The resulting deep green solution was stirred for 2 h at room temperature, and then all the volatiles were removed under vacuum. The remaining solid was washed with hexane (15 mL) and filtered out to yield the pure product as a dark green powder.

General procedure for the catalytic ROP of L- and rac-LA. It was conducted in a glovebox by dissolving LiHMDS (2 mg, 0.012 mmol) and the corresponding ligand 1 (0.012 mmol) in 1.2 mL of DCM or THF in a 5 mL capped vial equipped with a magnetic stirring bar. Once the catalyst was completely dissolved, the addition of L- or rac-Lactide (87 mg, 0.6 mmol) was carried out and the reaction was left to stir overnight at room temperature until complete conversion of the starting material was reached. The reaction was then quenched with HCl 1 M (few drops), precipitated with cold methanol, and washed and centrifuged (11000 rpm, 18ºC, 10 min.) with cold MeOH (3 x 10 mL). The pure polymer was finally dried under vacuum.

General procedure for the catalytic ROP of ε-Caprolactone. It was conducted in a glovebox by dissolving LiHMDS (2 mg, 0.012 mmol) and the corresponding ligand 1 (0.012 mmol) in 1.2 mL of DCM or THF in a 5 mL capped vial equipped with a magnetic stirring bar. Once the catalyst was completely dissolved, the addition of ε-Caprolactone (64 μL, 0.6 mmol) was carried out and the reaction was left to stir overnight at room temperature until complete conversion of the starting material was reached. The reaction was then quenched with HCl 1 M (few drops), precipitated with cold methanol, and washed and centrifuged (11000 rpm, 18ºC, 10 min.) with cold MeOH (3 x 10 mL). The pure polymer was finally dried under vacuum.

General procedure for NMR monitored reactions. In a glovebox, the corresponding Li-complex **2** (0.006 mmol) was dissolved in 0.6 mL of DCM-d_2 in a 1.5 mL capped vial equipped with a magnetic stirring bar. Then, addition of *L*- or *rac*-lactide (21.6 mg, 0.3 mmol) was carried out and the solution was then immediately transferred into an oven-dried 5 mm NMR J-Young tube. The sample tube was shaken to ensure the homogeneity of the mixture and then placed inside the NMR spectrometer to perform the corresponding measurements.

Quantitative NMR acquisition parameters. ^{1}H NMR determination of product conversion was carried out by comparing signals arising from both CH of substrate and product. The standard acquisition parameters were one-dimensional pulse sequence which includes a 30º flip angle (Bruker zg30), recycle time (D1 = 30 s), time domain (TD = 64k), number of scans (NS = 1), acquisition time (AQ = 2.97 s), transmitter (frequency) offset (O1P = 8.0 ppm), and spectral width (SW = 22.0 ppm).

Diffusion NMR Spectroscopy of complexes 2. NMR samples were prepared with different concentrations of complexes (10, 20, 40 mM) in 0.5 mL of THF-d_8 in an oven-dried 5 mm NMR tube. The Δ and δ values varied from 75 to 100 ms for ^{1}H and 75 ms for ^{7}Li; and from 2.5 to 3.5 ms, respectively. The gradient strength was incremented in steps of 4% starting from 8% to 96%, so that 23 points were used for regression analysis. The recovery delay was always set to 5 s. The number of scans per increment were 32 and typical experimental times were around 3 h. All experiments were run without spinning. To check reproducibility and lack of convection, two different measurements with different Δ were always carried out. The contribution of convection to the calculated D values seems to be negligible since it remains always constant under the two different diffusion times assayed. Determination of the D-values was performed by applying different algorithms. dART solutions were obtained by the use of an algebraic reconstruction technique.[1] TRAIn solutions were obtained by the use of the algorithm provided by Xu et al,[2] with an alpha parameter set to 1.05. LMS fittings were performed with the help of the DiffAtOnce package.[3]

Diffusion NMR Spectroscopy of cPLA polymers. NMR samples were prepared by just adding 1.5 mg of each polymer together with 0.5 mL of $CDCl_3$ in an oven-dried 5 mm NMR tube. The Δ and δ values varied from 75 to 100 ms, and from 2.5 to 3.5 ms, respectively. The gradient strength was incremented in steps of 4% starting from 8% to 96%, so that 23 points were used for regression analysis. The recovery delay was always set to 5 s. The number of scans per increment were 32 and typical experimental times were around 3 h. All experiments were run without spinning. To check reproducibility and lack of convection, two different measurements with different Δ were always carried out. The contribution of convection to the calculated D values

seems to be negligible since it remains always constant under the two different diffusion times assayed. Determination of the D-values was performed as mentioned before.

MALDI-TOF MS. Solutions of the polymer sample (10 mg/mL) and matrix DCTB (20 mg/mL) were prepared in dichloromethane (DCM):methanol (1:1). TFANa (10 mg/mL) in DCM:MeOH (1:1) was employed as additive. 1 μL of the 10:1:0.5 (v/v/v) mixture Matrix:Polymer:TFANa was spotted via micropipet for MALDI analysis.

FT-IR spectra were recorded in the range 400-4000 cm^{-1} with a Bruker Vertex 70 equipped with a cell for liquid samples.

Computational details. Density functional theory (DFT) simulations were carried out with the M06-2X density functional[4] and an ultrafine grid as implemented in Gaussian 16.[5] Geometry optimizations were performed in THF using the continuum solvent approach SMD.[6] The 6-31G(d,p) basis set was used for all atoms,[7] and diffuse functions were added for O atoms.[8] Vibrational frequencies were computed to confirm the nature of minima. Those frequencies below 50 cm−1 were replaced by 50 cm^{-1} when computing vibrational partition functions[9] using the software GoodVibes.[10] Gibbs energies are computed at 298 K and 1 M (12.33 M for a THF molecule in THF solution). Several conformations are searched for each species but only the most stables ones are reported. For the prediction of ^{15}N and ^{7}Li NMR chemical shifts, isotropic shielding constants were computed with the gauge-independent atomic orbital method (GIAO).[11] Single-point calculations were performed with the mPW1PW91 density functional[12] and the 6-311G(2d,p) basis set[8,13] in THF. This level of theory has been successful for predicting chemical shifts.[14] For ^{15}N, only chemical shift differences between the free ligand and the complexed ligand are reported. For ^{7}Li, the cation $[Li(THF)_4]^+$ is taken as reference, where the computed isotropic shielding constant is matched to the experimental chemical shift of −0.45 ppm.[15] All inputs and outputs can be consulted in the open-access ioChem-BD repository[16] via the following database.[17]

3. Numbering of ligands and complexes

3.1. Ligands

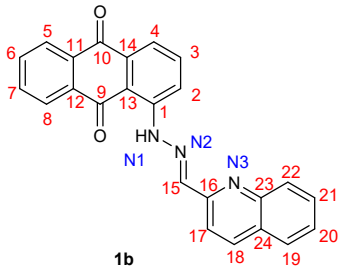

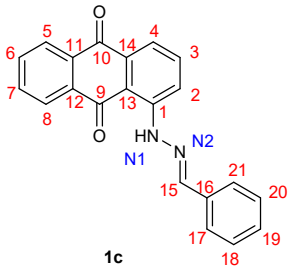

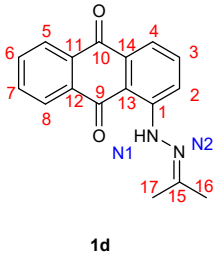

Scheme S1. Structure and numbering of ligands **1b-1d**.

3.2. Complexes

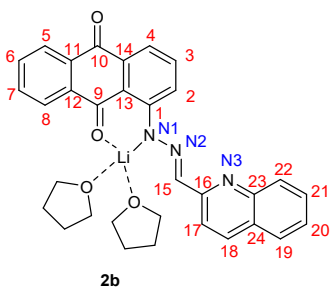

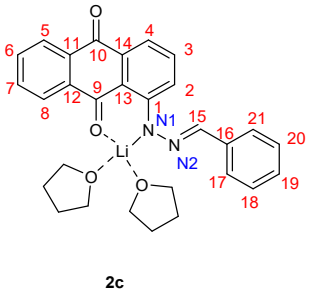

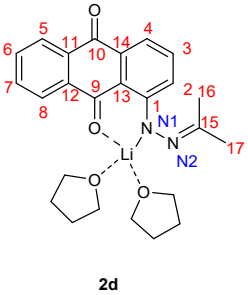

Scheme S2. Structure and numbering of complexes **2b-2d**.

4. Crystallographic Data of ligands 1b and 1d

Single-crystal diffraction data were collected at 100(2) K on a Bruker D8 Venture with a Photon detector equipped with graphite monochromated MoKα radiation (λ = 0.71073 Å). The data reduction was performed with the APEX2 software and corrected for absorption using SADABS. Crystal structures were solved by direct methods using the SIR97 program and refined by full-matrix least-squares on F2 including all reflections using anisotropic displacement parameters by means of the WINGX crystallographic package. Generally, anisotropic temperature factors were assigned to all atoms except for hydrogen atoms, which are riding their parent atoms with an isotropic temperature factor arbitrarily chosen as 1.2 times that of the respective parent. Several crystals of 1b and 1d were measured and the structure was solved from the best data we were able to collect, due to the fact that the crystals diffracted very little. Solvent mask routine (implemented in OLEX2 software) was used to eliminate one disordered crystallization dichloromethane molecule. Final R(F), wR(F2) and goodness of fit agreement factors, details on the data collection and analysis can be found in Table S1. Crystallographic data (excluding structure factors) for the structures reported in this paper have been deposited with the Cambridge Crystallographic Data Centre as supplementary publication nos. CCDC 2193241-2193242 for compounds. Copies of the data can be obtained free of charge on application to the Director, CCDC, 12 Union Road, Cambridge, CB2 1EZ, U.K. (Fax: +44-1223-335033; e-mail: deposit@ccdc.cam.ac.uk).

Table S1. Crystal data and structure refinement for compounds **1b** and **1d**.

	Compound 1b	**Compound 1d**
Empirical formula	$C_{25}\ H_{16}\ N_3\ O_2\ Cl_3$	$C_{34}\ H_{28}\ N_4\ O_4$
Formula weight	496.76	556.60
Temperature (K)	295 (2)	130 (2)
CCDC number	2193242	2193241
Wavelength (Å)	0.71073	0.71073
Crystal system	Monoclinic	Monoclinic
Space group	$P2_1/c$	Pc
a(Å)	15.3458(8)	11.1707(15)
b(Å)	15.7608(7)	3.8686(5)
c(Å)	9.4437(4)	30.877(4)
α(°)	90	90
β(°)	93.062(4)	91.966(5)
γ(°)	90	90
Volume(Å^3)	2280.81(18)	1333.6(3)
Z	4	2
Density (calculated) (g/cm^3)	1.447	1.386
Absorption coefficient (mm^{-1})	3.877	0.093
Goodness-of-fit on F^2	1.083	1.163
Final R indices [$I>2\sigma(I)$]	R1 = 0.0635 wR2 = 0.1785	R1 = 0.0771 wR2 = 0.1618
Largest diff. peak / hole	0.447 and -0.303	0.230 and -0.245

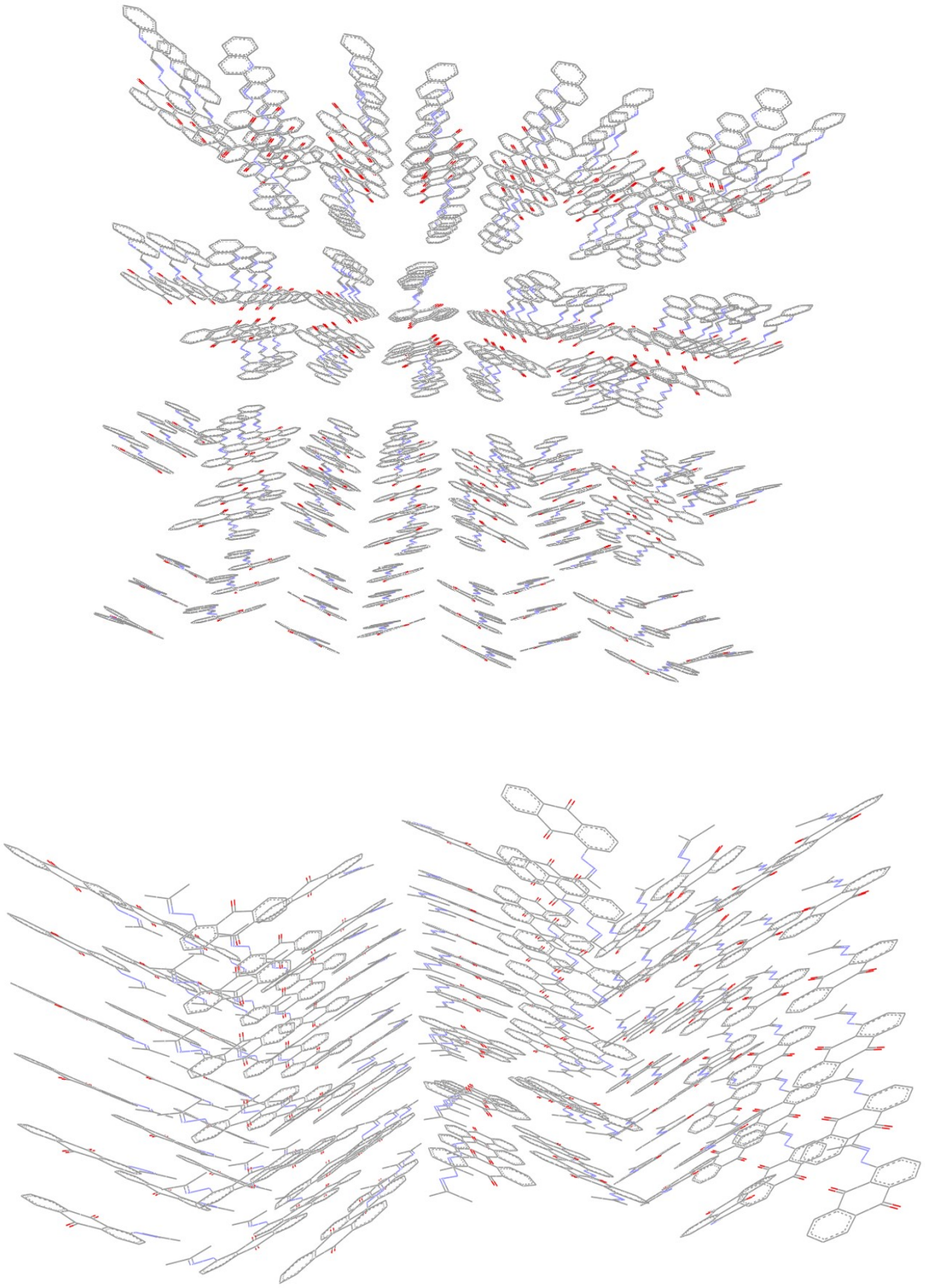

Figure S1. Planar geometry of ligand **1b** (top) and **1d** (bottom) favoring π-stacking interactions among anthraquinone units.

5. Diffusion data

Table S2. Diffusion coefficient (*D*) and Stokes-Einstein hydrodynamic radius (r_H) values for compounds **2b**, **2c** and **2d** at 292 K in THF-d_8.

Entry	Nucleus	Conc. (mM)	Complex	D x 10^9 (m^2s^{-1}) [a]	r_H (Å)[b]
1	^{1}H	10	**2b**	0.850556	5.0
	^{7}Li			0.907648	4.9
	^{1}H		THF	2.699488	1.6
2	^{1}H	10	**2c**	0.91713	4.7
	^{7}Li			0.92556	4.7
	^{1}H		THF	2.68569	1.7
3	^{1}H	20	**2c**	0.911063	4.7
	^{7}Li			0.923636	4.7
	^{1}H		THF	2.695803	1.6
4	^{1}H	40	**2c**	0.910831	4.7
	^{7}Li			0.899515	4.8
			THF	2.694559	1.6
5	^{1}H	20	**2d**	0.974004	4.4
	^{7}Li			0.984474	4.4
	^{1}H		THF	2.722127	1.6

[a] The experimental error in the *D* values is ± 2%. [b] The viscosity η used in the Stokes-Einstein equation was taken from Perry's Chemical Engineers' Handbook 8th Edition (www.knovel.com) for tetrahydrofuran h 0.4966 $Kg \cdot m^{-1} \cdot s^{-1}$.

Table S3. Diffusion coefficient (*D*), hydrodynamic radius (r_H) weight-average MW (M_w) and polydispersity index (*Đ*) values for cPLAs with ***L*-LA** at 292 K in $CDCl_3$.

LA, Catalyst	$[LA]_0/[Cat]$	Solvent	*D* x 10^{-9} (m^2 s^{-1})[a]	r_H (Å)[b]	Mw (kDa)[c]	Đ
2b	50:1	DCM	0.0730667	51.1	40.2	2.13
$CHCl_3$			2.337013	1.6		
2c	50:1	DCM	0.062655	59.5	52.7	2.26
$CHCl_3$			2.37369	1.6		
2d	50:1	DCM	0.0785621	47.5	35.4	1.77
$CHCl_3$			2.345989	1.6		

[a] The experimental error in the *D* values is ± 2%. Signal at δ_H 5.19 ppm assigned to the inner methine was always monitored. [b] The viscosity η used in the Stokes-Einstein equation was taken from Perry's Chemical Engineers' Handbook 8th Edition (www.knovel.com) and is 0.545 10^{-3} kg m^{-1} s^{-1}. [c] Determined by ^{1}H PGSE diffusion NMR using polystyrene standards and without the use of any correction factor. See ref. 1 for details.

Table S4. Diffusion coefficient (*D*), hydrodynamic radius (r_H) weight-average MW (Mw) and polydispersity index (*Đ*) values for cPLAs with *rac*-LA at 294 K in $CDCl_3$.

LA, Catalyst	$[LA]_0/[Cat]$	Solvent	*D* x 10^{-9} (m^2 s^{-1})[a]	r_H (Å)[b]	Mw (kDa)[c]	Đ	Pr
2b	50:1	DCM	0.078747	48.7	34.6	1.59	0.486
$CHCl_3$			2.41818	1.6			
2c	50:1	DCM	0.0639976	59.9	49.9	1.49	0.452
$CHCl_3$			2.427372	1.6			
2d	50:1	DCM	0.0681884	56.2	44.6	1.98	0.461
$CHCl_3$			2.39270	1.6			

[a] The experimental error in the *D* values is ± 2%. Signal at δ_H 5.19 ppm assigned to the inner methine was always monitored. [b] The viscosity η used in the Stokes-Einstein equation was taken from Perry's Chemical Engineers' Handbook 8th Edition (www.knovel.com) and is 0.5615 10^{-3} kg m^{-1} s^{-1}. [c] Determined by ^{1}H PGSE diffusion NMR using polystyrene standards and without the use of any correction factor. See ref. 1 for details.

Table S5. ^{7}Li and ^{15}N NMR chemical shifts for ligands **1b-1d** and complexes **2b-2d** in THF-d_8 at 292 K and their corresponding ligands.

Compound	δ_{Li} (ppm)	Half width (Hz)	T_1 ^{7}Li (ms)	δ_{N1} (ppm)	δ_{N2} (ppm)
1b	-		-	-249.2	-69.3
2b	1.99	15.7	257	-134.3	-9.8
1c	-		-	-249.2	-69.3
2c	1.88	30.8	176	-134.4	-25.9
1d	-		-	-256.1	-92.9
2d	1.31	6.0	192	-130.4	-43.9

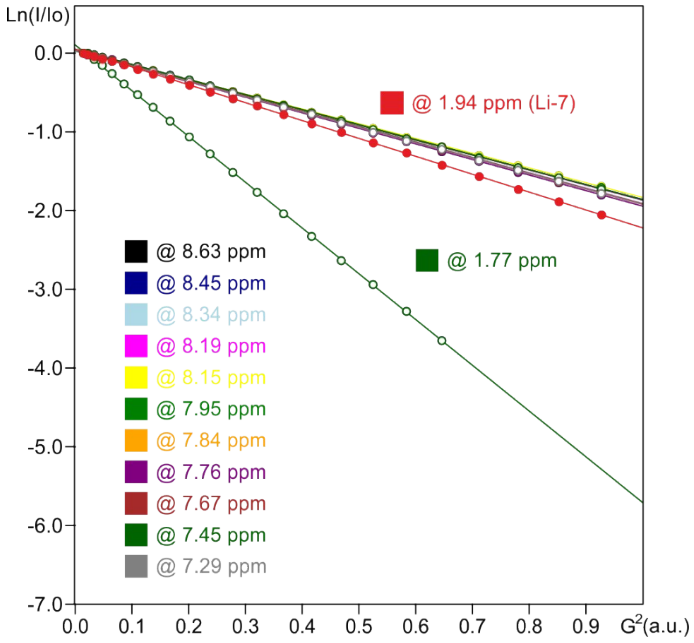

Figure S2. Stejskal-Tanner plots from ^{1}H and ^{7}Li PGSE NMR diffusion experiments in THF-d_8 at 292 K using the stimulated echo with bipolar pair pulses (stebpgp1s1d) sequence for complex **2b** (1 mM). The solid lines represent linear least-squares fits to the experimental data.

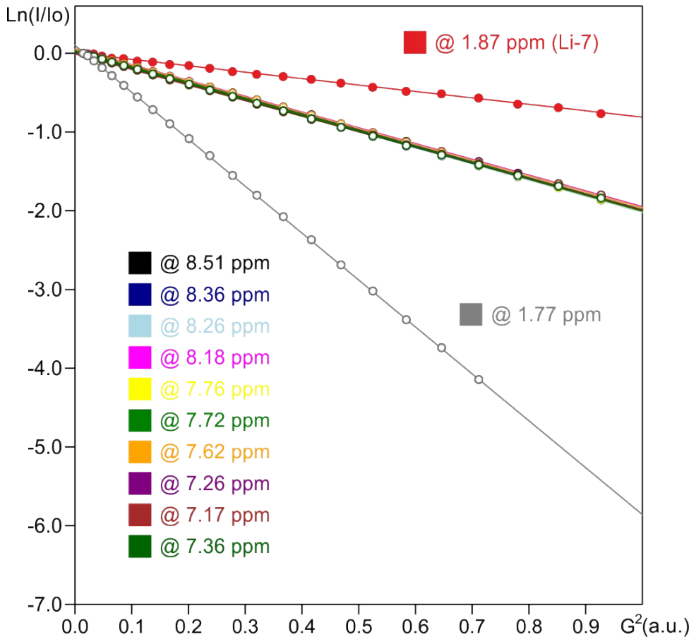

Figure S3. Stejskal-Tanner plots from ^{1}H and ^{7}Li PGSE NMR diffusion experiments in THF-d_8 at 292 K using the stimulated echo with bipolar pair pulses (stebpgp1s1d) sequence for complex **2c** (20 mM). The solid lines represent linear least-squares fits to the experimental data.

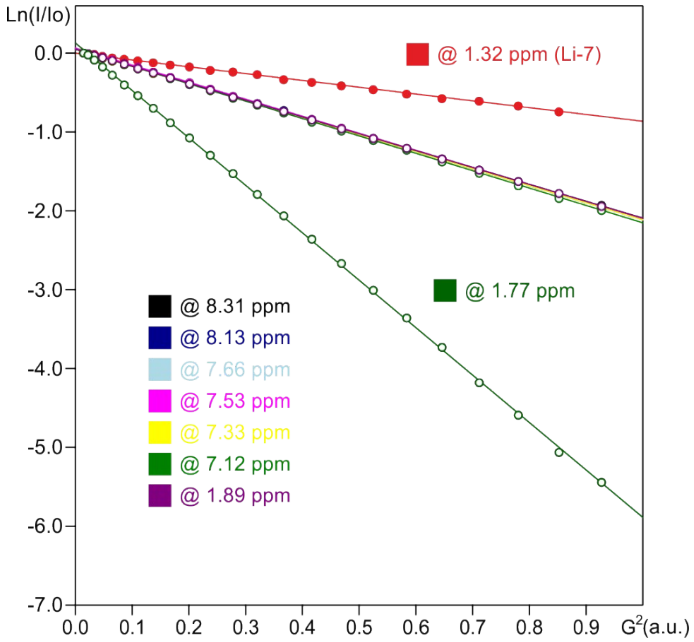

Figure S4. Stejskal-Tanner plots from ^{1}H and ^{7}Li PGSE NMR diffusion experiments in THF-d_8 at 292 K using the stimulated echo with bipolar pair pulses (stebpgp1s1d) sequence for complex **2d** (20 mM). The solid lines represent linear least-squares fits to the experimental data.

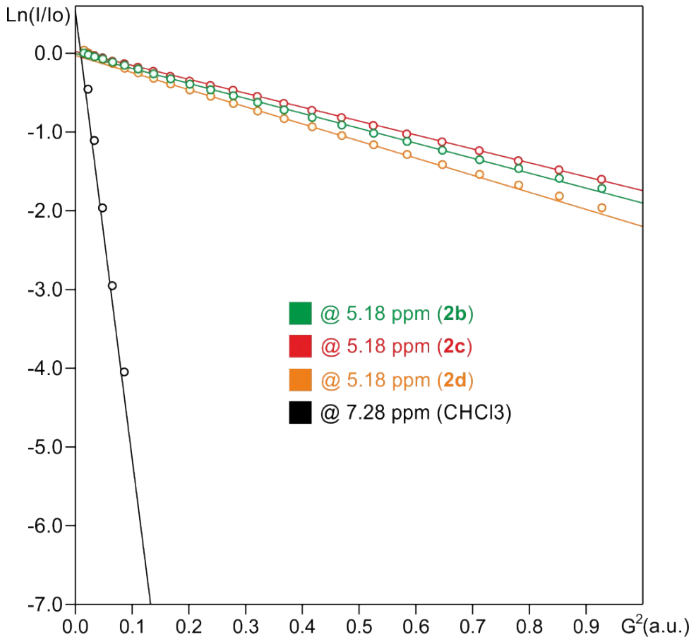

Figure S5. Stejskal-Tanner plots from ^{1}H PGSE NMR diffusion experiments in $CDCl_3$ at 292 K using the stimulated echo with bipolar pair pulses (stebpgp1s1d) sequence for **cPLA** obtained with the different catalysts and *L*-Lactide in DCM (50:1). The solid lines represent linear least-squares fits to the experimental data.

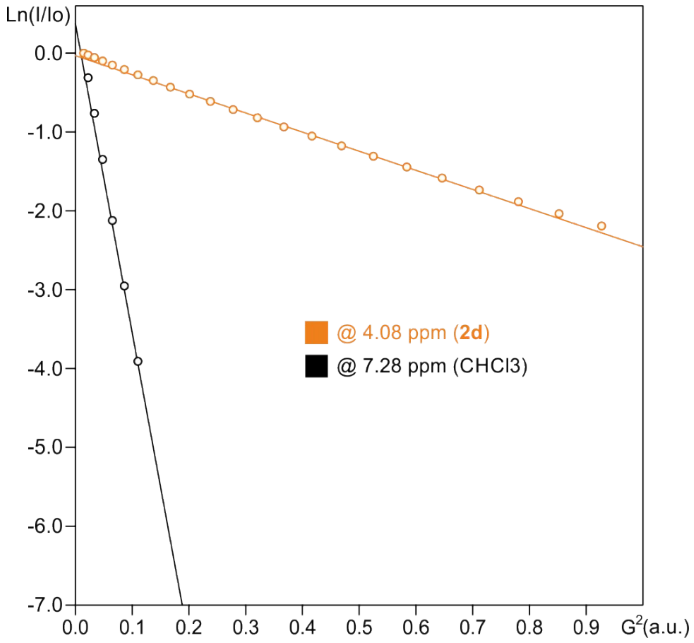

Figure S6. Stejskal-Tanner plots from ^{1}H PGSE NMR diffusion experiments in $CDCl_3$ at 292 K using the stimulated echo with bipolar pair pulses (stebpgp1s1d) sequence for **cPCL** obtained with **2d** in THF (50:1). The solid lines represent linear least-squares fits to the experimental data

6. Kinetic profiles

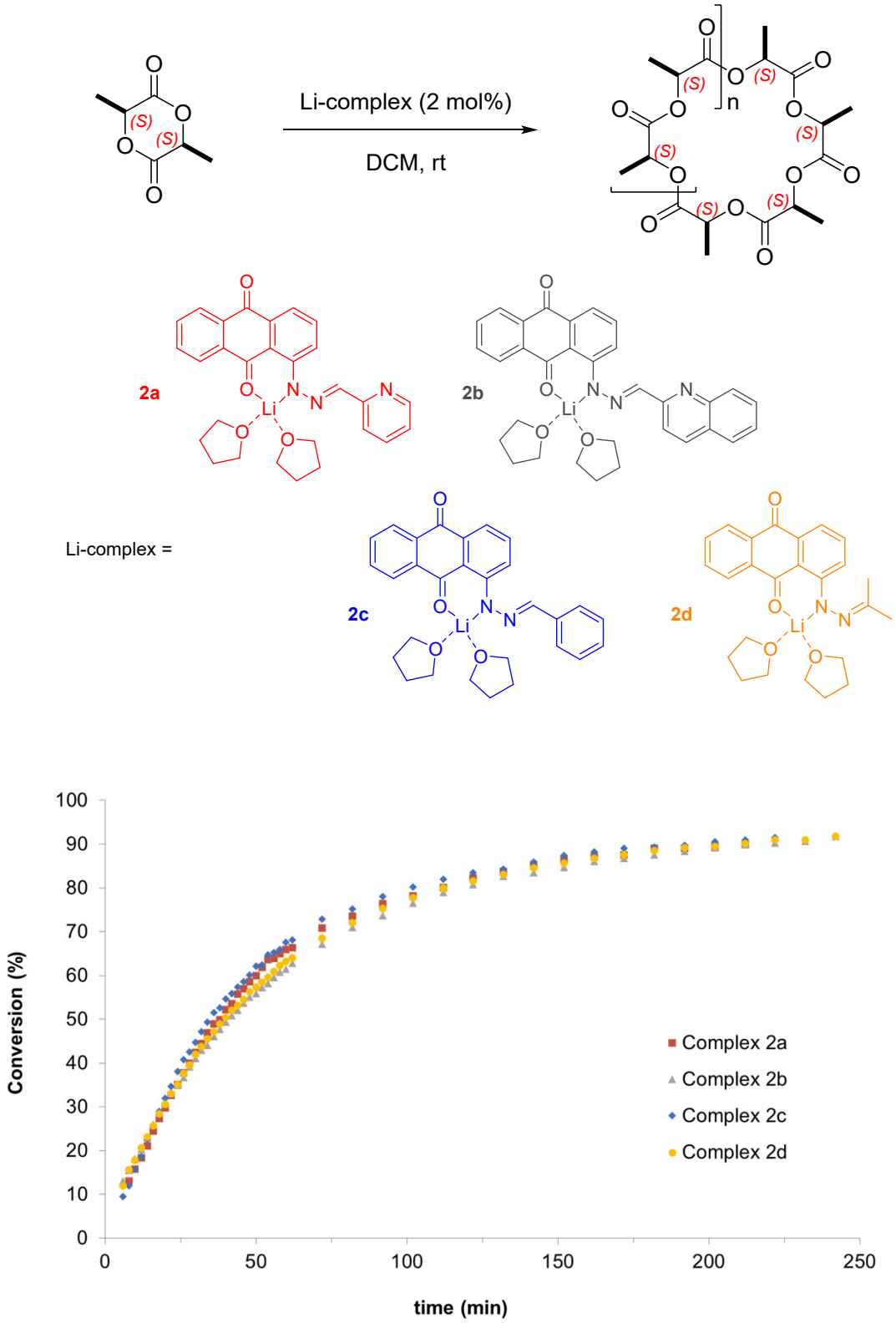

Figure S7. Kinetic profile for the catalytic ROP of ***L*-Lactide** with complex **2a** (red), complex **2b** (grey), complex **2c** (blue) and complex **2d** (yellow) at 25ºC in DCM.

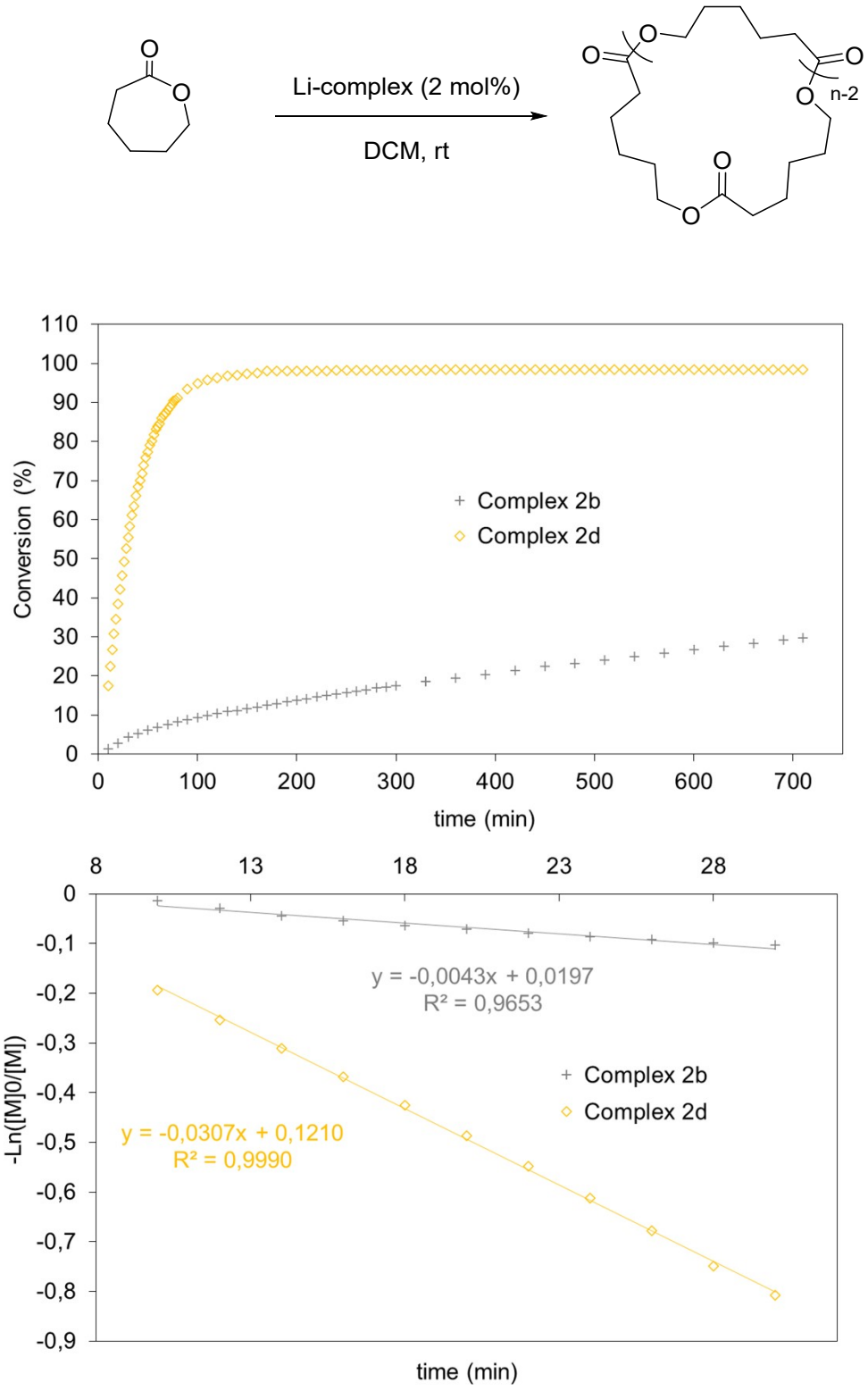

Figure S8. a) Kinetic profiles and b) -Ln(M/M_0) dependence for the catalytic ROP of **CL** with **2b** (+) and **2d** (◊) at 25ºC in DCM.

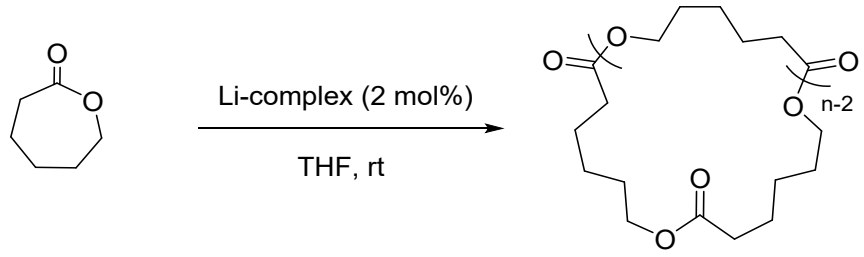

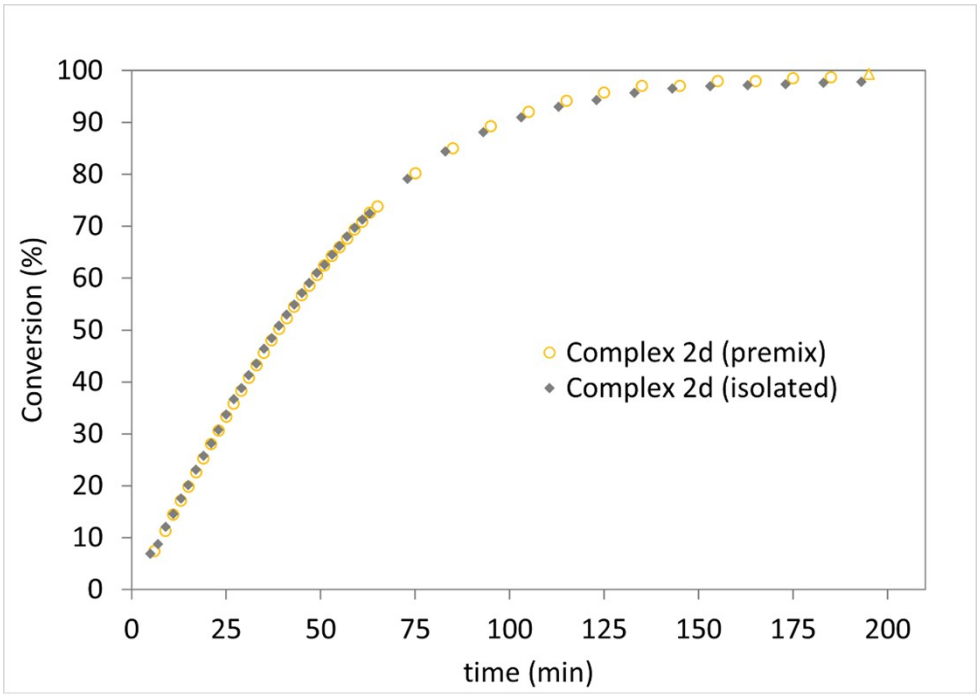

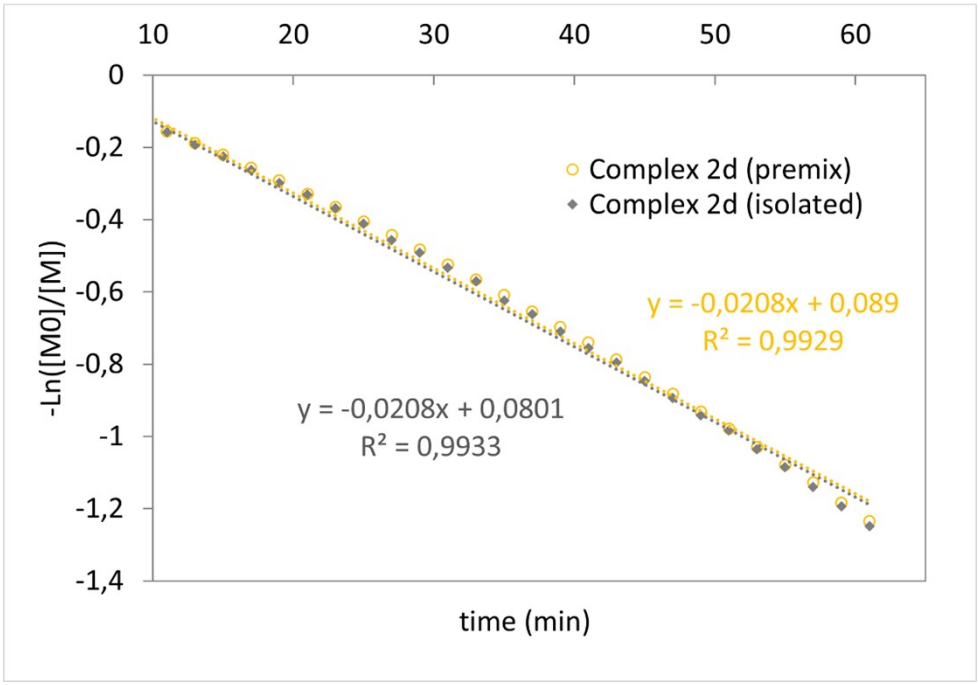

Figure S9. a) Kinetic profiles and b) -Ln(M_0/M) dependence for the catalytic ROP of **ε-CL** with **2d (premix)** (o) and **2d (isolated)** (♦) at 25ºC in THF.

7. Characterization data

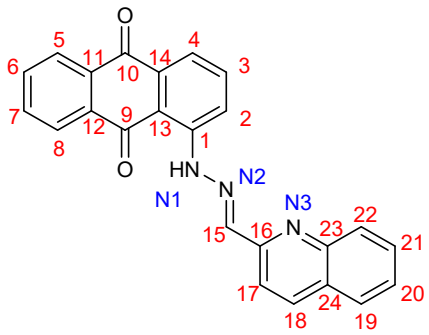

(*E*)-1-(2-(Quinolin-2-ylmethylene)hydrazineyl)anthracene-9,10-dione (1b):

^{1}H-NMR (600.13 MHz, $CDCl_3$): δ 12.95 (s, 1H, N*H*), 8.32 (m, 1H, H8), 8.30 (s, 1H, H15), 8.28-8.25 (m, 2H, H2, H5), 8.19 (d, *J* = 8.60 Hz, 1H), 8.15 (d, *J* = 8.60 Hz, 1H), 8.09 (d, *J* = 8.30 Hz, 1H), 7.85 (dd, *J* = 1.05 Hz, 7.35 Hz, 1H, H4), 7.83-7.79 (m, 2H), 7.79-7.73 (m, 2H), 7.73-7.69 (2H, m, H3), 7.54 (m, 1H) ppm.

^{13}C-NMR (150.91 MHz, $CDCl_3$): δ 186.0 (CO, C9), 183.3 (CO, C10), 154.2 (C16), 148.0 (C23), 147.7 (C1), 143.4 (C15), 136.4, 135.5, 134.5 (C_{ipso}), 134.30, 134.28 (C11), 134.23 (C12), 133.8, 133.2 (C_{ipso}), 130.0, 129.3, 128.2 (C_{ipso}), 127.8, 127.4, 127.2, 127.1 (C5), 120.4 (C2), 119.5 (C4), 118.1, 113.5 (C13) ppm.

IR (ATR): υ 3050 (s), 1673 (m), 1633 (m), 1579 (w), 1502 (w), 1464 (s), 1425 (s), 1298 (m), 1267 (w), 1169 (s), 1125 (w), 1069 (m), 1005 (m), 922 (s), 884 (m), 830 (s), 739 (m), 706 (w), 635 (s), 615 (m) cm^{-1}.

ESI-MS: calcd (m/z) for $[C_{24}H_{15}N_3O_2]^+$: 377.1164; found: 378.1228 $[M + H]^+$.

Elemental Analysis: Calcd for $C_{24}H_{15}N_3O_2$: C, 76.38; H, 4.01; N, 11.13; found: C, 73.51; H, 4.28; N, 11.34.

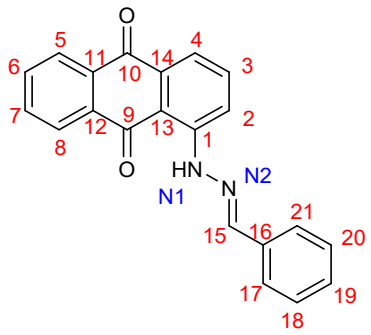

(*E*)-1-(2-Benzylidenehydrazineyl)anthracene-9,10-dione (1c):

^{1}H-NMR (500.13 MHz, $CDCl_3$): δ 12.75 (s, 1H, NH), 8.29 (dd, *J* = 7.7, 1.1 Hz, 1H, H5), 8.27 (dd, *J* = 7.7, 1.2 Hz, 1H, H8), 8.20 (d, *J* = 8.6 Hz, 1H, H2), 8.05 (s, 1H, H15), 7.78 (d, *J* = 7.5 Hz, 2H, ArH, H4), 7.76–7.73 (m, 3H, ArH, H17, H21), 7.67–7.64 (m, 1H, H3), 7.44–7.41 (m, 2H, ArH), 7.39–7.36 (m, 1H, H19) ppm.

^{13}C-NMR (125.77 MHz, $CDCl_3$): δ 185.6 (C9), 183.3 (C10), 148.2 (C1), 143.0 (C15), 135.3 (C3), 134.7 (C16), 134.6 (C_{ipso}), 134.04 (C7), 134.00 (C_{ipso}), 133.5 (C6), 133.1, 129.5 (19), 128.8, 127.0 (C5), 126.9 (C17, C21), 126.8 (C8), 120.3 (C2), 118.6, 112.5 (C3) ppm.

^{15}N NMR (60.8 MHz, THF-d8, via gHMBC): δ -81.5 (N2), -250.2 (N1) ppm.

IR (ATR): υ 3061 (s), 1670 (m), 1628 (m), 1584 (w), 1501 (w), 1452 (s), 1298 (m), 1266 (w), 1168 (m), 1115 (m), 1067 (m), 1003 (m), 929 (s), 928 (s), 829 (s), 806 (s), 739 (m), 706 (w), 640 (m) cm^{-1}.

ESI-MS: calcd. (m/z) for $[C_{21}H_{14}N_2O_2]^+$: 326.1055; found: 327.1121 $[M + H]^+$.

Elemental Analysis: Calcd. for $C_{21}H_{14}N_2O_2$: C, 77.29; H, 4.32; N, 8.58; found: C, 75.67; H, 4.23; N, 8.36.

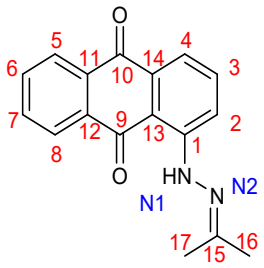

1-(2-(Propan-2-ylidene)hydrazineyl)anthracene-9,10-dione (1d):

^{1}H-NMR (600.13 MHz, $CDCl_3$): δ 12.30 (s, 1H, NH), 8.29 (dd, *J* = 7.7, 1.0 Hz, 1H, H8), 8.27 (dd, *J* = 7.7, 1.1 Hz, 1H, H5), 8.09 (dd, *J* = 8.6, 1.0 Hz, 1H, H2), 7.77 (td, *J* = 7.5, 1.5 Hz, 1H, H7), 7.74–7.71 (m, 2H, H6, H4), 7.62–7.60 (m, 1H, H3), 2.15 (s, 3H, CH_3), 2.13 (s, 3H, CH_3) ppm.

^{13}C-NMR (150.9 MHz, $CDCl_3$): δ 185.3 (C9), 183.6 (C10), 149.6 (C15), 148.7 (C_{ipso}), 135.3 (C3), 134.7 (C_{ipso}), 133.9 (C7), 133.2 (C6), 133.1 (C_{ipso}), 126.9 (C5), 126.7 (C8), 119.9 (C2), 117.8 (C4), 111.9 (C13), 25.3 (C16/C17), 17.1 (C17/C16) ppm.

^{15}N NMR (60.8 MHz, $CDCl_3$, via gHMBC): δ 143.92, -93.45 ppm.

^{15}N NMR (60.8 MHz, THF-d8, via gHMBC): δ -92.72, -255.89 ppm.

IR (ATR): υ 2909 (s), 1665 (m), 1628 (m), 1584 (w), 1503 (m), 1436 (s), 1394 (s), 1366 (m), 1303 (s), 1274 (w), 1162 (m), 1119 (m), 1068 (s), 966 (m), 891 (s), 828 (m), 800 (m), 730 (m), 702 (w), 663 (s), 618 (s) cm^{-1}.

ESI-MS: calcd. (m/z) for $[C_{17}H_{14}N_2O_2]^+$: 278.1055; found: 279.1121 $[M + H]^+$.

Elemental Analysis: Calcd. for $C_{17}H_{14}N_2O_2$: C, 73.37; H, 5.07; N, 10.07; found: C, 72.67; H, 4.95; N, 10.22.

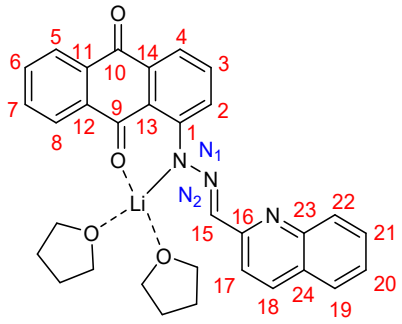

Lithium *E*)-1-(2-(quinolin-2-ylmethylene)hydrazineyl)anthracene-9,10-dione (2b):

^{1}H-NMR (600.13 MHz, THF-d$_8$): δ 8.6 (dd, *J* = 9.15, 1.04 Hz, 1H, H2), 8.45 (s, 1H, H15), 8.37 (d, *J* = 7.79 Hz, 1H, H8), 8.34 (d, *J* = 8.64 Hz, 1H, H17), 8.20 (d, *J* = 7.6 Hz, 1H, H5), 8.14 (d, *J* = 8.66 Hz, 1H, H18), 7.95 (d, *J* = 8.33 Hz, 1H, H22), 7.83 (d, *J* = 7.45 Hz, 1H, H19), 7.79-7.73 (m, 1H, H6), 7.70-7.62 (m, 2H, H7, H21), 7.49-7.43 (m, 2H, H4, H20), 7.29 (dd, *J* = 9.13, 6.84 Hz, 1H, H3).

^{13}C-NMR (150.9 MHz, THF-d$_8$): 183.2 (C10), 179.0 (C9), 161.3 (C1), 157.1 (C16), 148.7 (C23), 143.8 (C15), 137.0 (C11), 135.2 (C14), 134.7 (C18), 133.2 (C12), 132.9 (C6), 131.9 (C3), 131.1 (C7), 129.0 (C22), 128.7 (C21), 127.8 (C24), 127.4 (C19), 126.6 (C8), 125.8 (C5), 125.3 (C20), 124.7 (C2), 118.2 (C17), 116.3 (C4), 112.4 (C13).

IR (ATR): 2980 (w), 2875 (w), 1654 (m), 1585 (m), 1509 (m), 1433 (m), 1409 (m), 1354 (m), 1319 (m), 1300 (m), 1254 (s), 1188 (m), 1148 (m), 1092 (m), 1057 (s), 1001 (m), 904 (m), 801 (m), 733 (m), 598 (w), 559 (w) cm^{-1}.

ESI-MS: calcd (m/z) for $[C_{24}H_{14}N_3O_2Li(THF)_2+Na]^+$: 550.22941; found: 550.62946 $[M + Na]^+$.

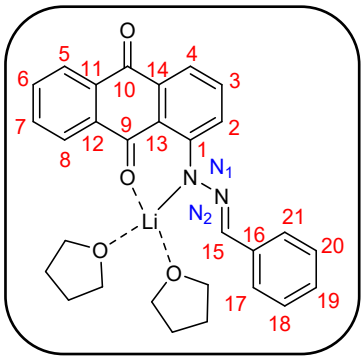

Lithium (*E*)-1-(2-benzylidenehydrazineyl)anthracene-9,10-dione (2c):

^{1}H-NMR (600.13 MHz, THF-d$_8$): δ ppm 8.50 (d, *J* = 9.1 Hz, H2), 8.36 (d, *J* = 7.6 Hz, 1H, H8), 8.27 (s, 1H, H15), 8.18 (d, *J* = 7.6 Hz, 1H, H5), 7.77 (d, *J* = 7.4 Hz, 2H, H17, H21), 7.72 (t, *J* = 7.6 Hz, 1H, H7), 7.62 (t, *J* = 7.6 Hz, 1H, H6), 7.40-7,30 (m, 3H, H4, H18, H20), 7.26 (t, *J* = 7.4 Hz, 1H, H19), 7.17 (t, *J* = 8.0 Hz, 1H, H3).

^{13}C-NMR (150.9 MHz, THF-d$_8$): δ 183.29 (C10), 177.08 (C9), 161.24 (C1), 143.12 (C15), 137.87 (C16), 137.41 (C12), 135.18 (C14), 133.10 (C11), 132.74 (C7), 131.22 (C3), 130.56 (C6), 128.22 (C18, C20), 127.51 (C19), 126.37 (C8), 126.24 (C17, C21), 125.67 (C5), 124.92 (C2), 115.73 (C4), 111.25 (C13).

IR (ATR): υ 3060 (w), 3024 (w), 2975 (w), 2871 (w), 2361 (w), 2341 (w), 2237 (w), 1653 (w), 1629 (m), 1580 (m), 1529 (w), 1496 (m), 1457 (w), 1446 (w), 1429 (w), 1411 (w), 1398 (w), 1388 (w), 1361 (m), 1302 (w), 1261 (m), 1234 (w), 1189 (w), 1150 (w), 1098 (w), 1069 (m), 1051 (m), 994 (m), 911 (w), 847 (w), 826 (w), 792 (w), 782 (w), 757 (w), 720 (m), 701 (m), 694 (m), 652 (w), 620 (w), 594 (w), 559 (w), 441 (s), 430 (s), 412 (s) cm^{-1}.

ESI-MS: calcd (m/z) for $[C_{21}H_{13}N_2O_2Li(THF)_2+Na]^+$: 449.49070; found: 499.32474 $[M+Na]^+$.

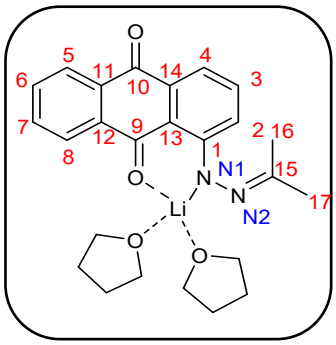

Lithium 1-(9,10-dioxo-9,10-dihydroanthracen-1-yl)-2-(propan-2-ylidene)hydrazin-1-ide (2d):

^{1}H-NMR (600.13 MHz, THF-d$_8$): δ ppm 8.25 (d, *J* = 7.8, 1H, H8), 8.05 (d, *J* = 7.8, 1H, H5), 7.59 (dt, *J* = 7.8, 1.1 Hz, 1H, H7), 7.45 (dt, *J* = 7.8, 1.1 Hz, 1H, H6), 7.26 (d, *J* = 9.3 Hz, 1H, H2), 7.06 (d, *J* = 6.6 Hz, 1H, H4), 6.84 (dd, *J* = 9.3, 6.6 Hz, 1H, H3), 2.01 (s, 3H, CH_3), 1.81 (s, 3H, CH_3).

^{13}C-NMR (150.9 MHz, THF-d$_8$): δ 184.6 (C10), 174.2 (C9), 156.2 (C1), 154.3 (C15), 139.4 (C12), 136.5 (C14), 134.1 (C11), 133.6 (C7), 131.3 (C3), 130.5 (C5), 127.1 (C8), 126.6 (C5), 124.8 (C2), 115.2 (C4), 110.9 (C13), 25.5 (C16/C17), 17.4 (C17/C16)

IR (ATR): υ 2361 (w), 1647 (m), 1588 (m), 1547 (w), 1499 (m), 1431 (m), 1415 (m), 1396 (m), 1311 (m), 1273 (m), 1162 (w), 1069 (w), 1047 (w), 1024 (w), 860 (w), 824 (w), 796 (w), 728 (m), 707 (m), 663 (w), 624 (w), 594 (w), 559 (w), 448 (s), 436 (s), 414 (s) cm^{-1}.

ESI-MS: calcd (m/z) for $[C_{17}H_{13}N_2O_2Li(THF)_2]^+$: 429.46500; found: 429.23141 $[M + H]^+$.

8. NMR data

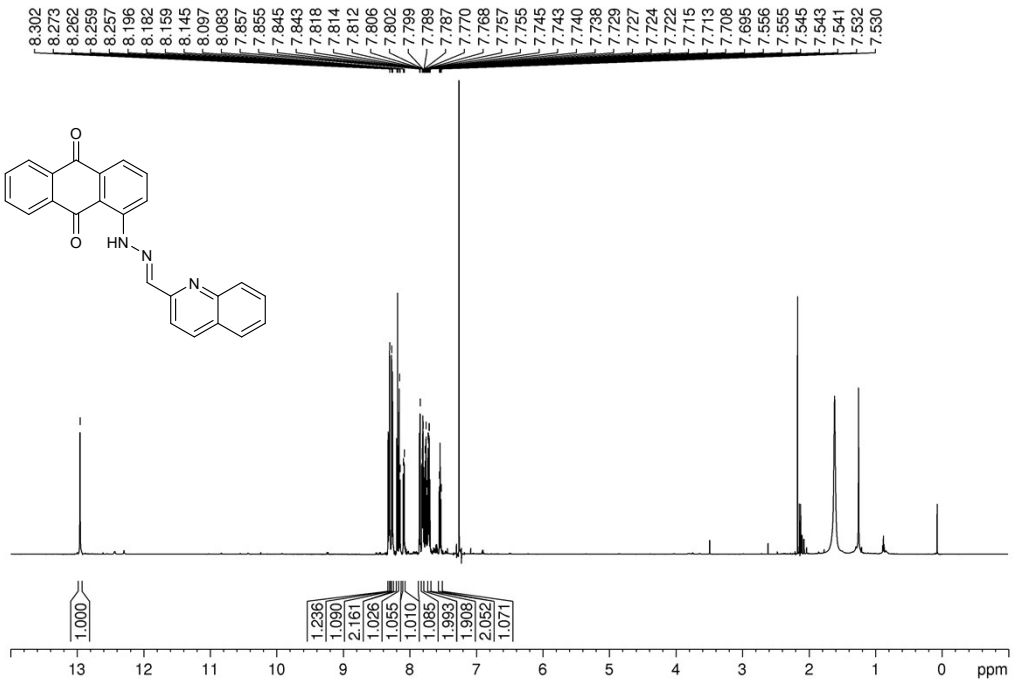

Figure S10. ^{1}H NMR (600.13 MHz, $CDCl_3$) spectrum of **1b**.

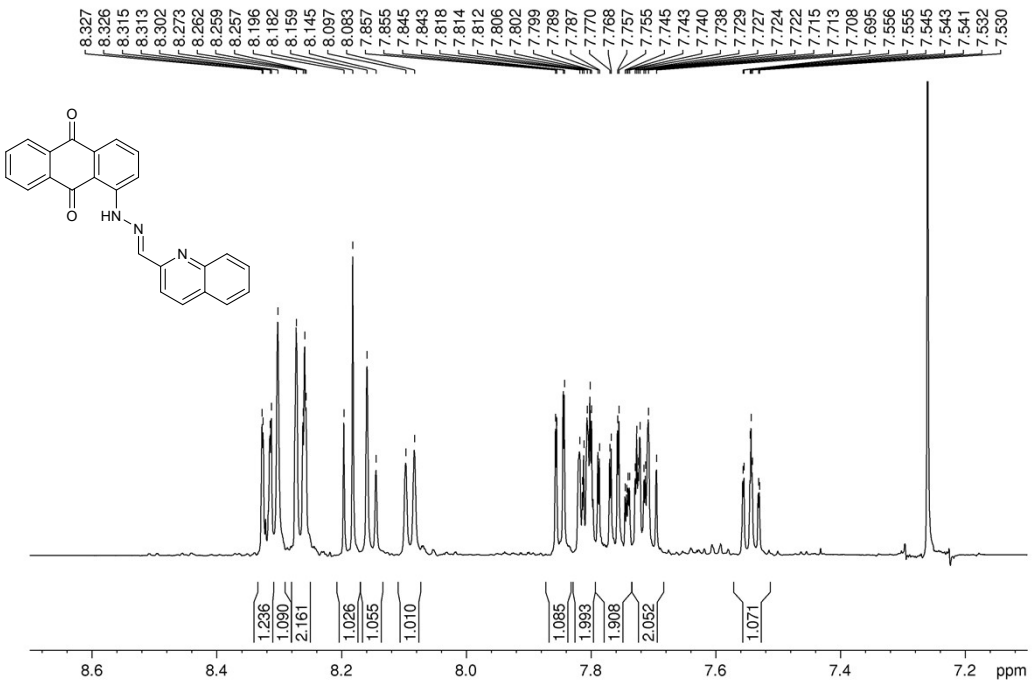

Figure S11. Expanded ^{1}H NMR (600.13 MHz, $CDCl_3$) spectrum of **1b**.

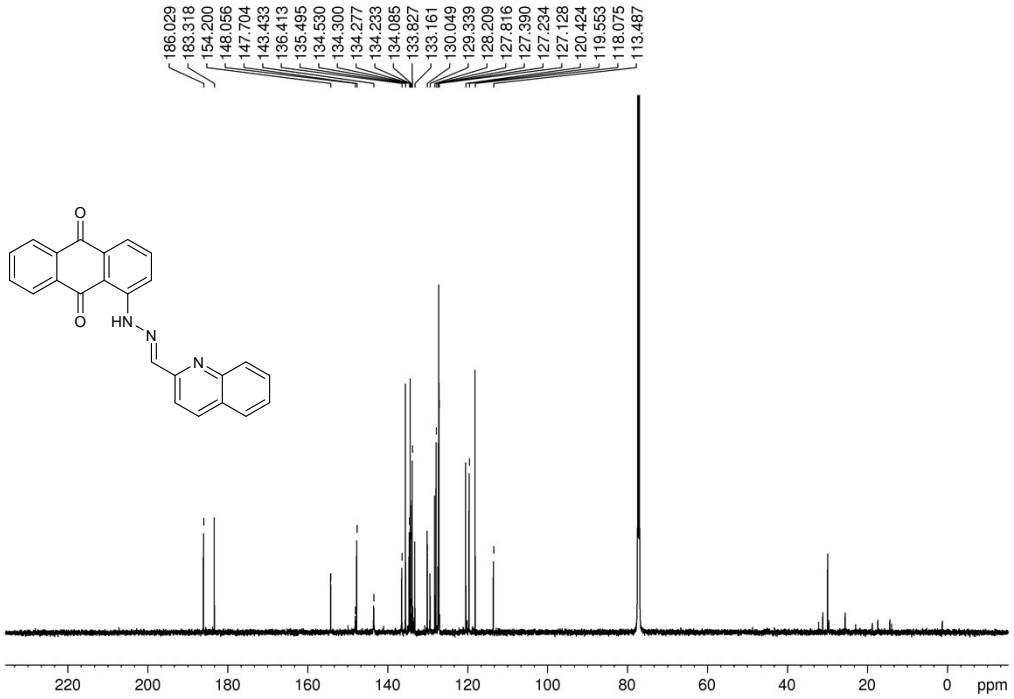

Figure S12. ^{13}C NMR (125.77 MHz, $CDCl_3$) spectrum of **1b**.

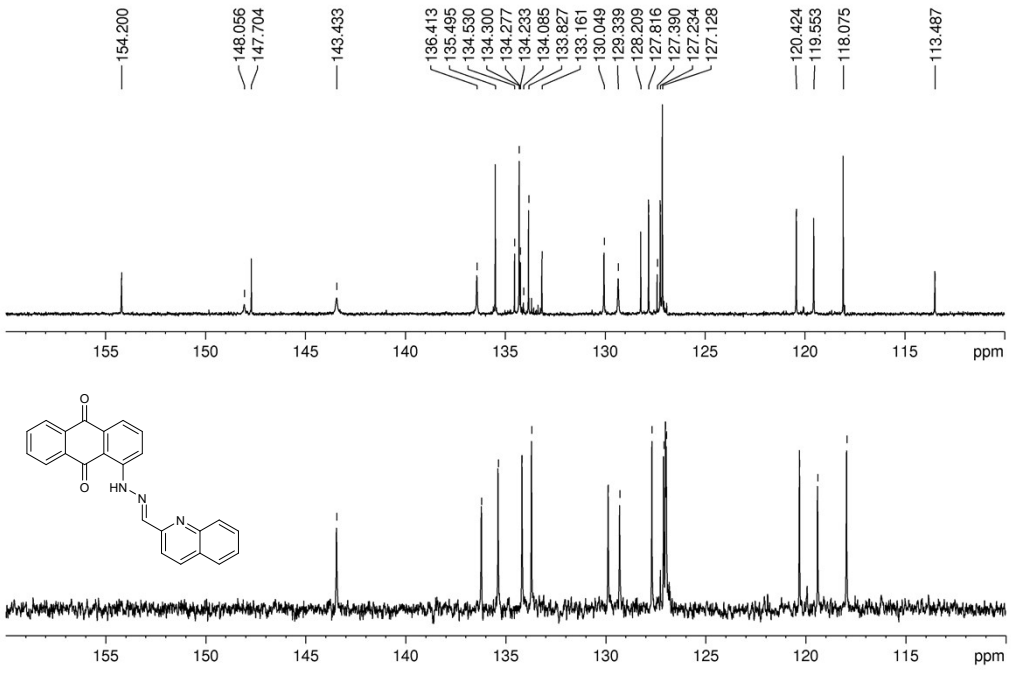

Figure S13. Expanded ^{13}C NMR (125.77 MHz, $CDCl_3$) and DEPT-135 spectrum of **1b**.

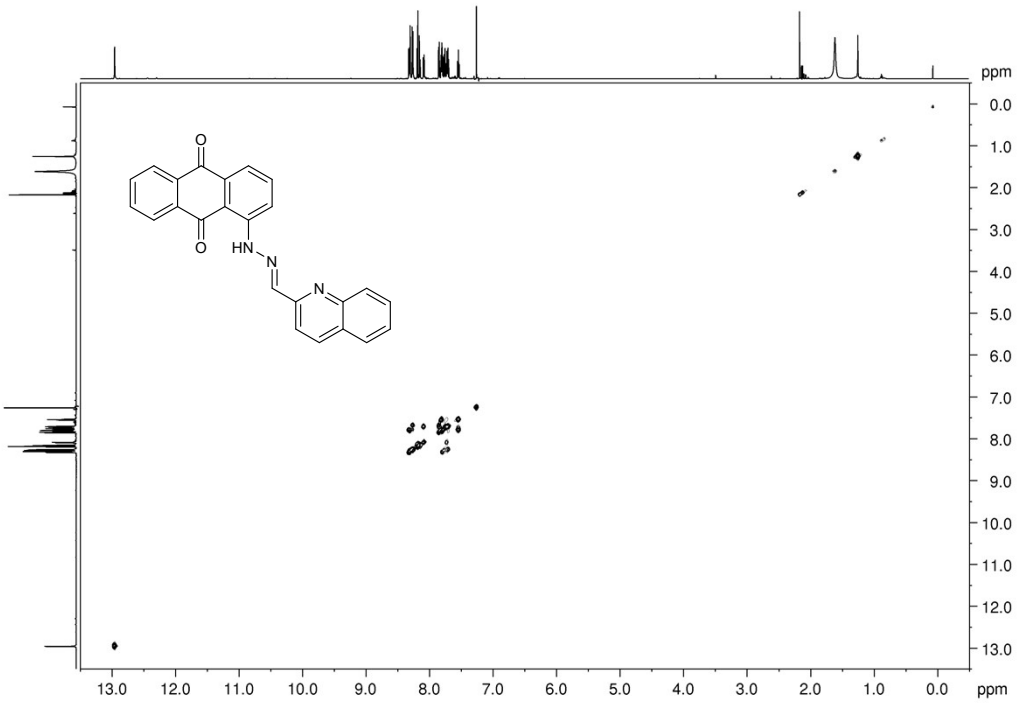

Figure S14. COSY spectrum of **1b**.

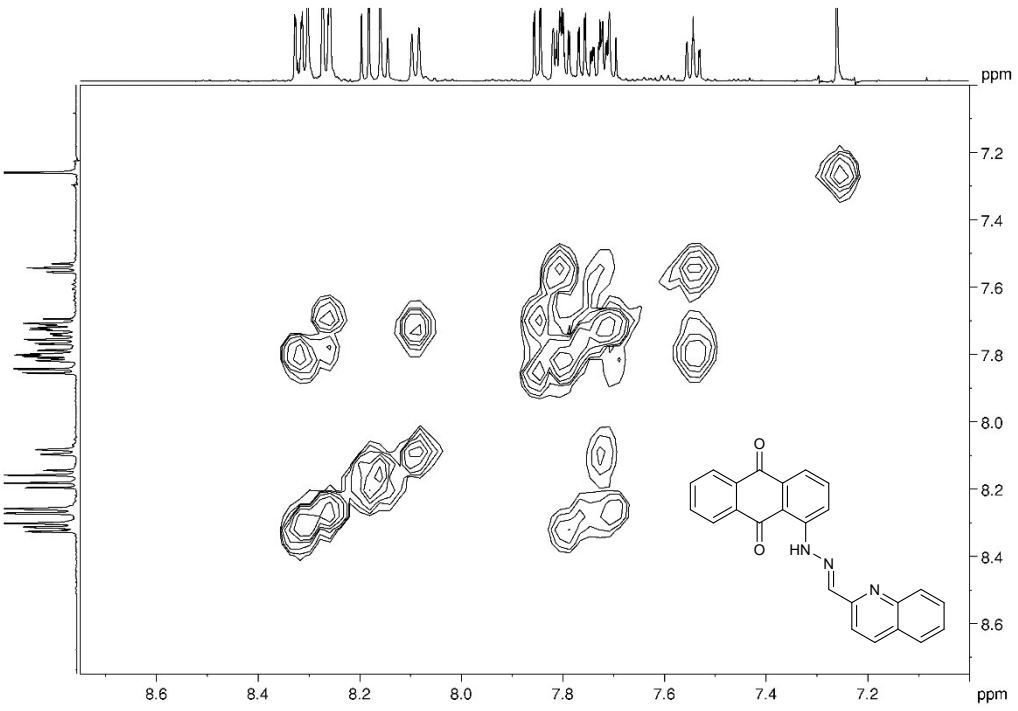

Figure S15. Expanded COSY spectrum of **1b**.

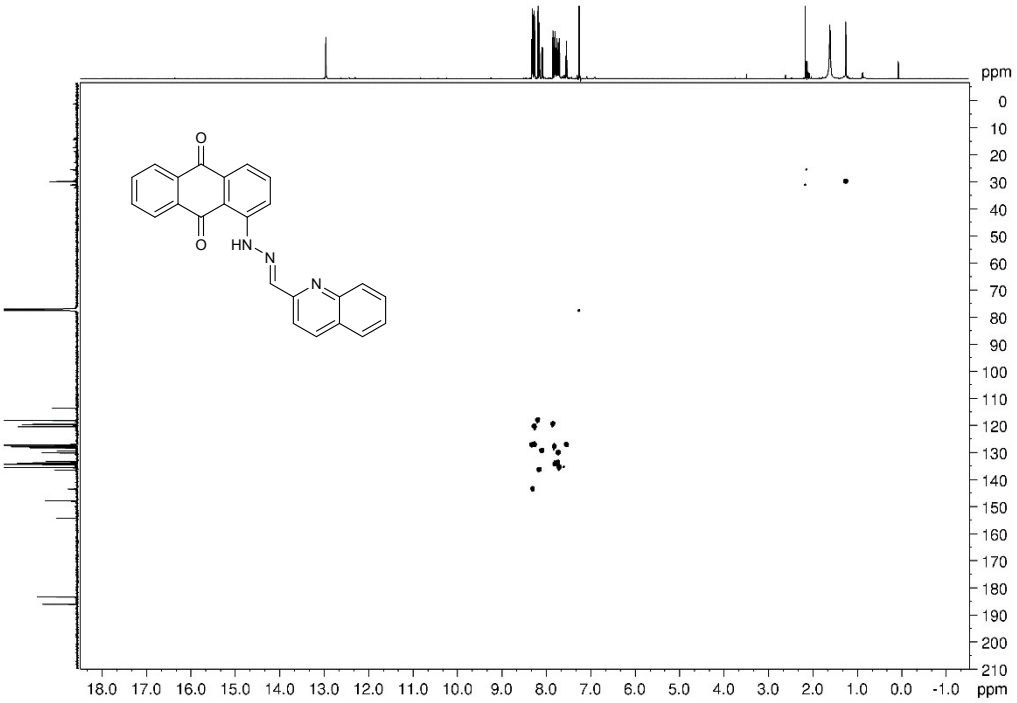

Figure S16. HSQC spectrum of **1b**.

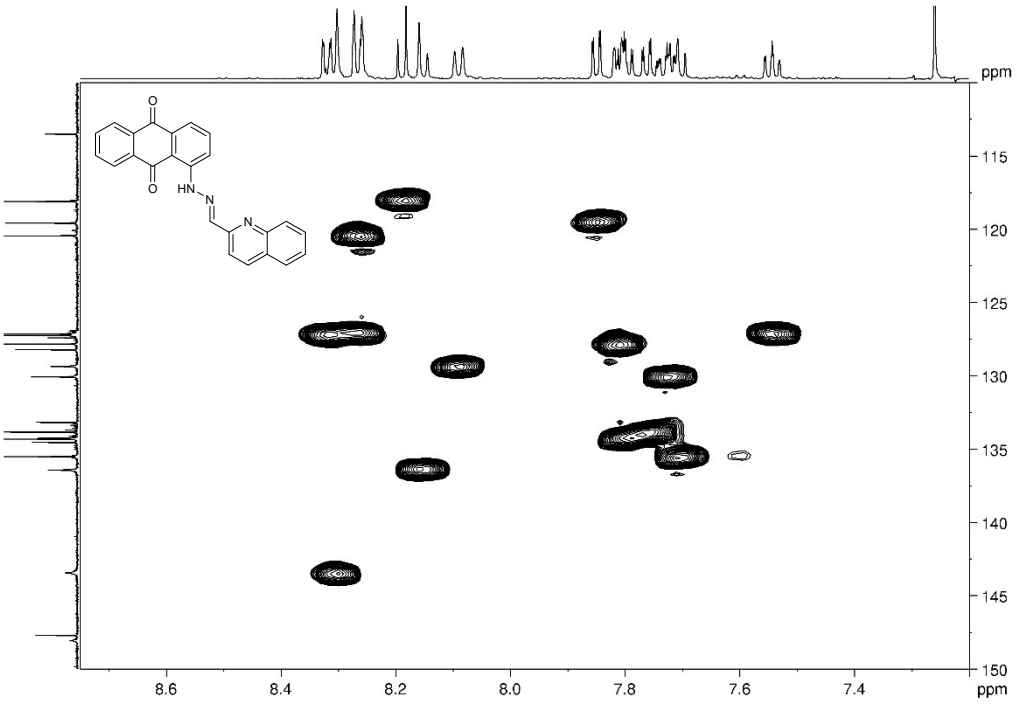

Figure S17. Expanded HSQC spectrum of **1b**.

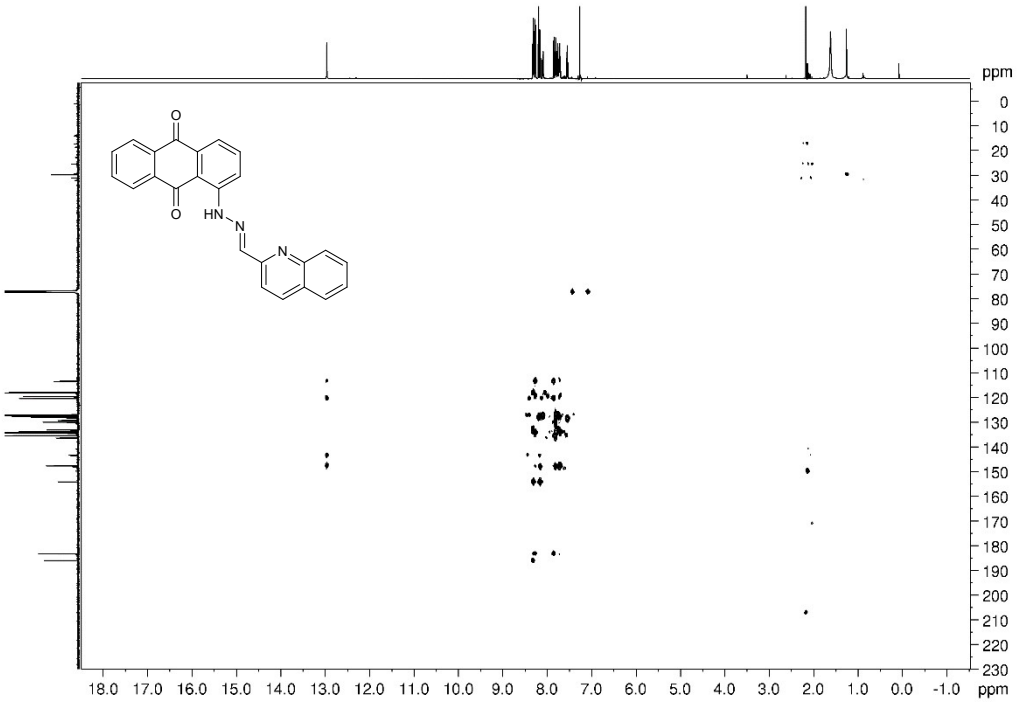

Figure S18. HMBC spectrum of **1b.**

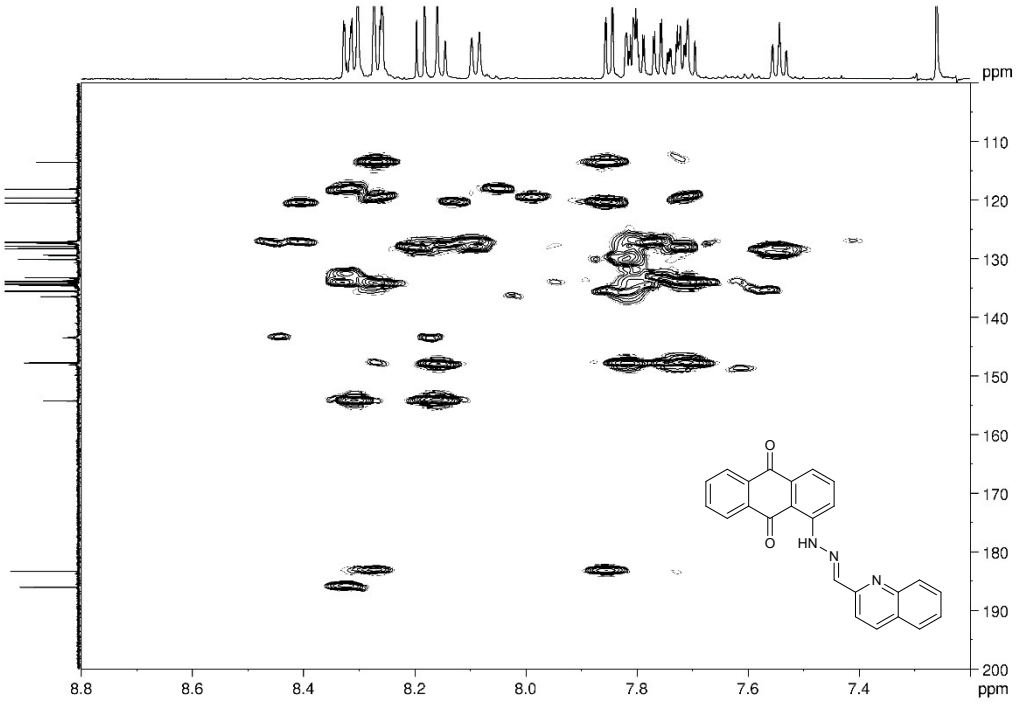

Figure S19. Expanded HMBC spectrum of **1b.**

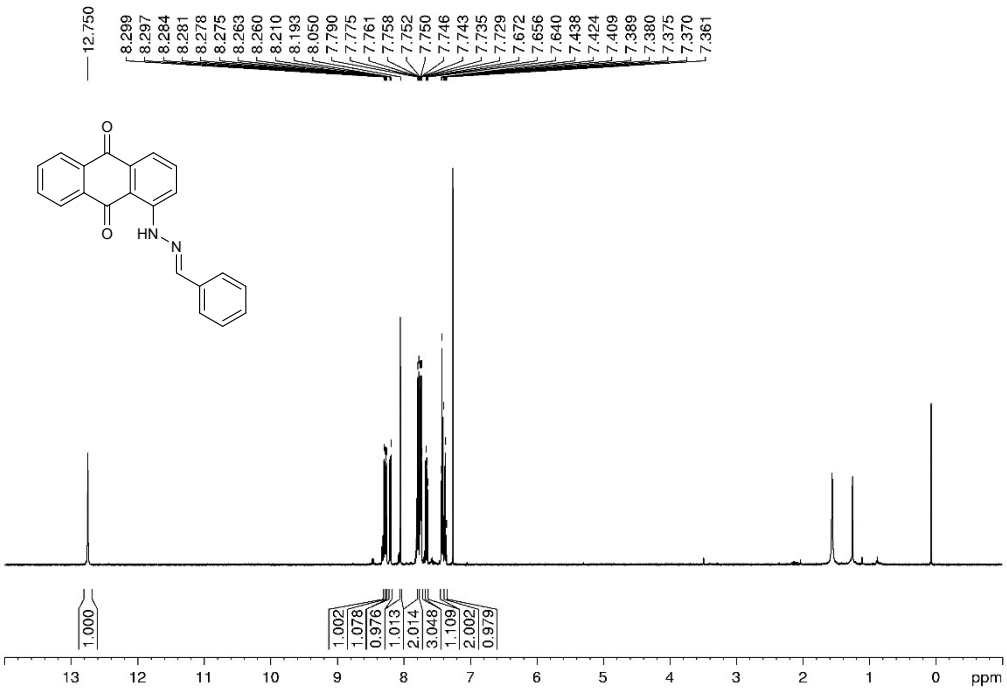

Figure S20. ^{1}H NMR (500.13 MHz, $CDCl_3$) spectrum of **1c**.

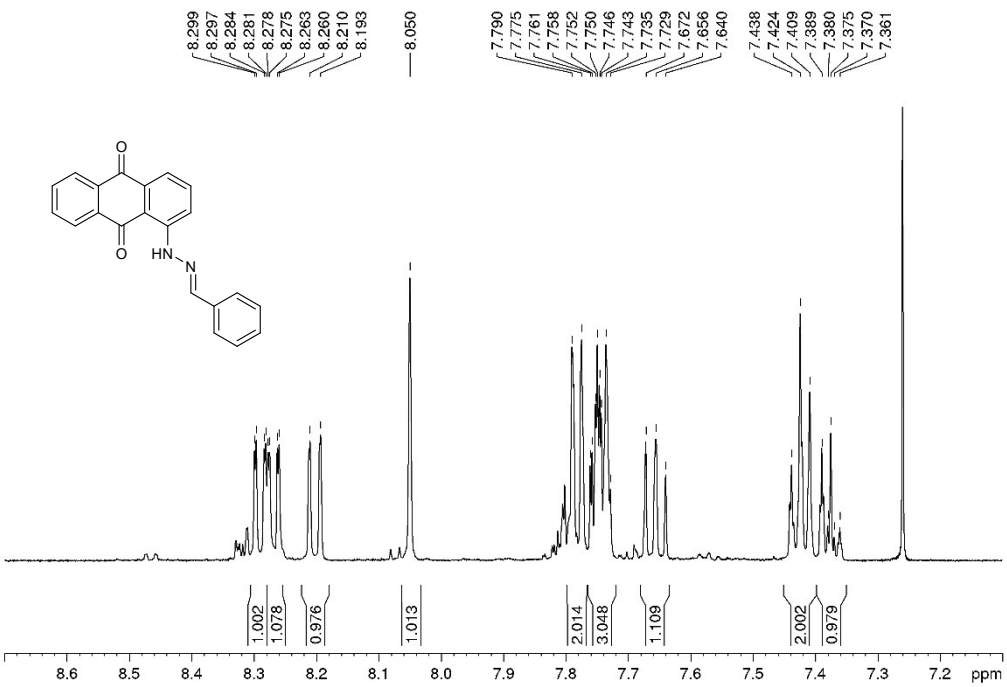

Figure S21. Expanded ^{1}H NMR (500.13 MHz, $CDCl_3$) spectrum of **1c**.

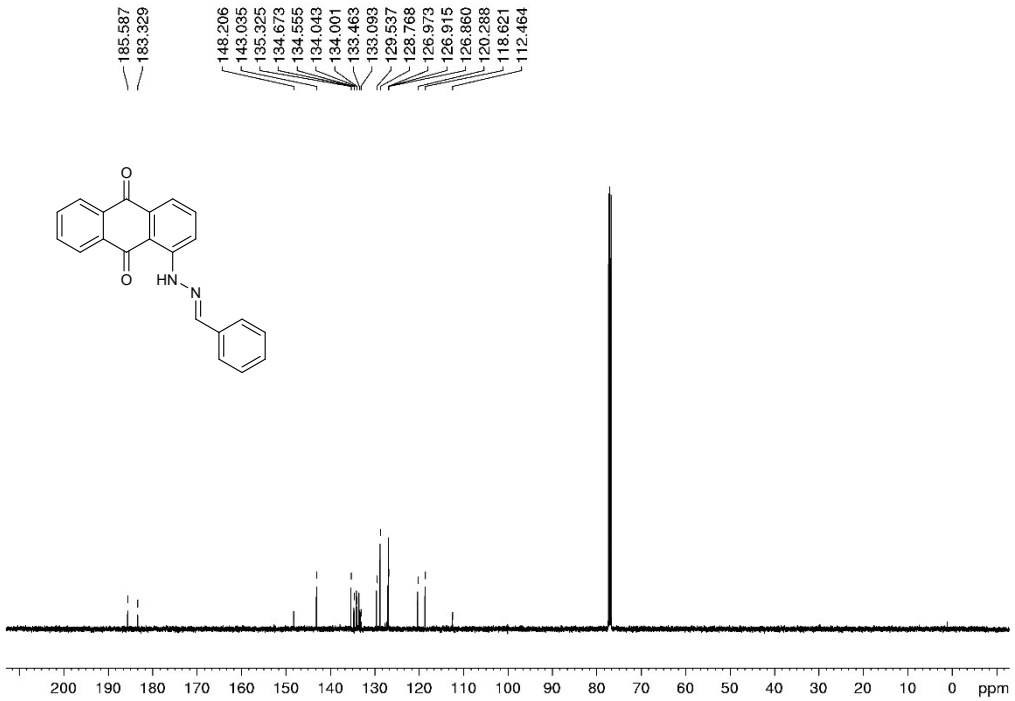

Figure S22. ^{13}C NMR (125.77 MHz, $CDCl_3$) spectrum of **1c**.

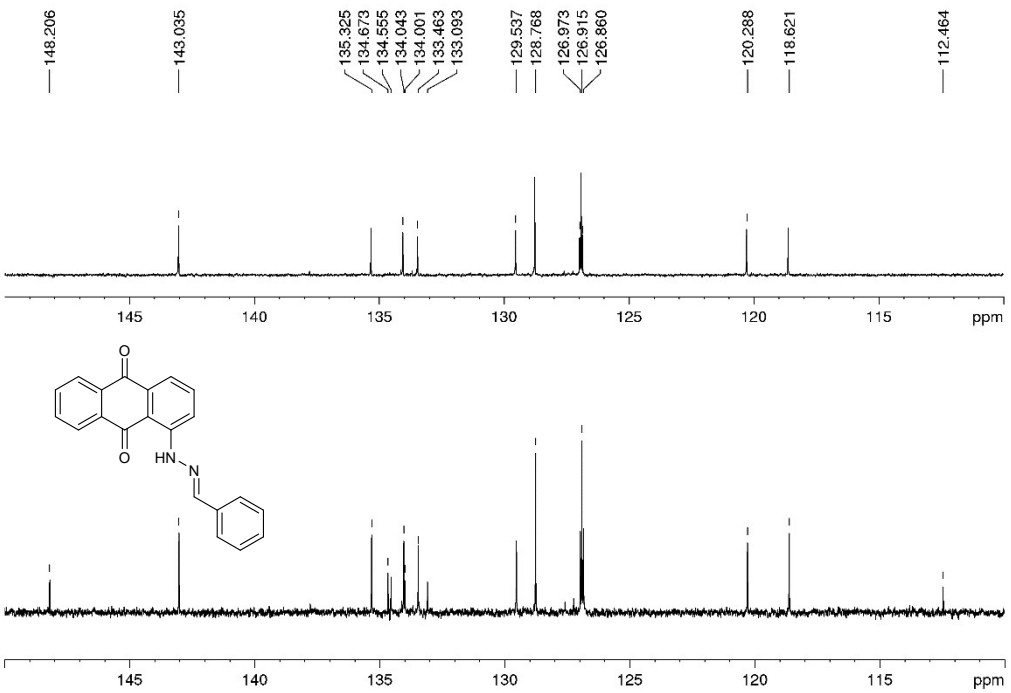

Figure S23. Expanded ^{13}C NMR (125.77 MHz, $CDCl_3$) and DEPT-135 spectrum of **1c**.

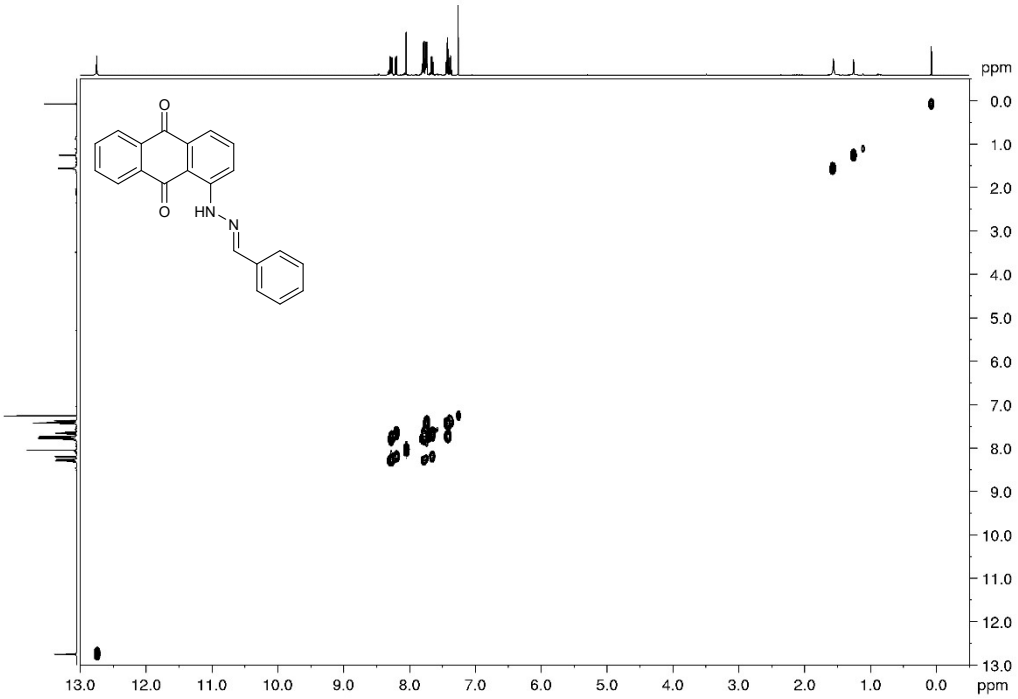

Figure S24. COSY spectrum of **1c**.

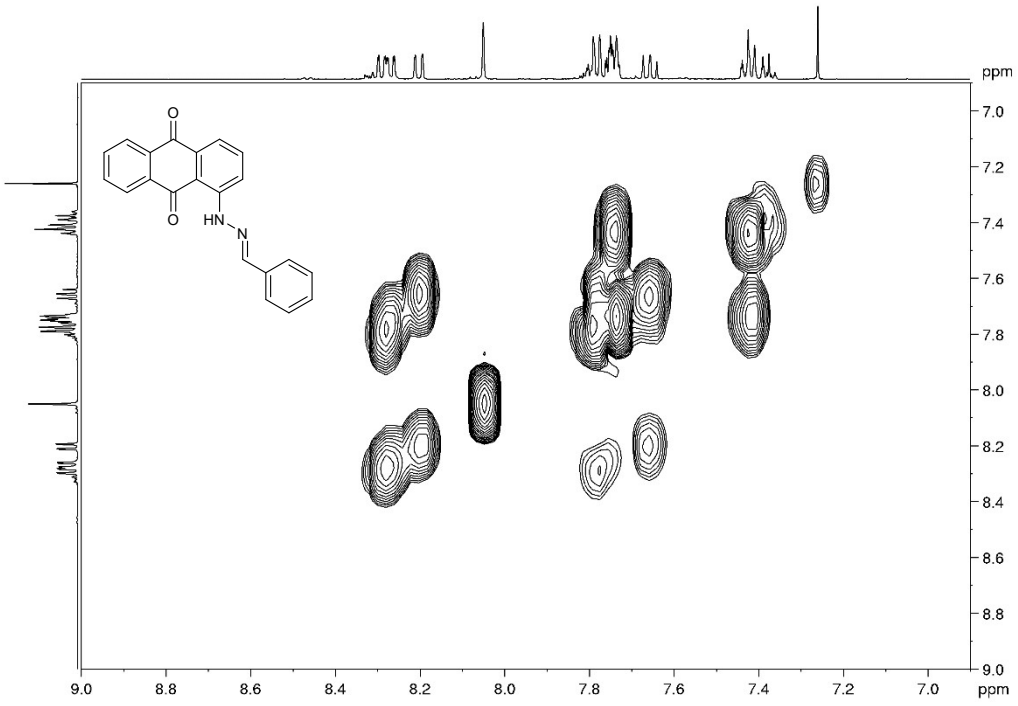

Figure S25. Expanded COSY spectrum of **1c**.

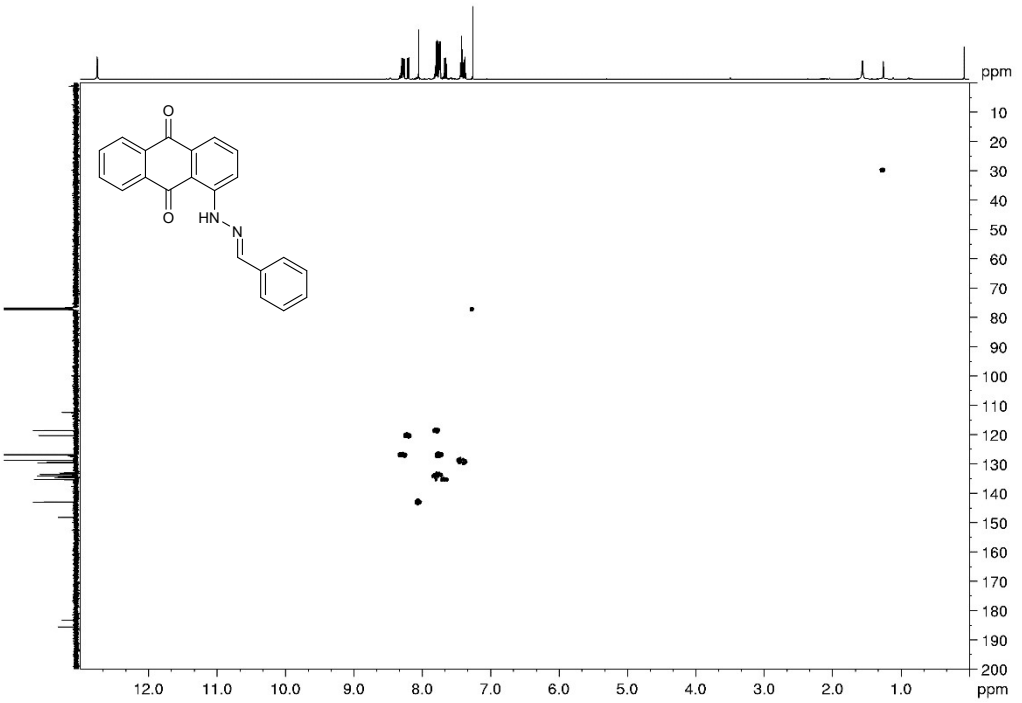

Figure S26. HSQC spectrum of **1c**.

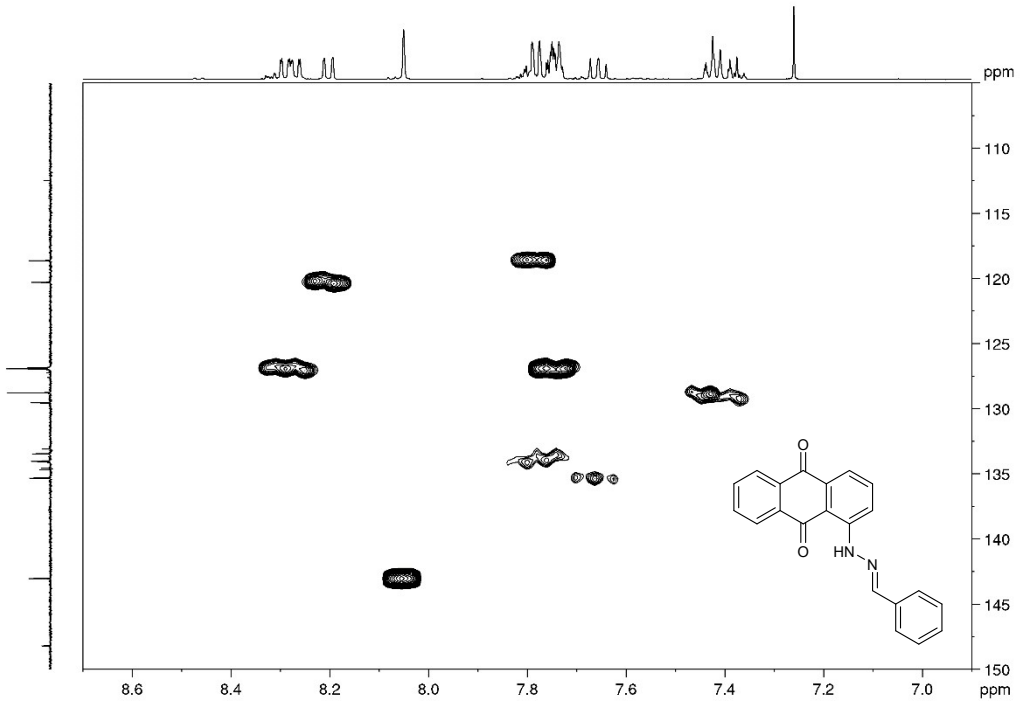

Figure S27. Exspanded HSQC spectrum of **1c**.

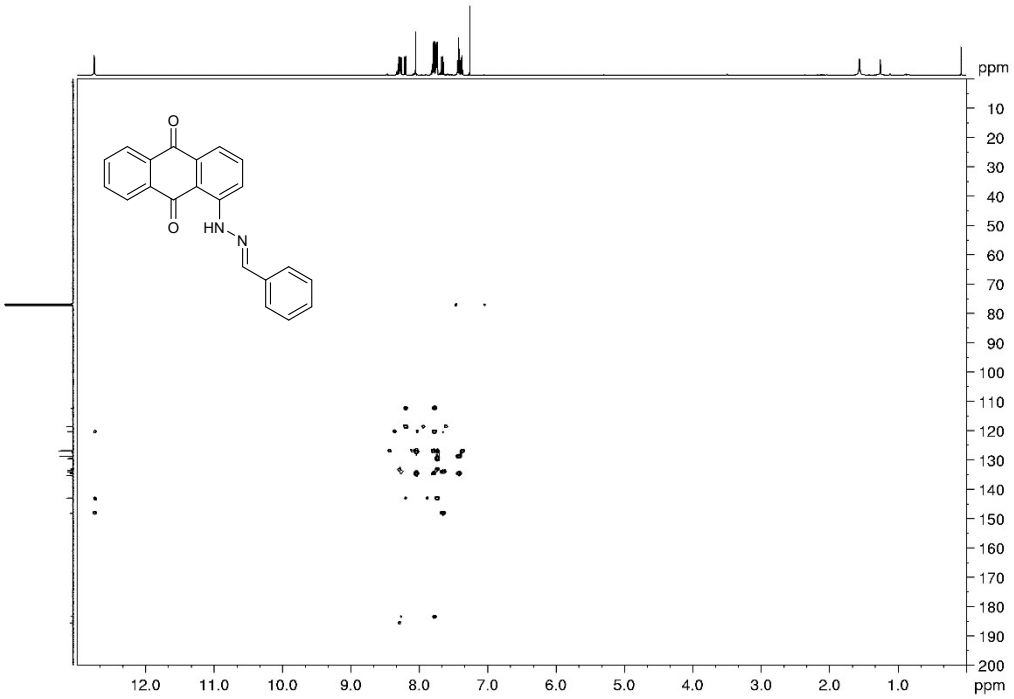

Figure S28. HMBC spectrum of **1c.**

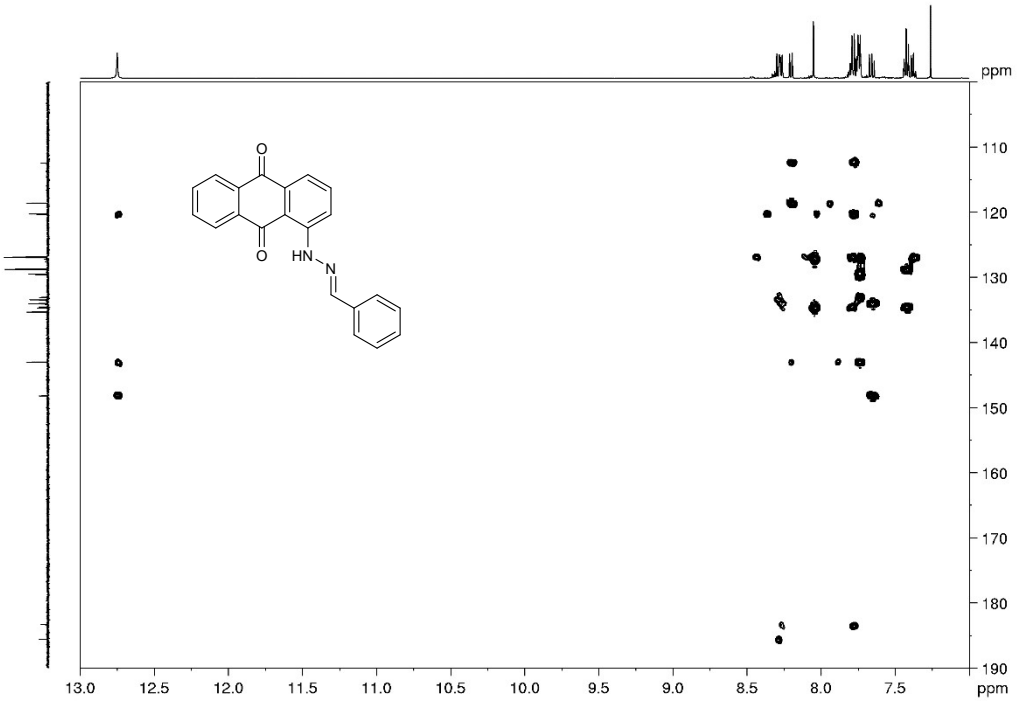

Figure S29. Expanded HMBC spectrum of **1c.**

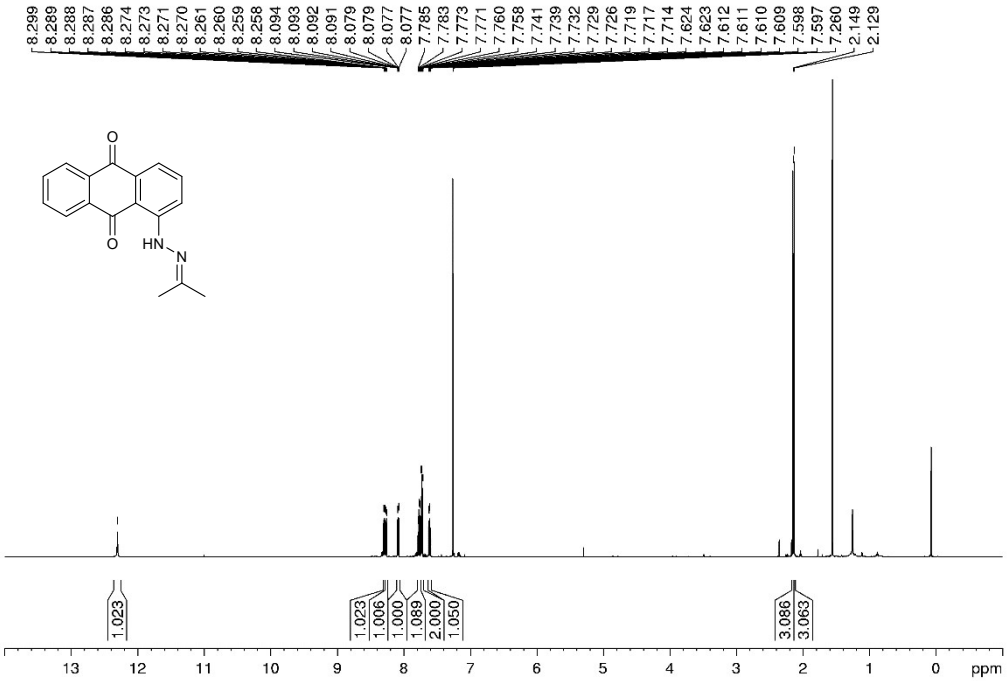

Figure S30. ^{1}H NMR (500.13 MHz, $CDCl_3$) spectrum of **1d**.

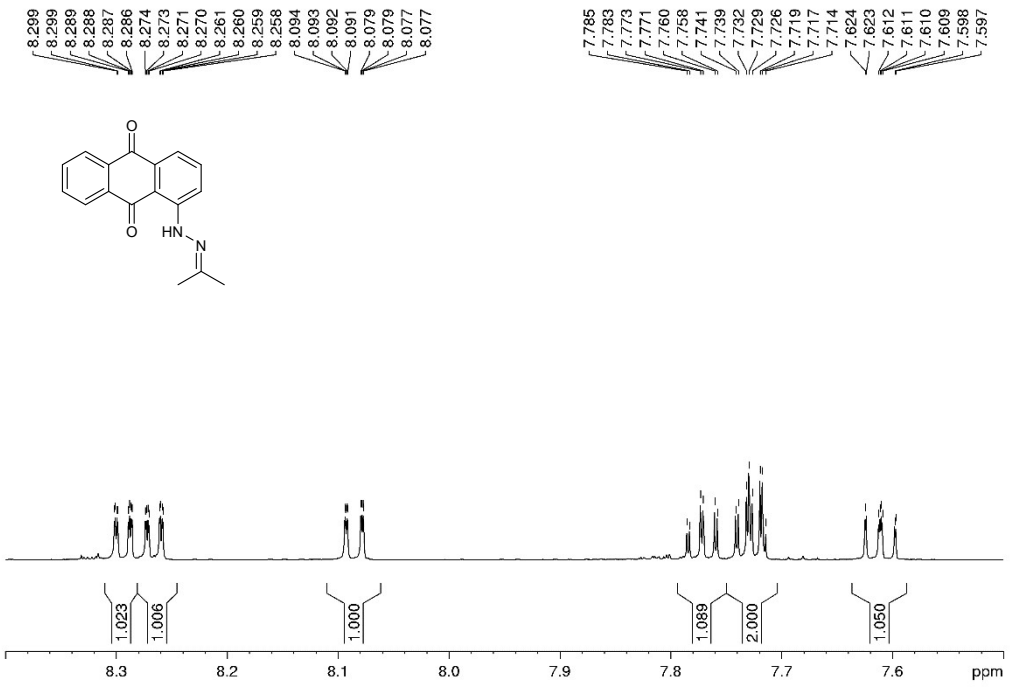

Figure S31. Expanded ^{1}H NMR (500.13 MHz, $CDCl_3$) spectrum of **1d**.

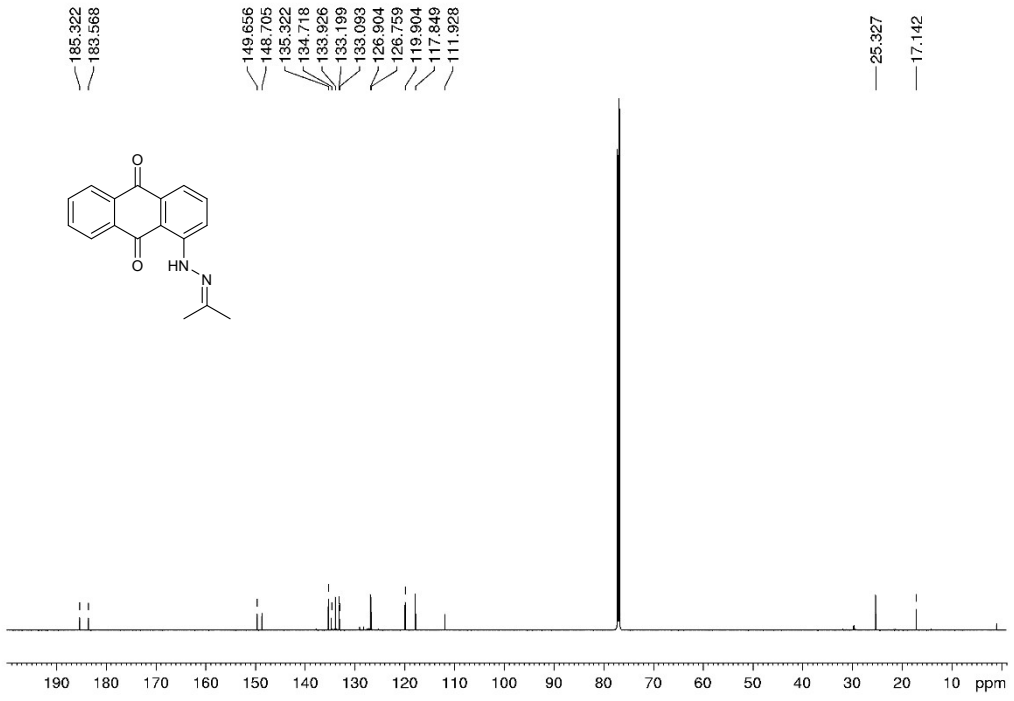

Figure S32. ^{13}C NMR (125.77 MHz, $CDCl_3$) spectrum of **1d**.

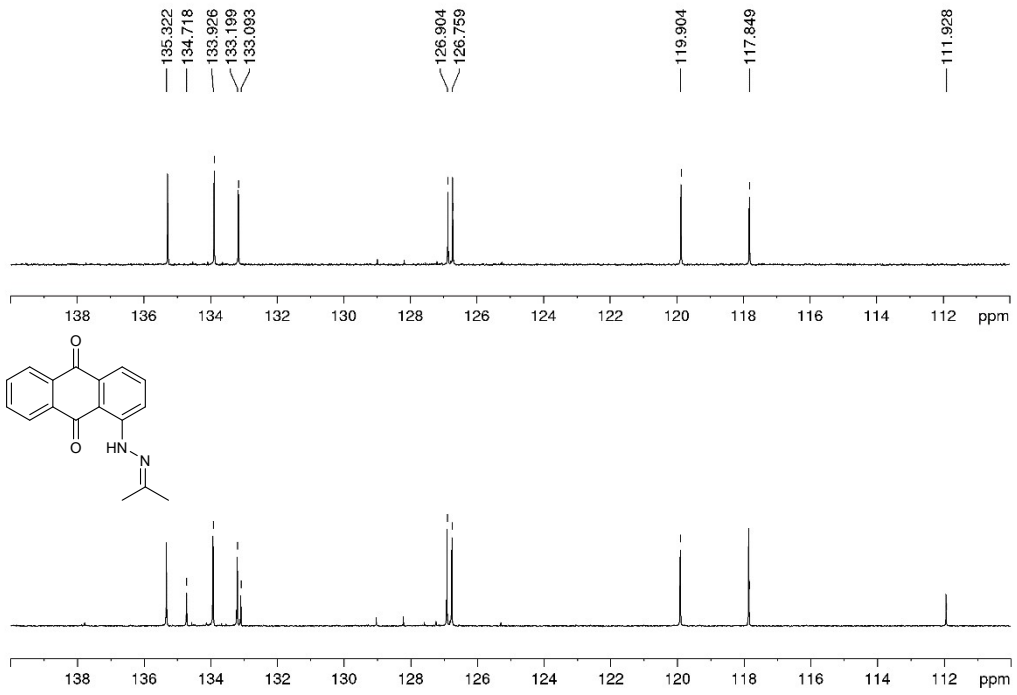

Figure S33. Expanded ^{13}C NMR (125.77 MHz, $CDCl_3$) and DEPT-135 spectrum of **1d**.

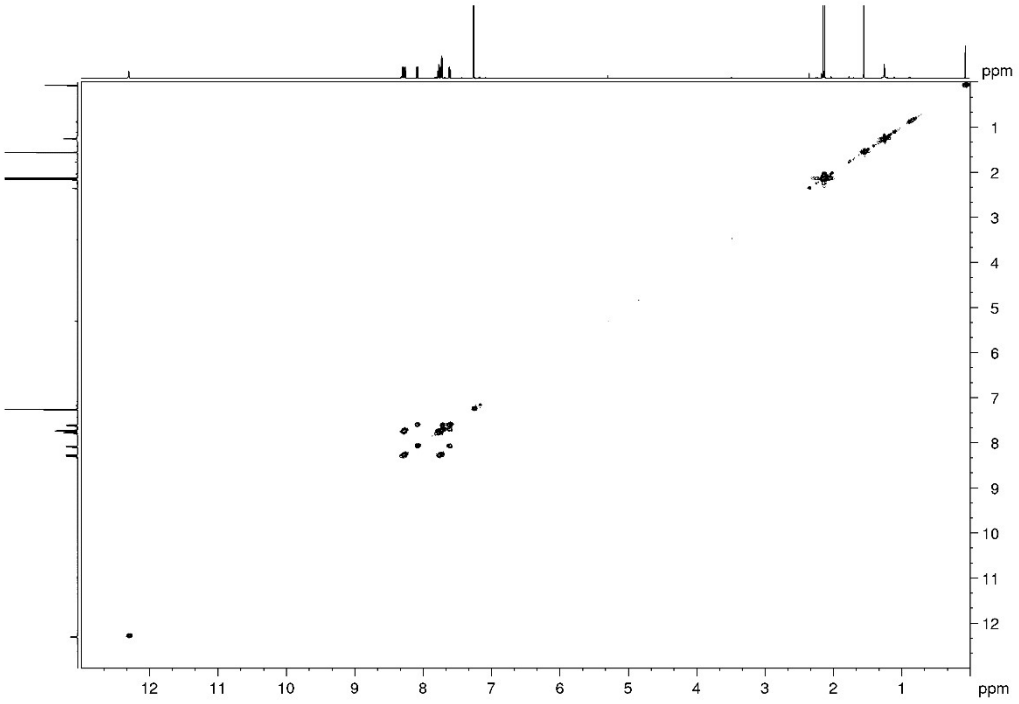

Figure S34. COSY spectrum of **1d.**

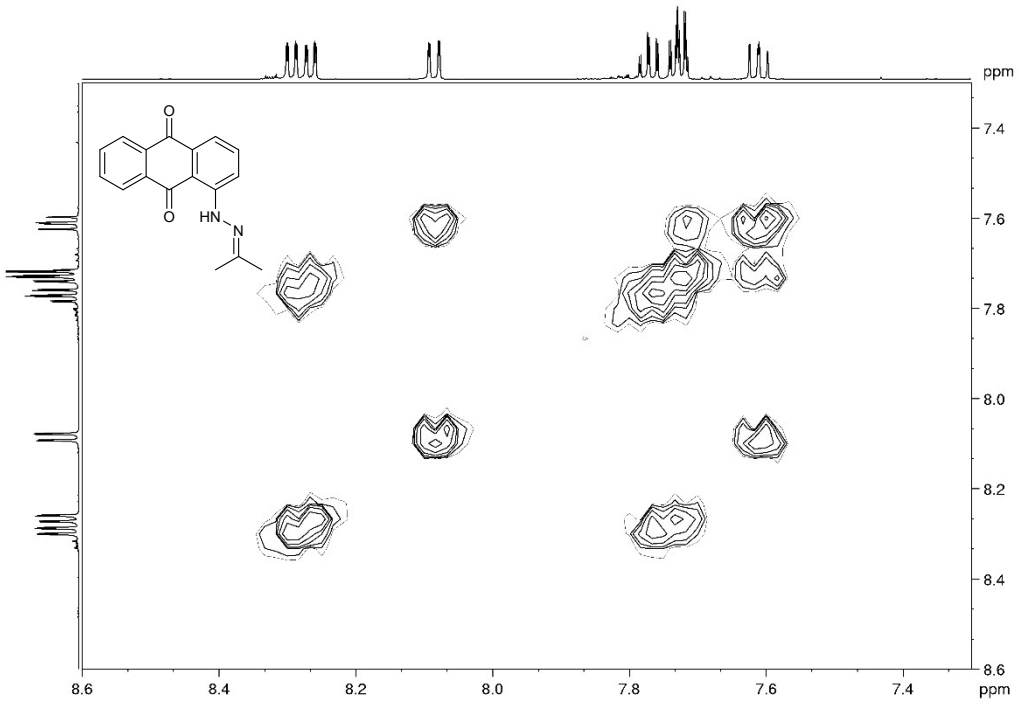

Figure S35. Expanded COSY spectrum of **1d**.

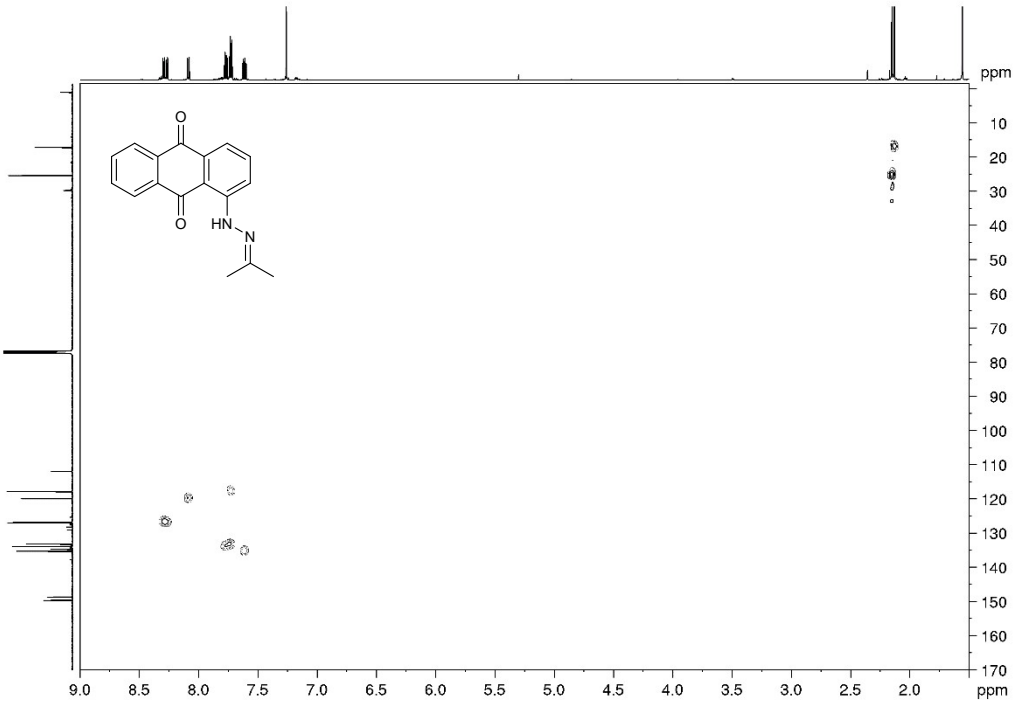

Figure S36. HSQC spectrum of **1d**.

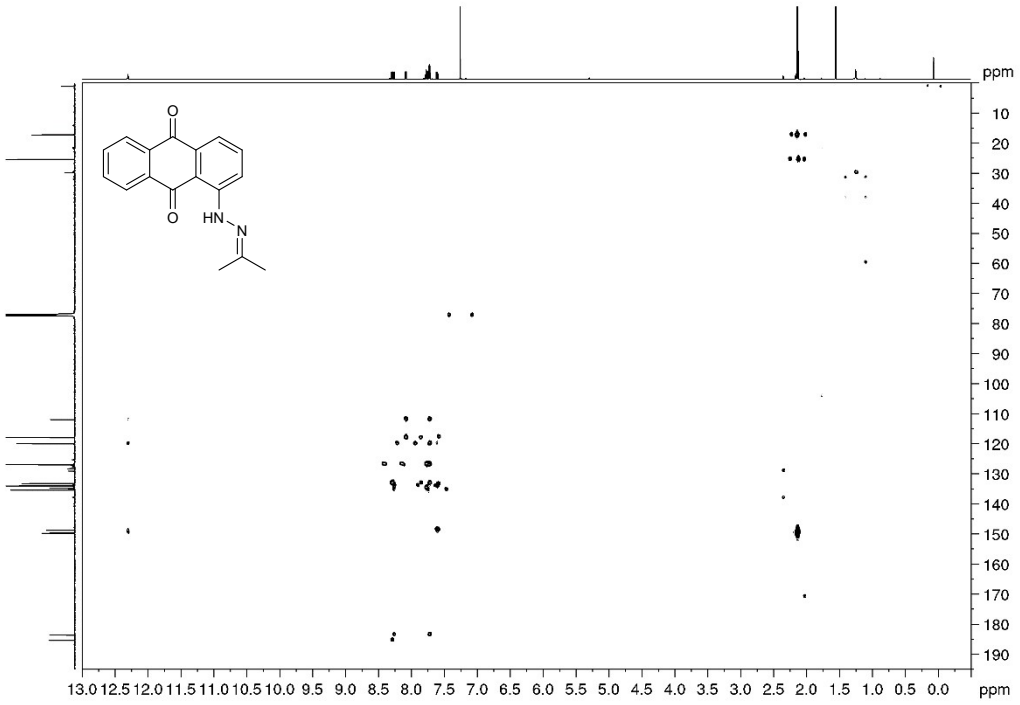

Figure S37. HMBC spectrum of **1d**.

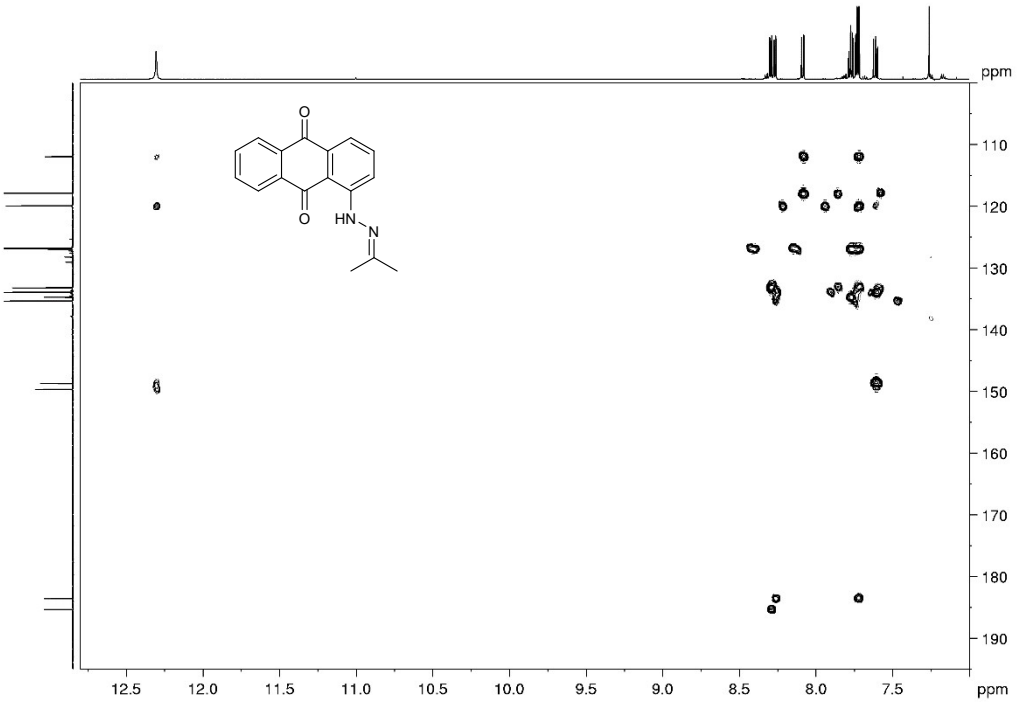

Figure S38. Expanded HMBC spectrum of **1d**.

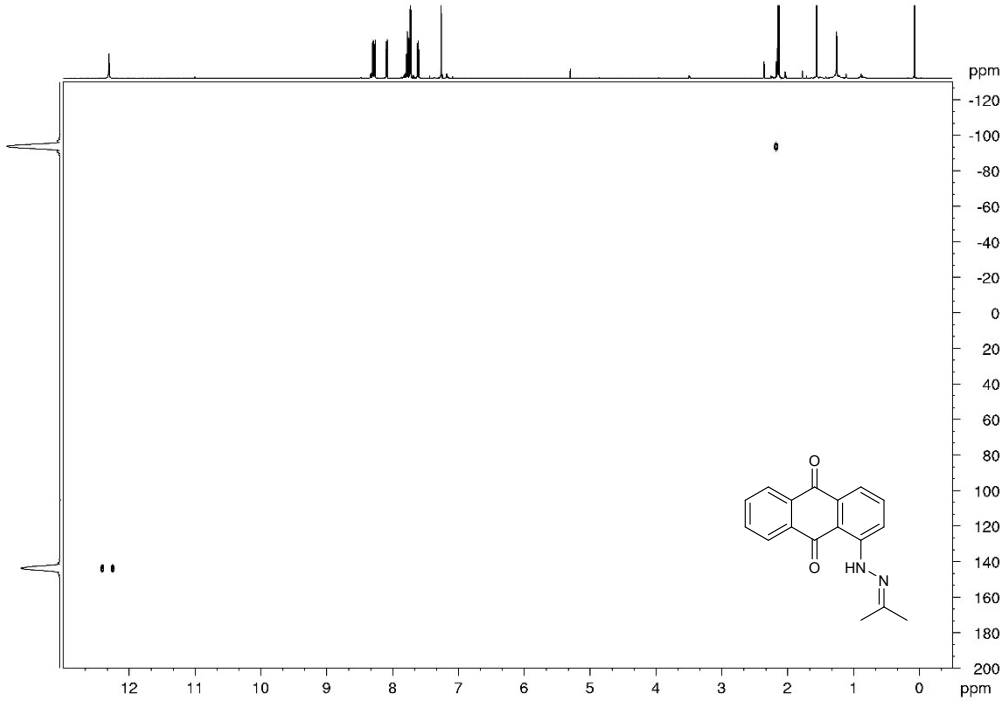

Figure S39. $^{1}H,^{15}N$ gHMBC spectrum of **1d**.

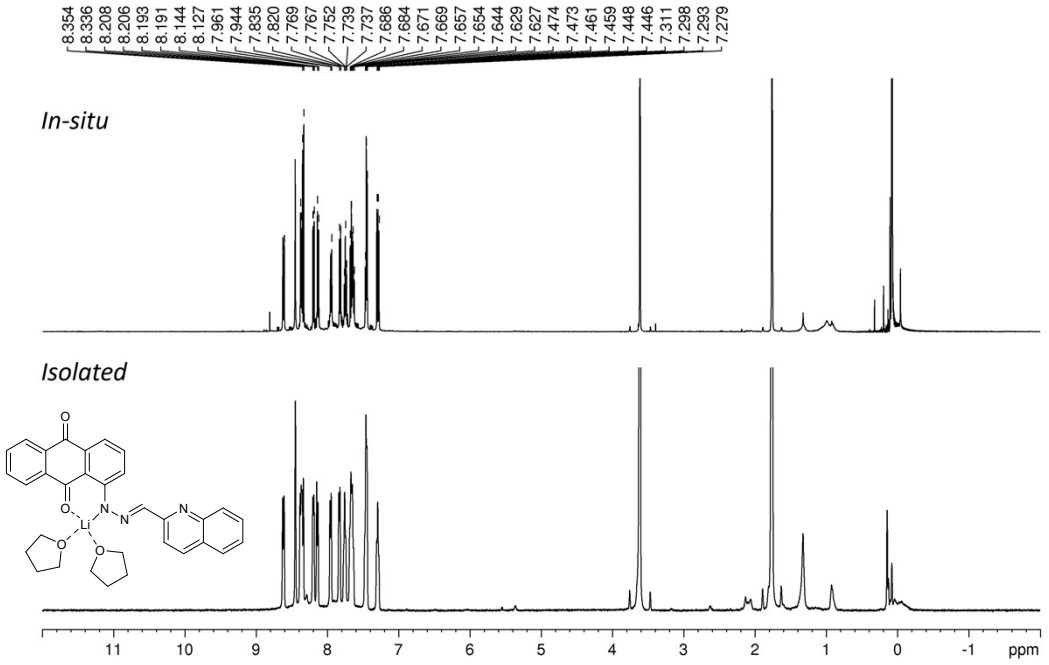

Figure S40. [1]H NMR (500.13 MHz, THF-d_8) spectrum of **2b (in-situ)** and **2b (isolated)**.

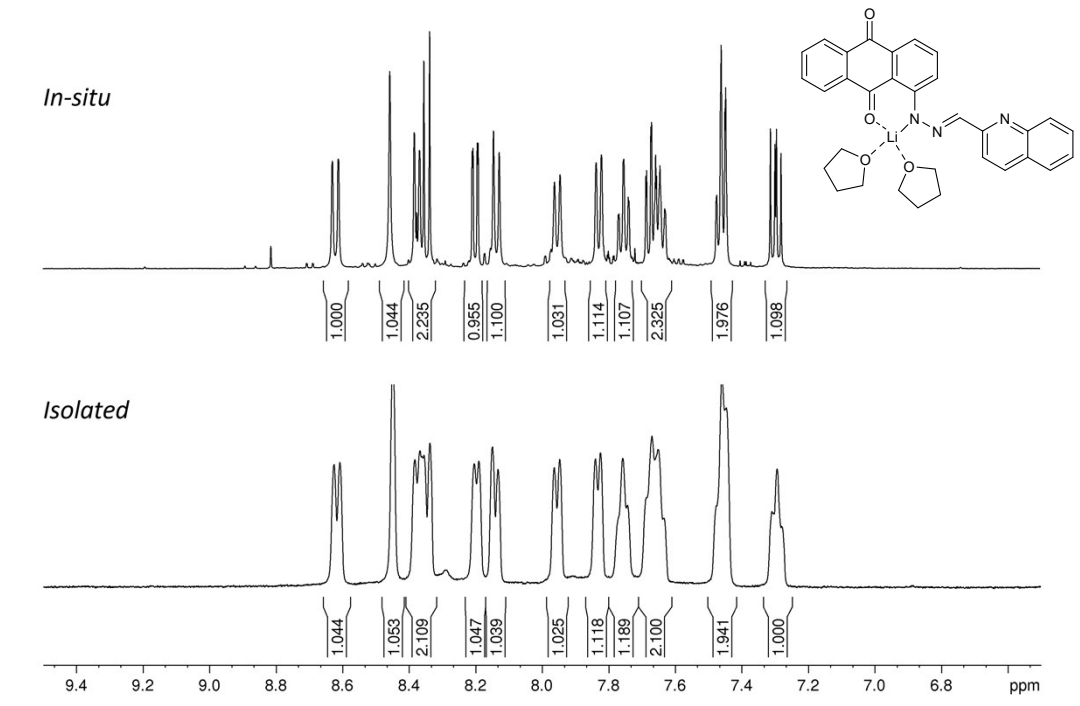

Figure S41. Expanded [1]H NMR (500.13 MHz, THF-d_8) spectrum of **2b (in-situ)** and **2b (isolated)**.

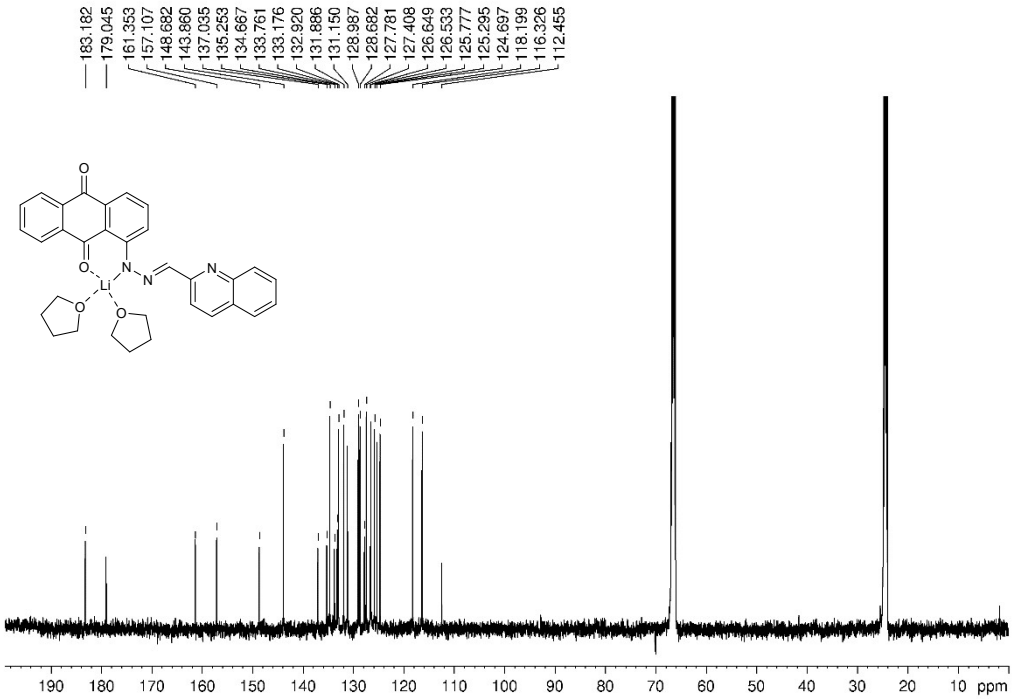

Figure S42. ^{13}C NMR (125.77 MHz, THF-d_8) spectrum of **2b**.

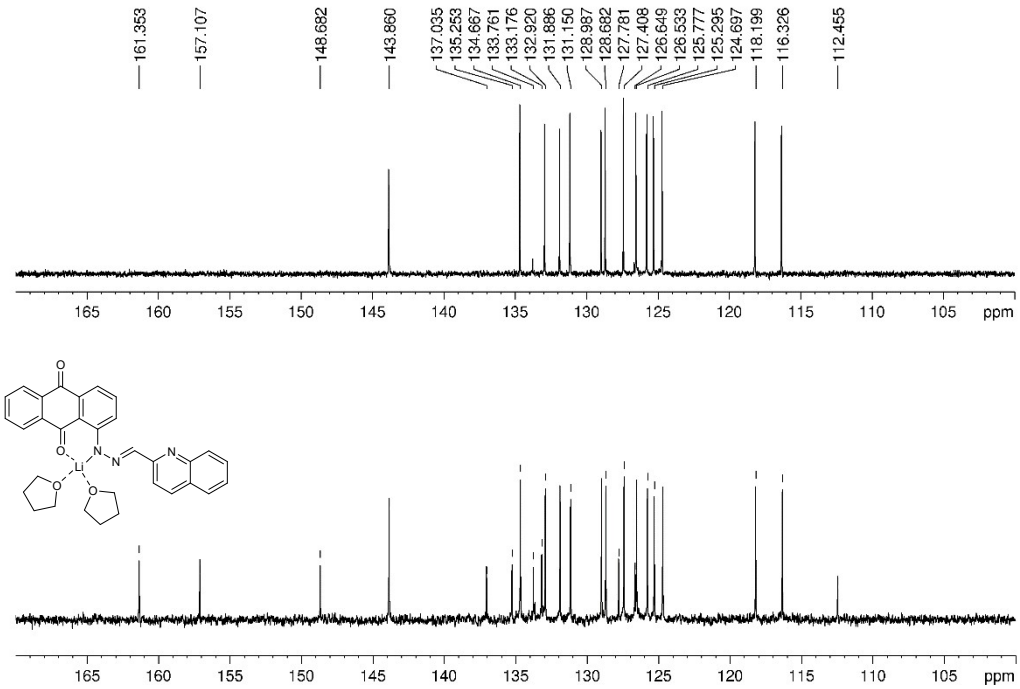

Figure S43. Expanded ^{13}C NMR (125.77 MHz, THF-d_8) and DEPT-135 spectrum of **2b**.

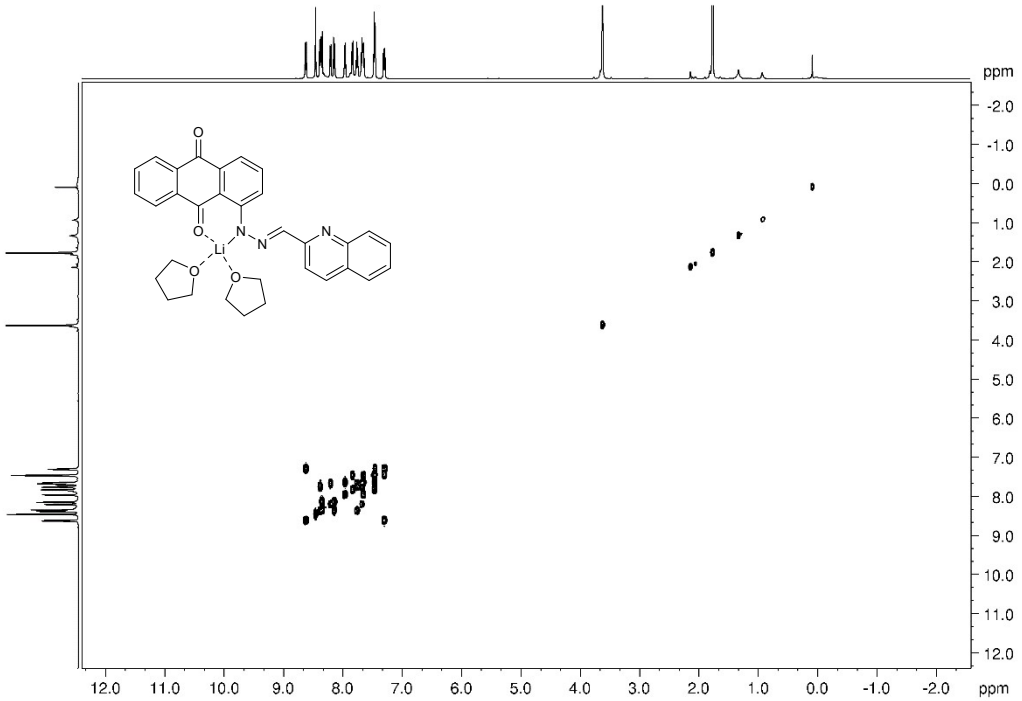

Figure S44. COSY spectrum of **2b**.

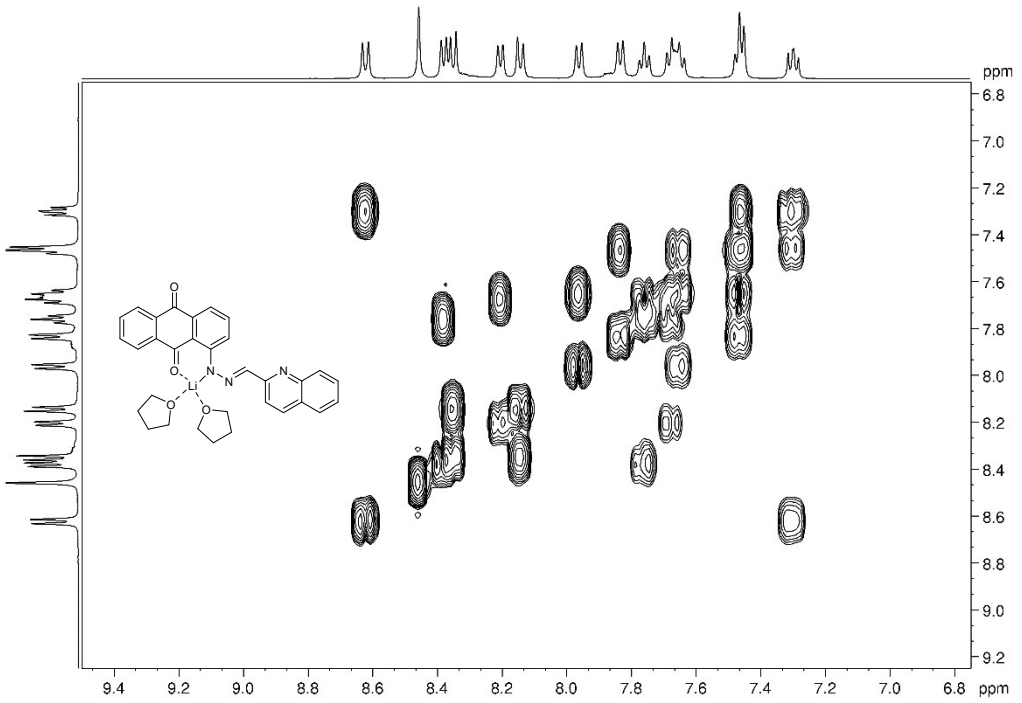

Figure S45. Expanded COSY spectrum of **2b**.

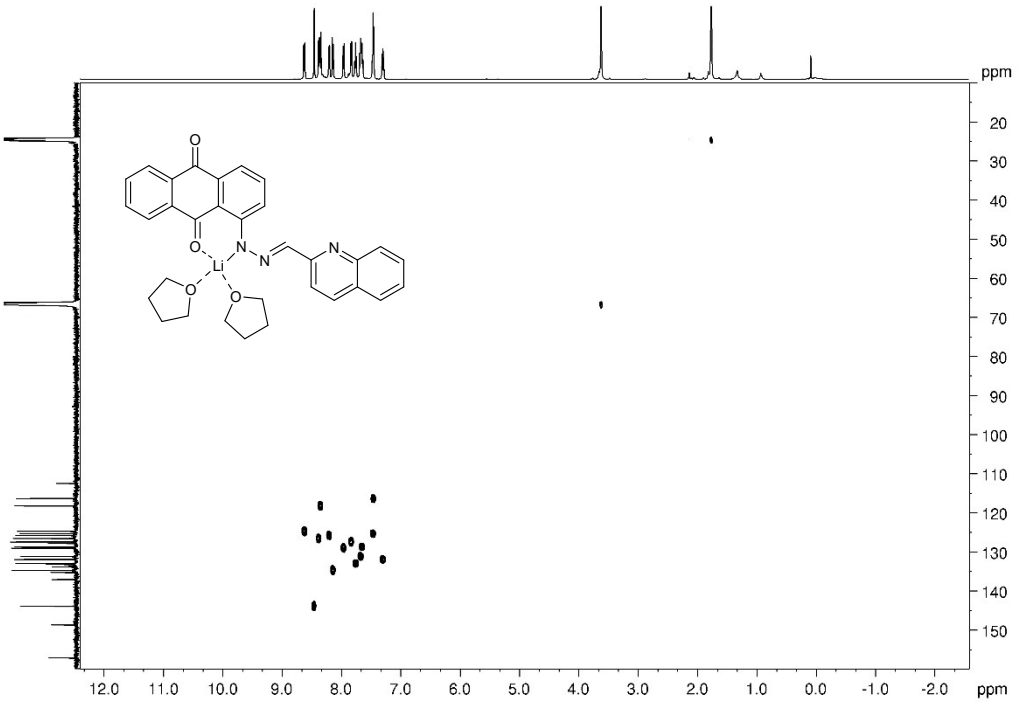

Figure S46. HMQC spectrum of **2b**.

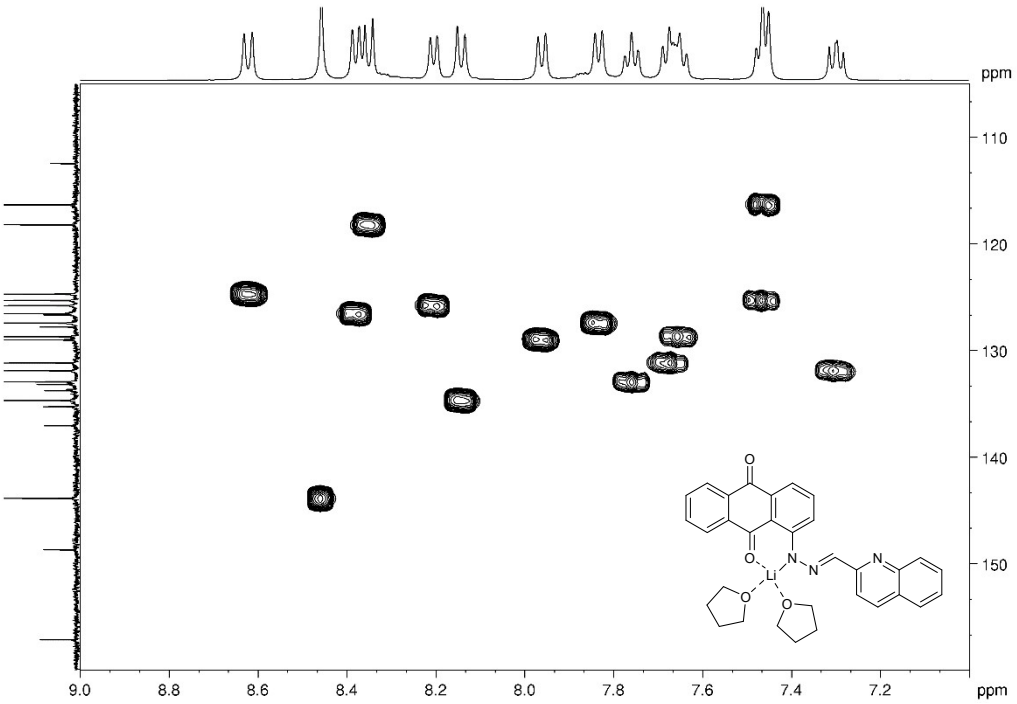

Figure S47. Expanded HMQC spectrum of **2b**.

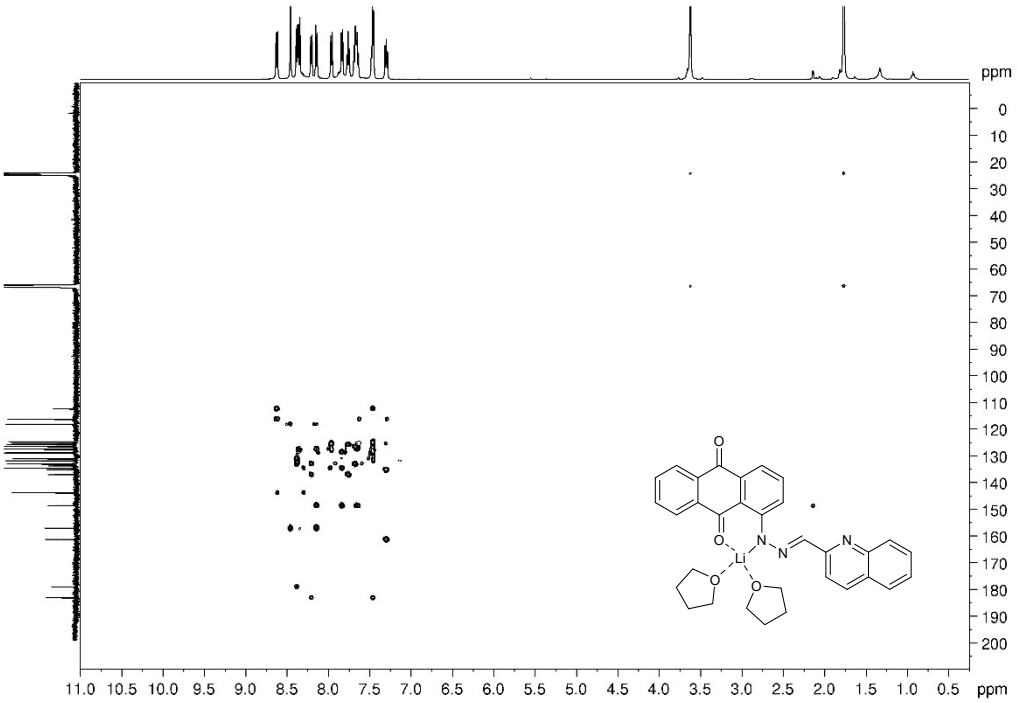

Figure S48. HMBC spectrum of **2b.**

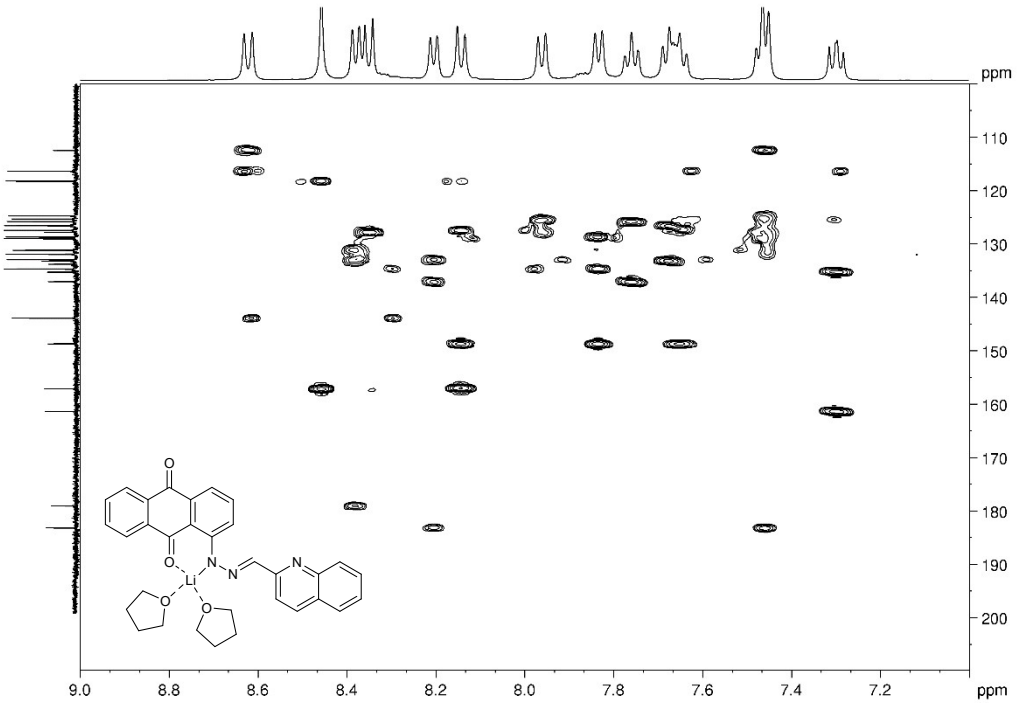

Figure S49. Expanded HMBC spectrum of **2b.**

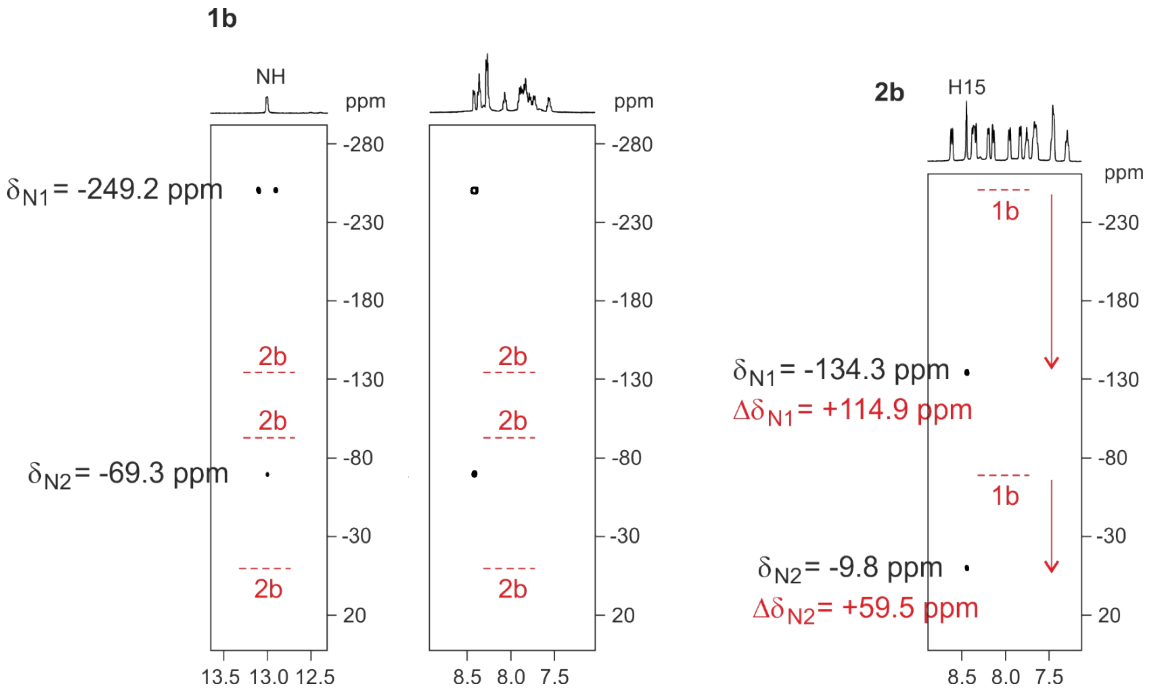

Figure S50. $^{1}H,^{15}N$ gHMBC spectrum of **1b** and **2b**.

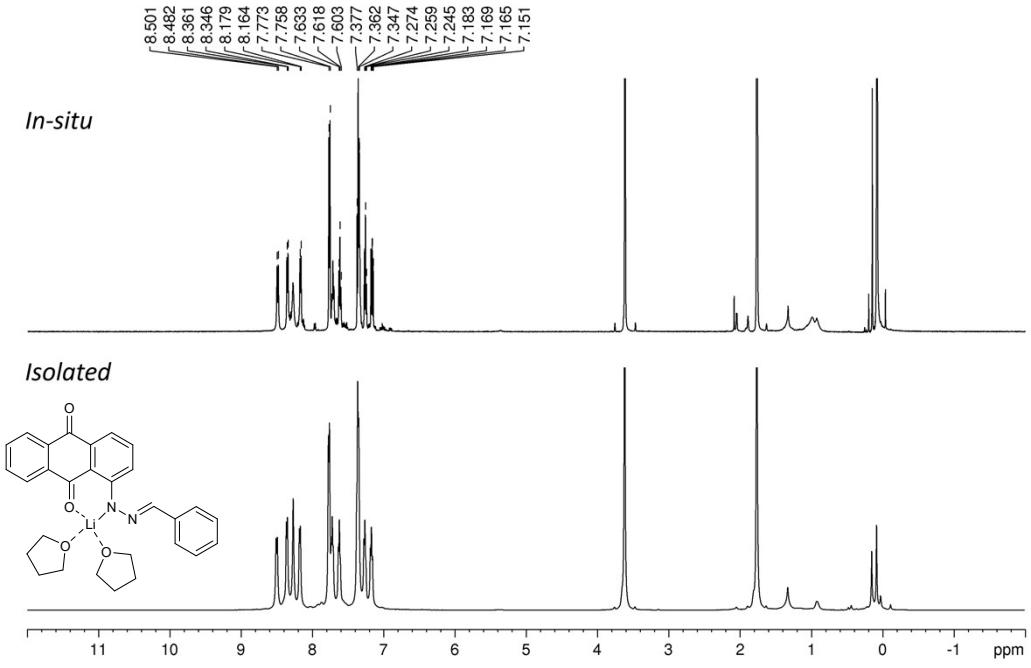

Figure S51. ^{1}H NMR (500.13 MHz, THF-d_8) spectrum of **2c (in-situ)** and **2c (isolated)**.

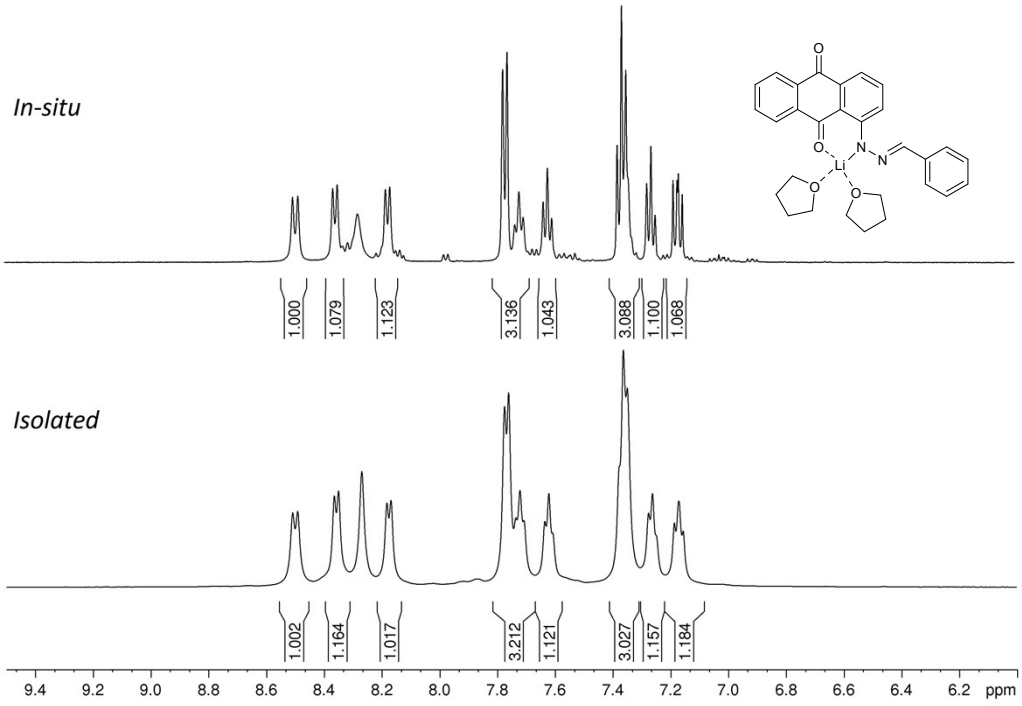

Figure S52. Expanded ^{1}H NMR (500.13 MHz, THF-d_8) spectrum of **2c (in-situ)** and **2c (isolated)**.

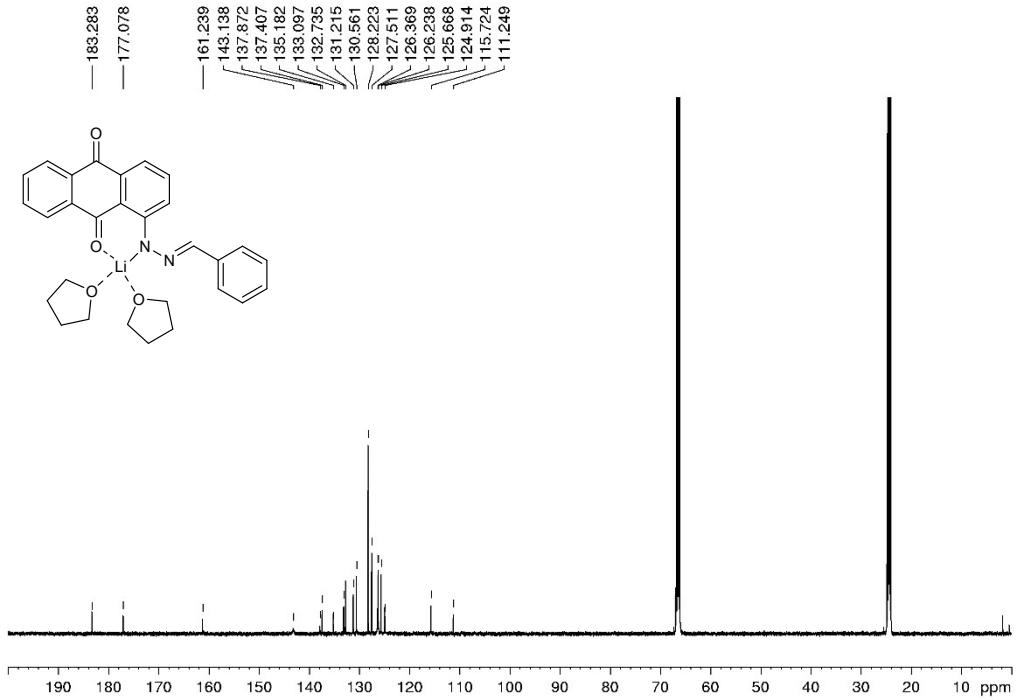

Figure S53. ^{13}C NMR (125.77 MHz, THF-d_8) spectrum of **2c**.

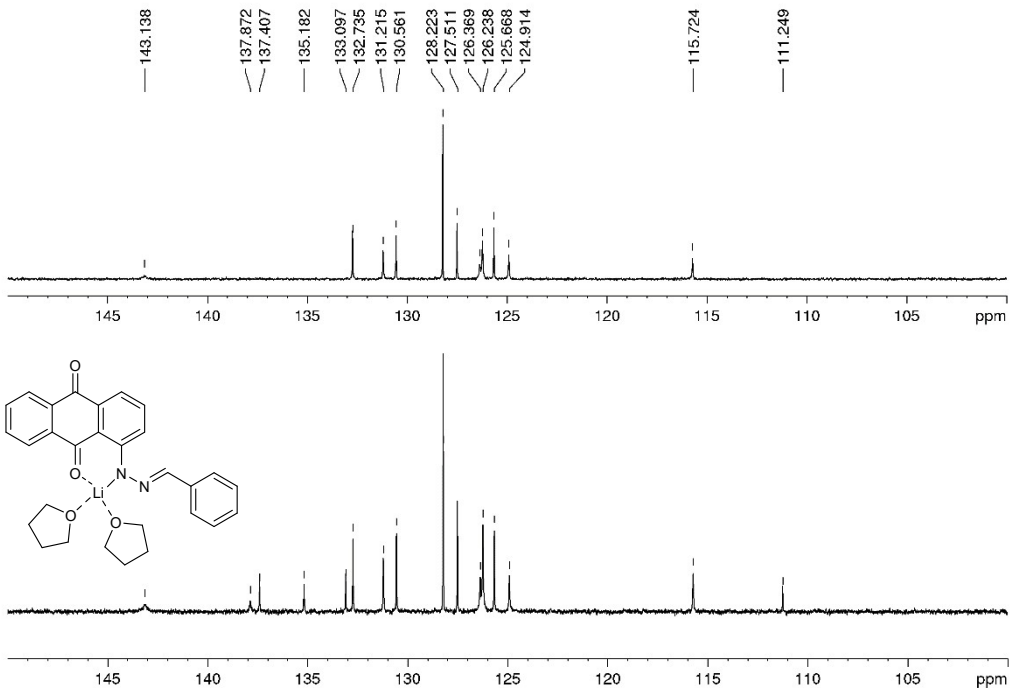

Figure S54. Expanded ^{13}C NMR (125.77 MHz, THF-d_8) and DEPT-135 spectrum of **2c**.

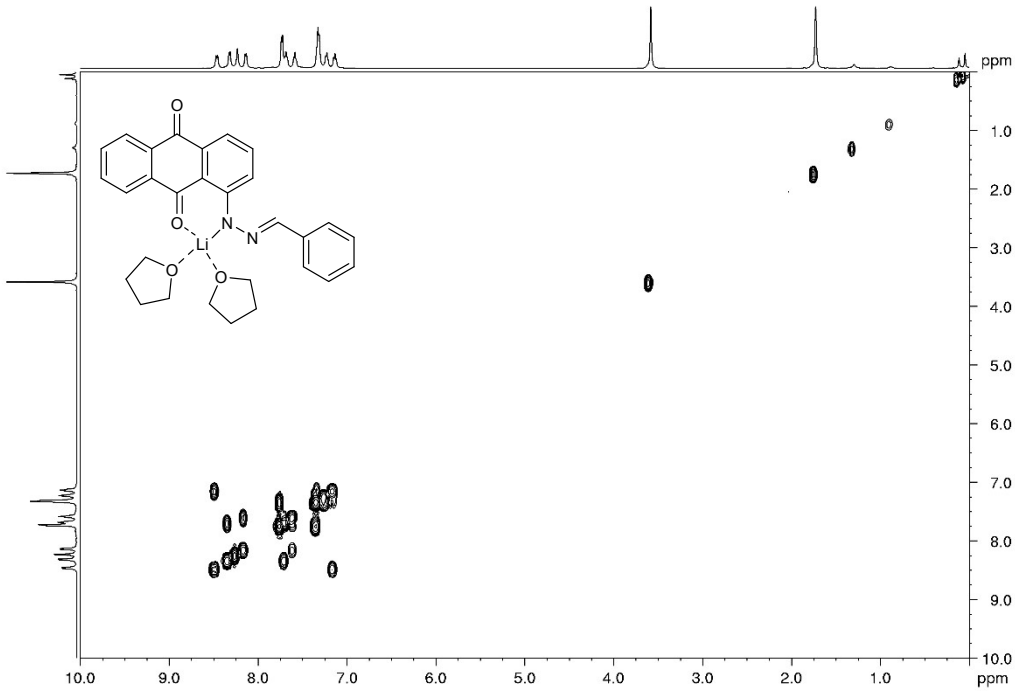

Figure S55. COSY spectrum of **2c**.

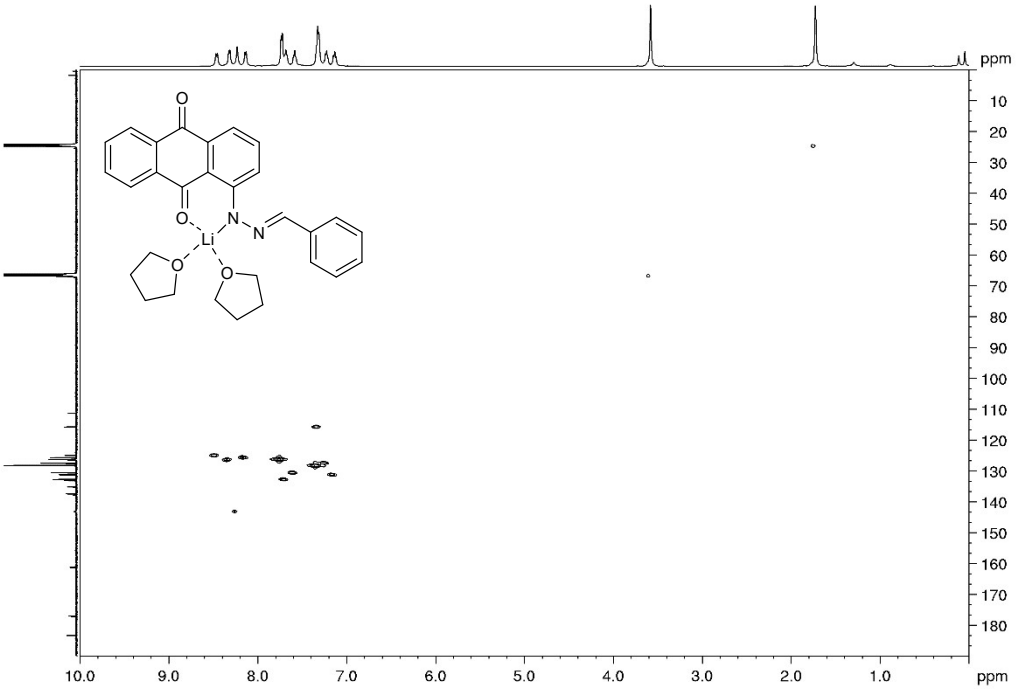

Figure S56. HMQC spectrum of **2c**.

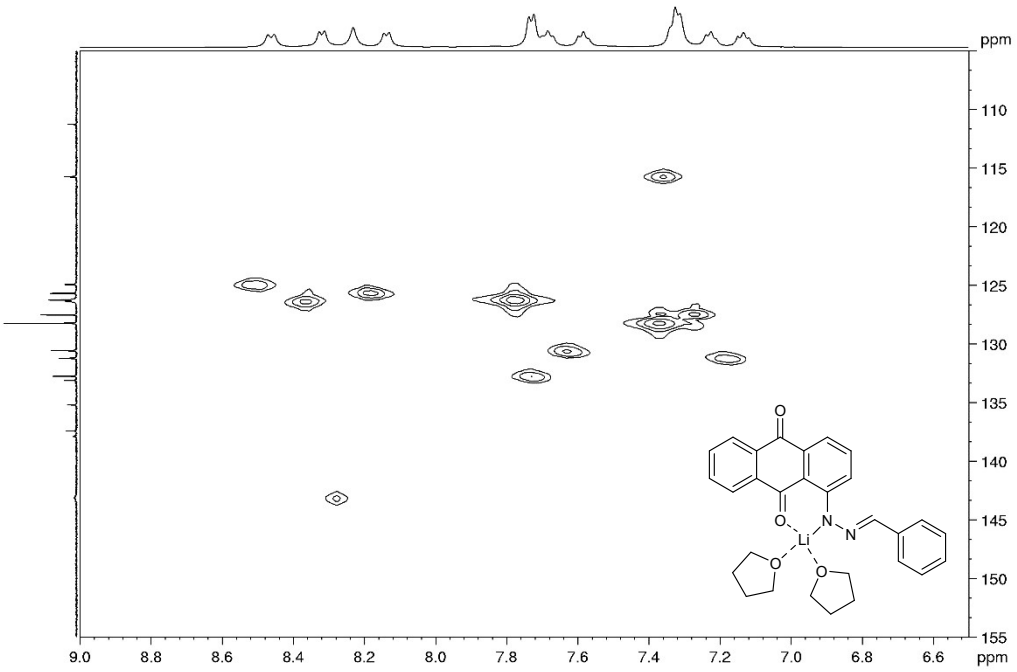

Figure S57. Expanded HMQC spectrum of **2c**.

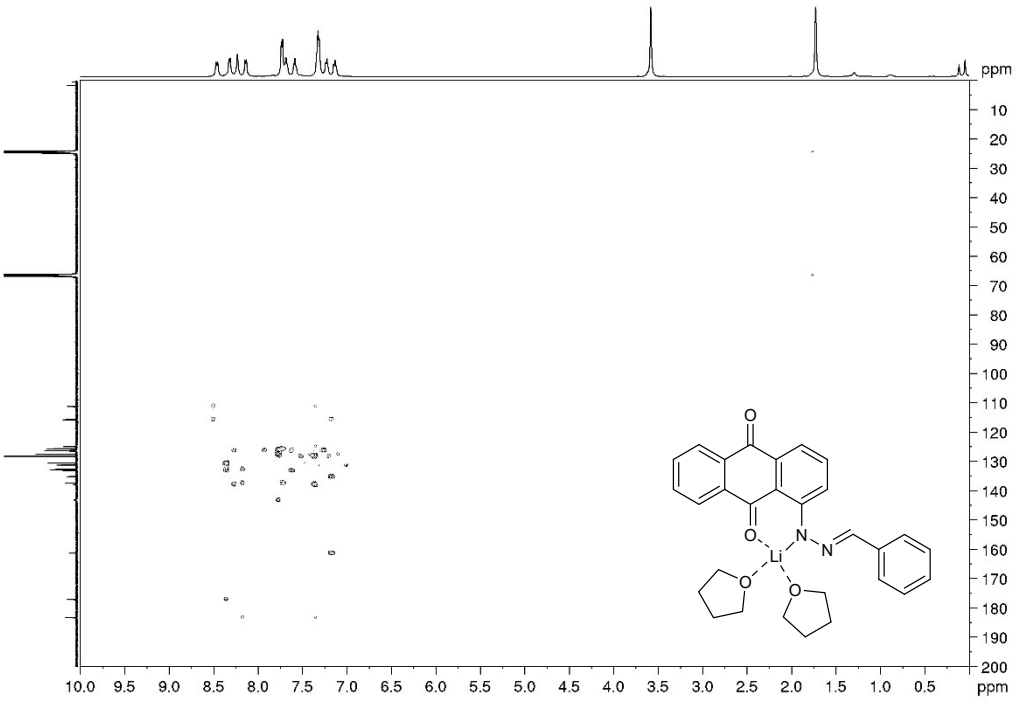

Figure S58. HMBC spectrum of **2c**.

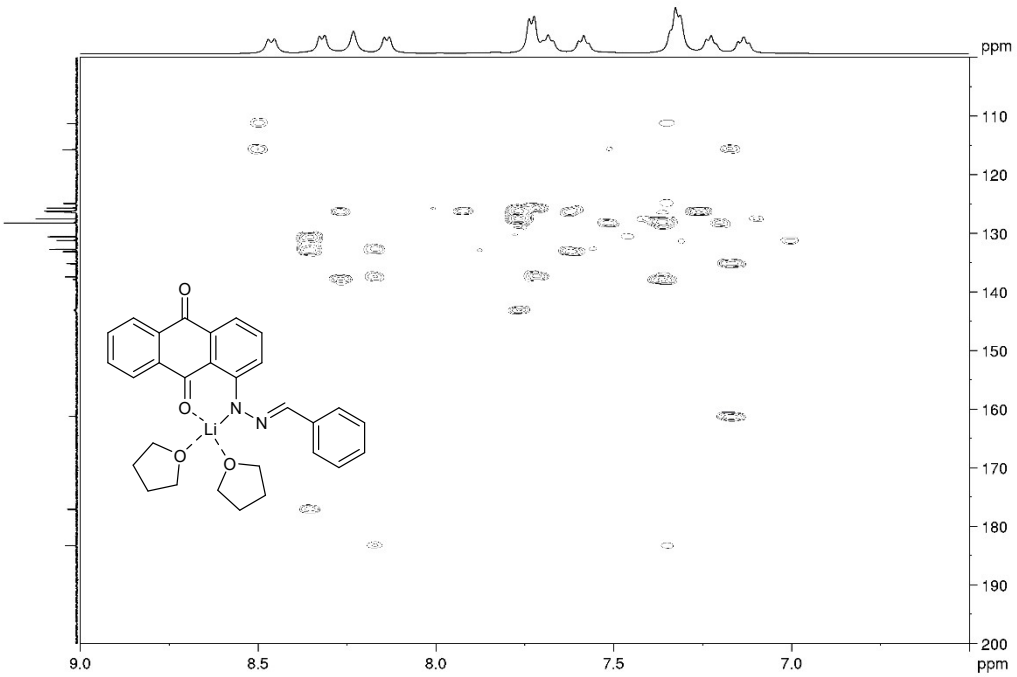

Figure S59. Expanded HMBC spectrum of **2c**.

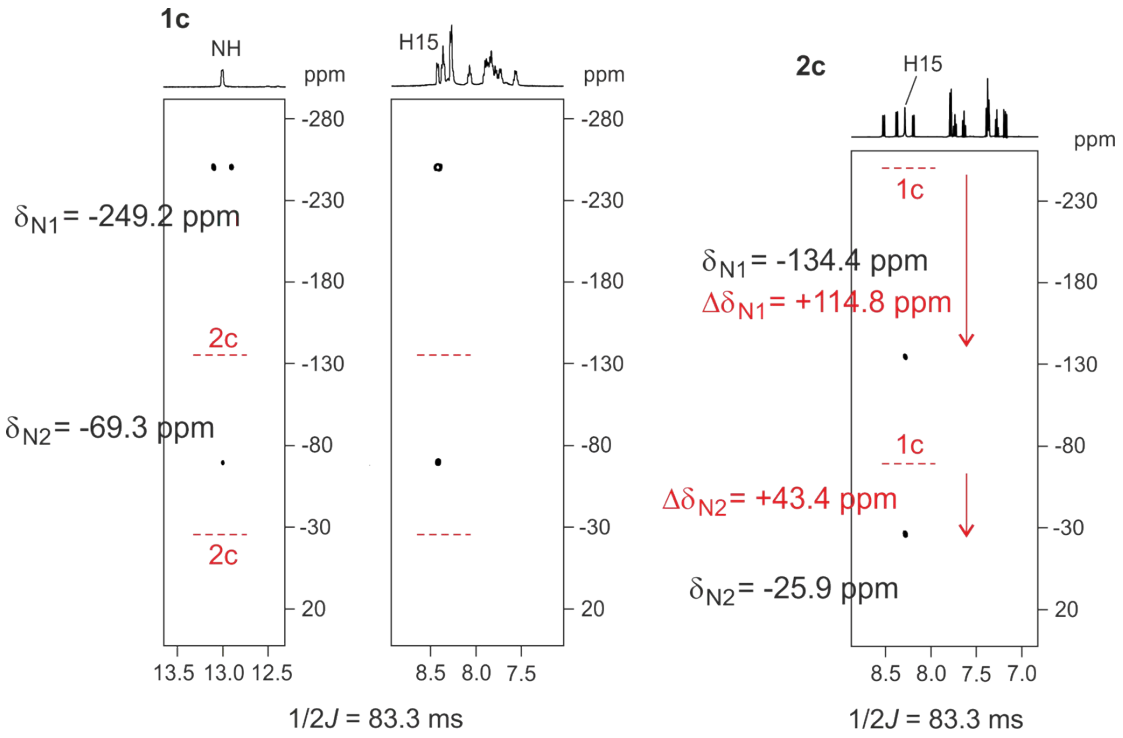

Figure S60. $^{1}H,^{15}N$ gHMBC spectrum of **1c** and **2c**.

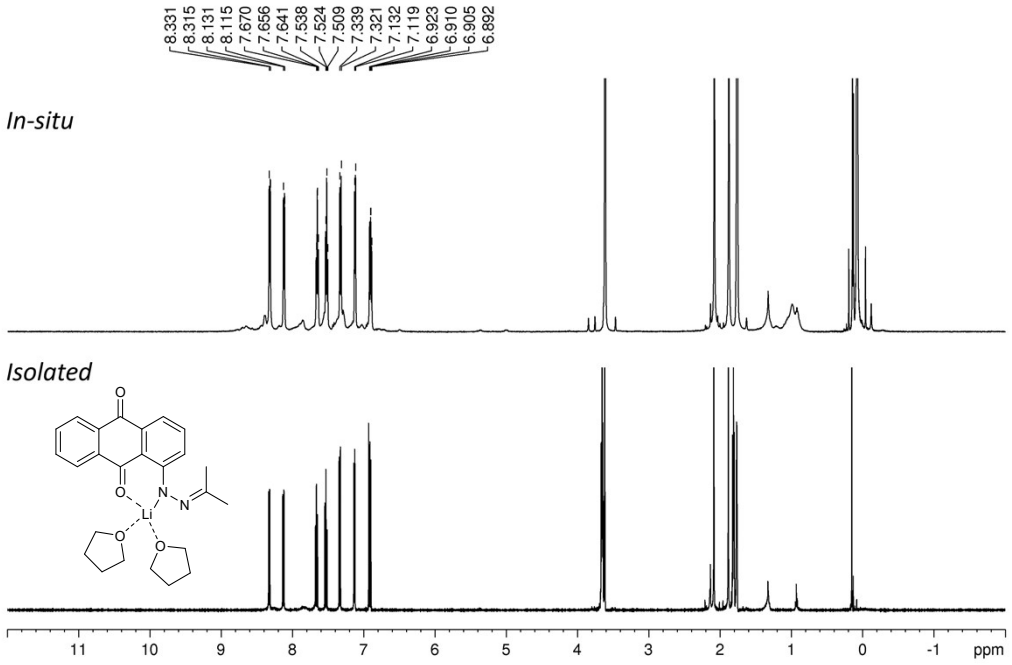

Figure S61. ^{1}H NMR (500.13 MHz, THF-d_8) spectrum of **2d (in-situ)** and **2d (isolated)**.

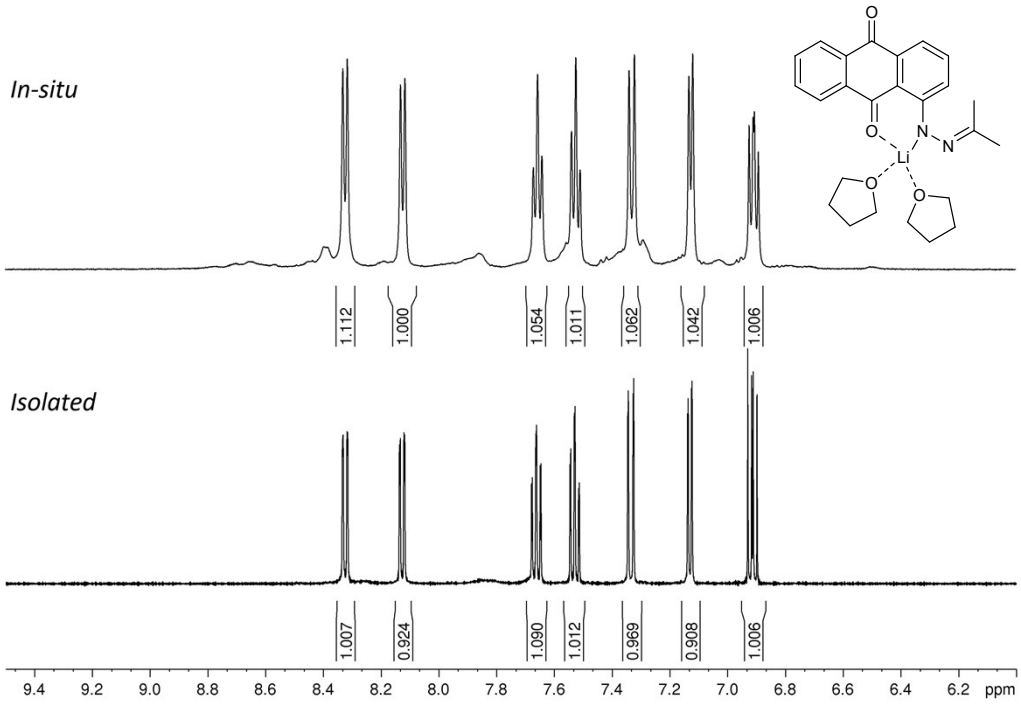

Figure S62.Expanded ^{1}H NMR (500.13 MHz, THF-d_8) spectrum of **2d (in-situ)** and **2d (isolated)**.

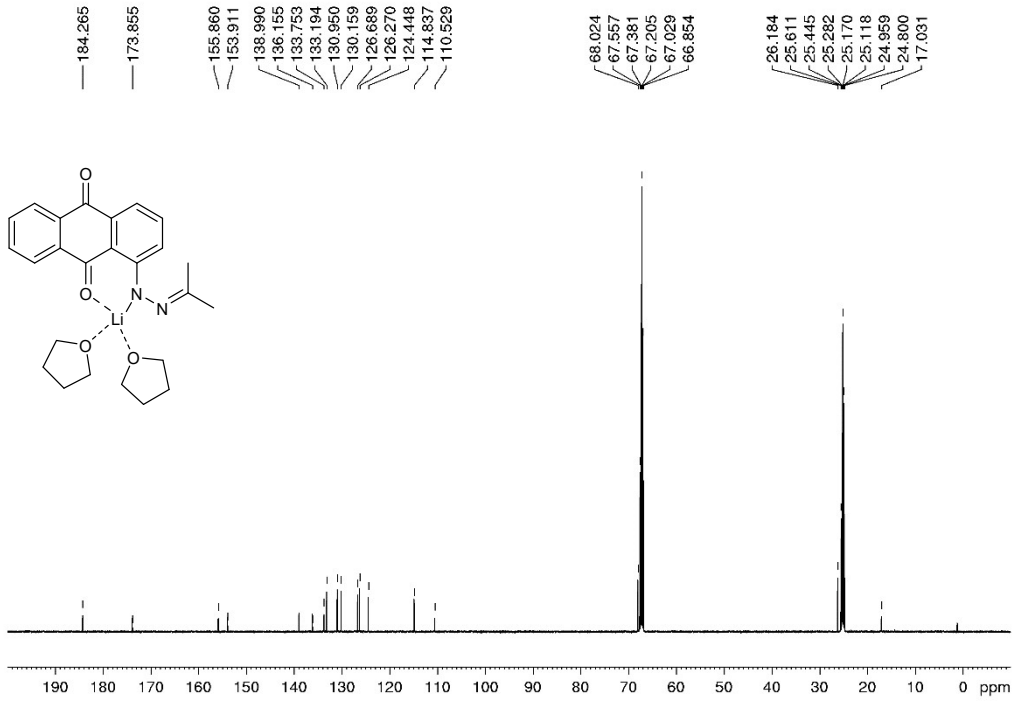

Figure S63. ^{13}C NMR (125.77 MHz, THF-d_8) spectrum of **2d**.

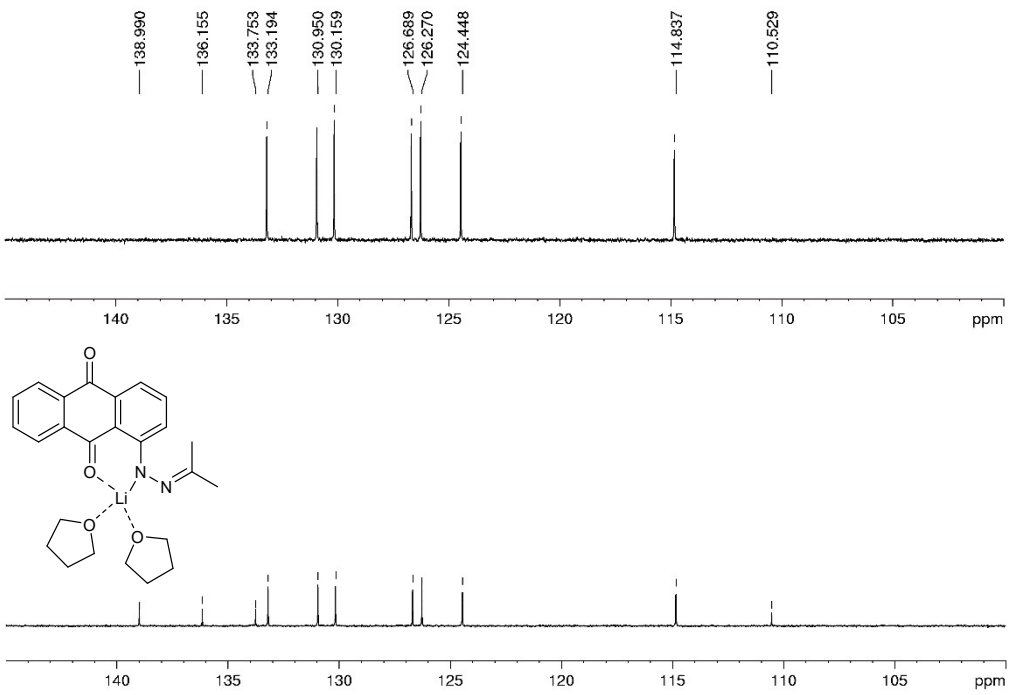

Figure S64. Expanded ^{13}C NMR (125.77 MHz, THF-d_8) and DEPT-135 spectrum of **2d**.

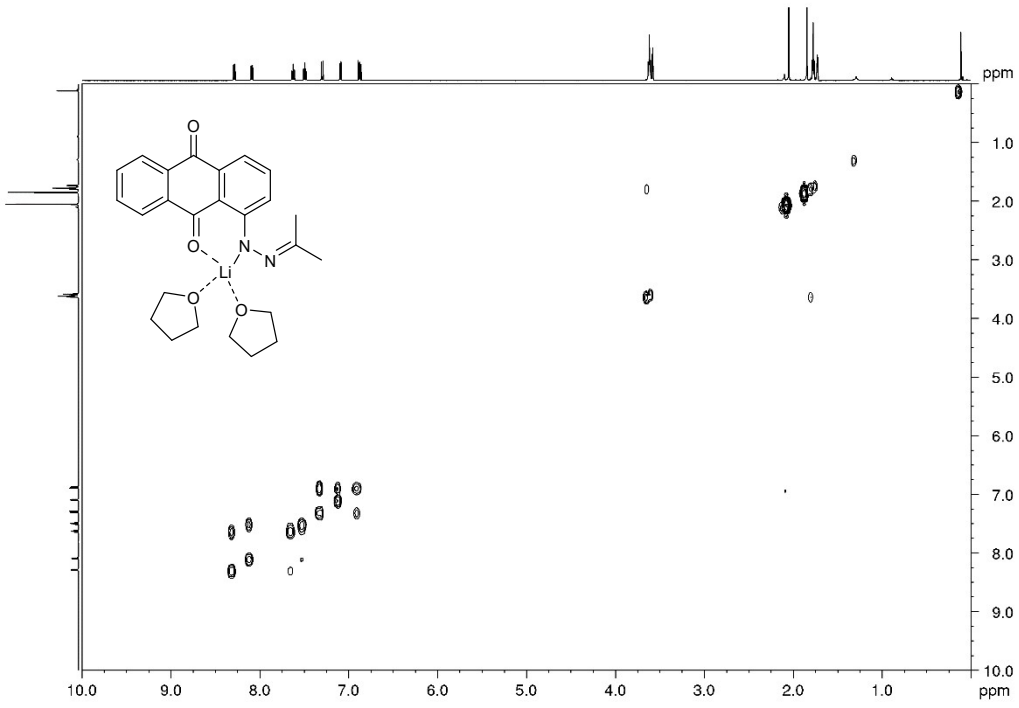

Figure S65. COSY spectrum of **2d**.

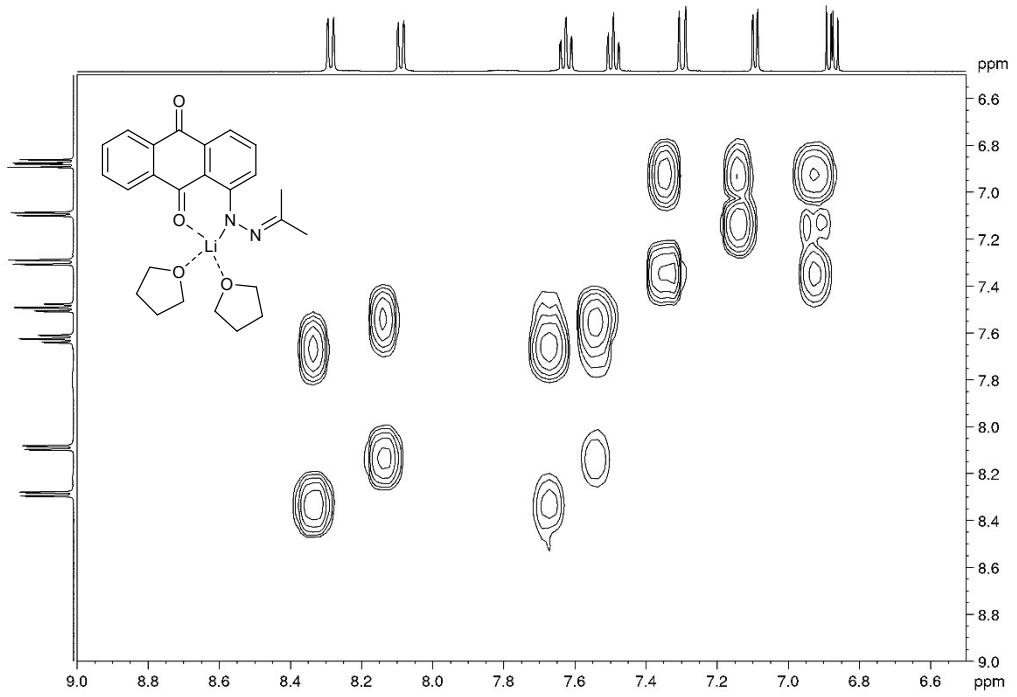

Figure S66. Expanded COSY spectrum of **2d**.

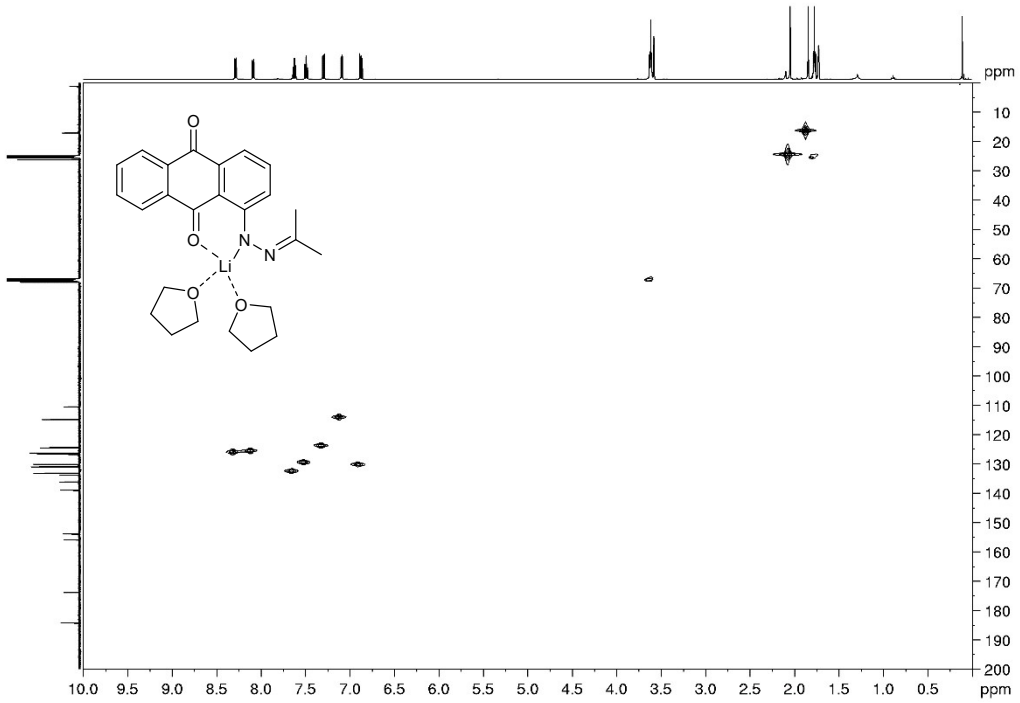

Figure S67. HMQC spectrum of **2d**.

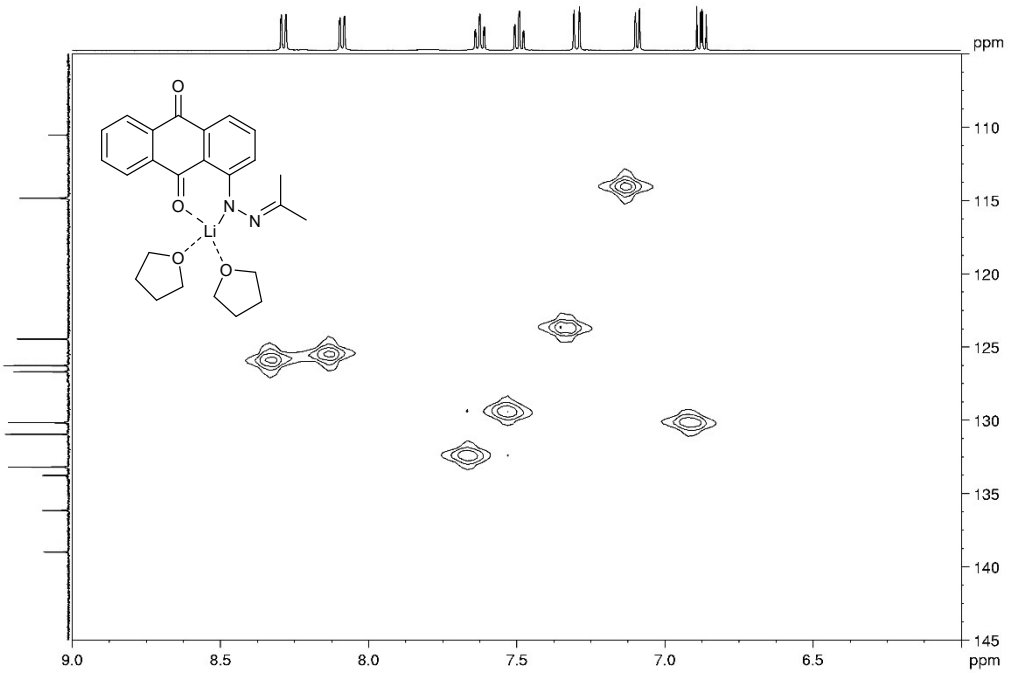

Figure S68. Expanded HMQC spectrum of **2d**.

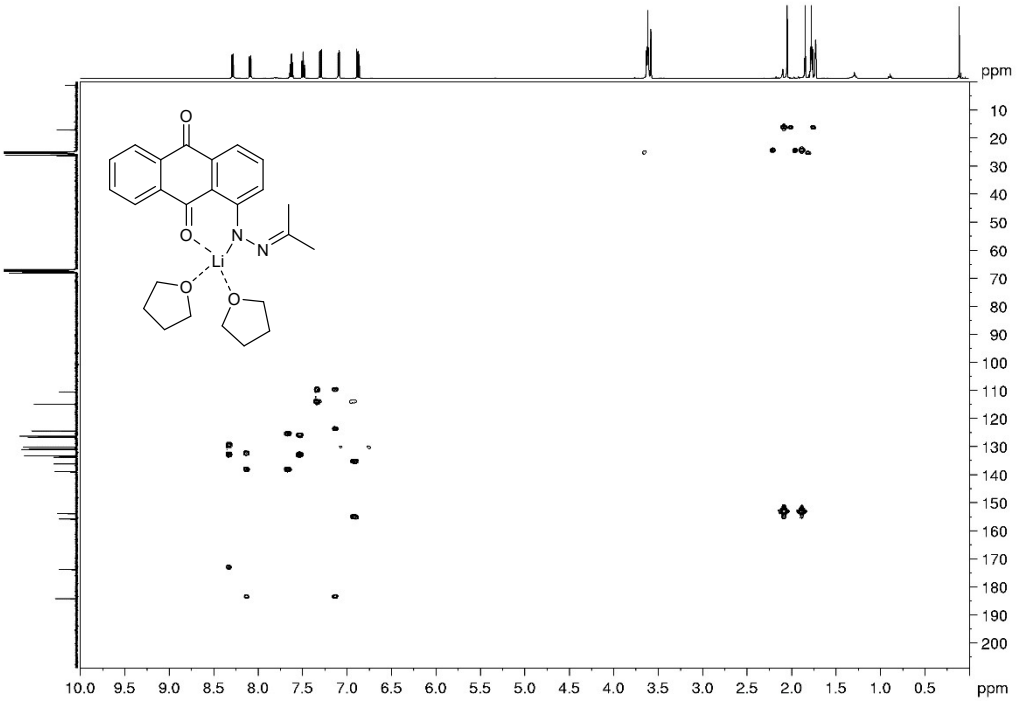

Figure S69. HMBC spectrum of **2d**.

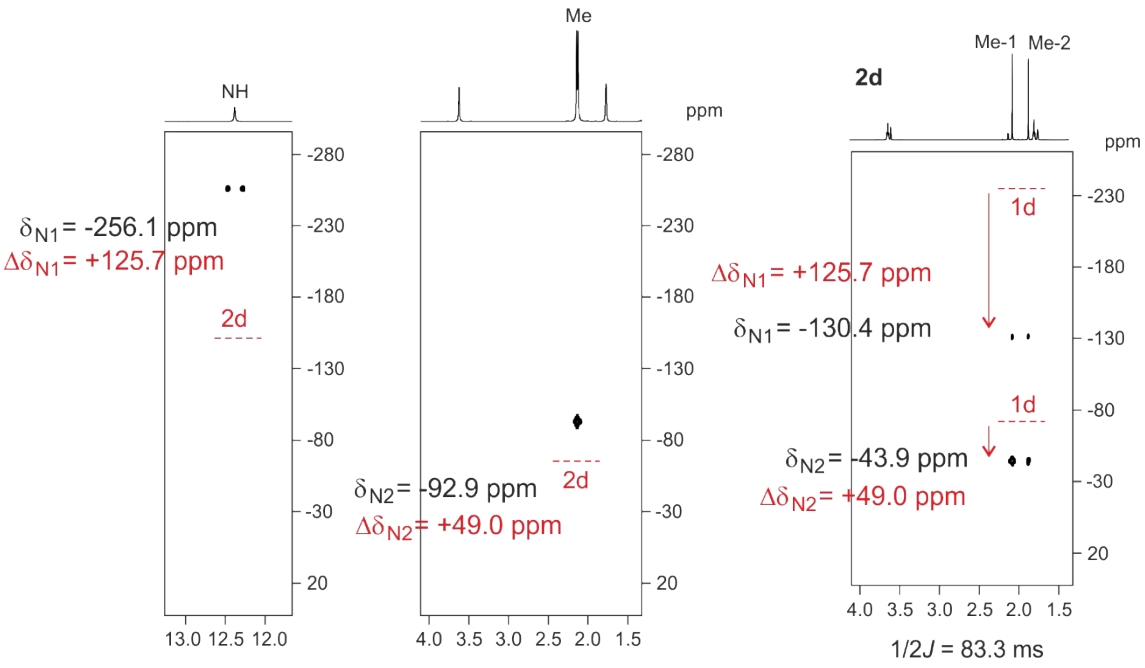

Figure S70. $^{1}H,^{15}N$ gHMBC spectrum of **1d** and **2d**.

9. IR Spectra

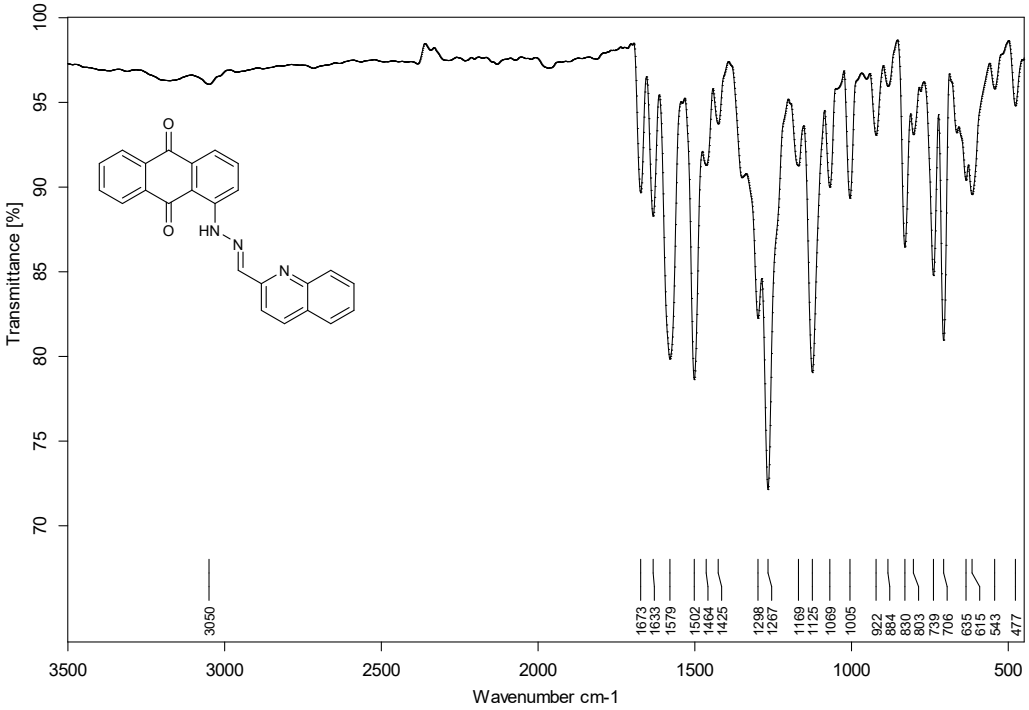

Figure S71. IR (ATR) spectrum of **1b**.

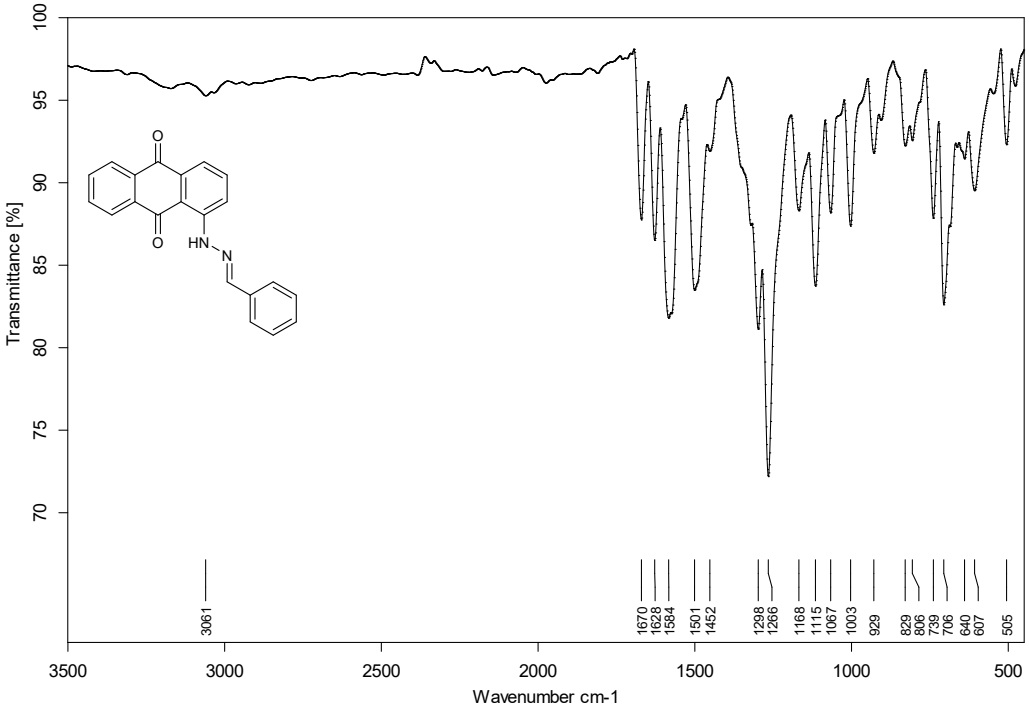

Figure S72. IR (ATR) spectrum of **1c**.

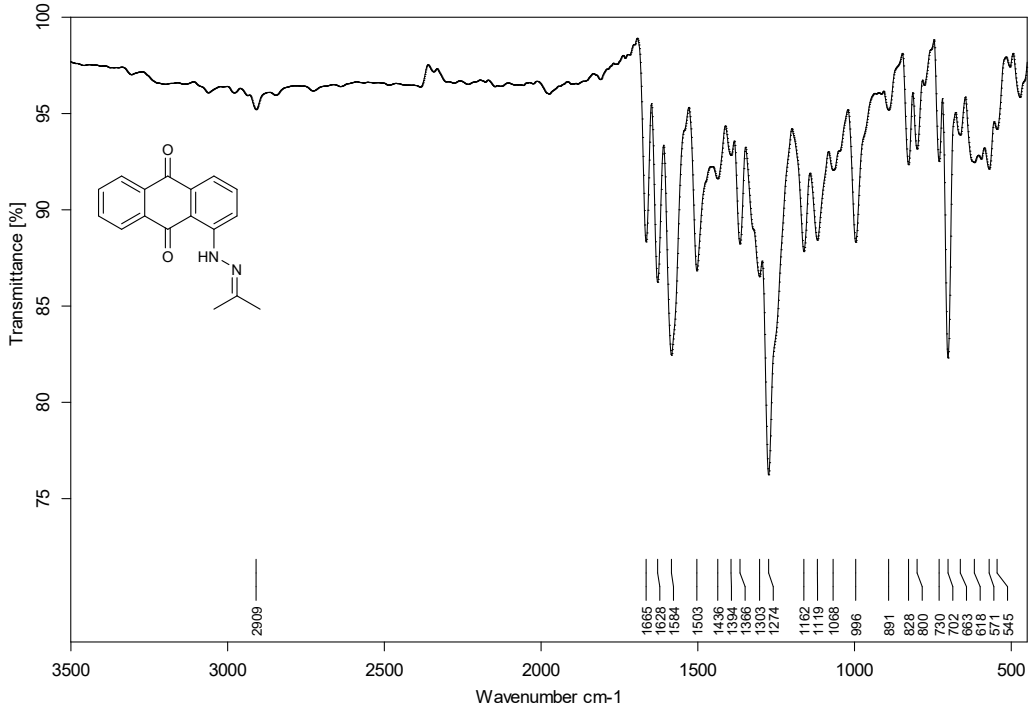

Figure S73. IR (ATR) spectrum of **1d**.

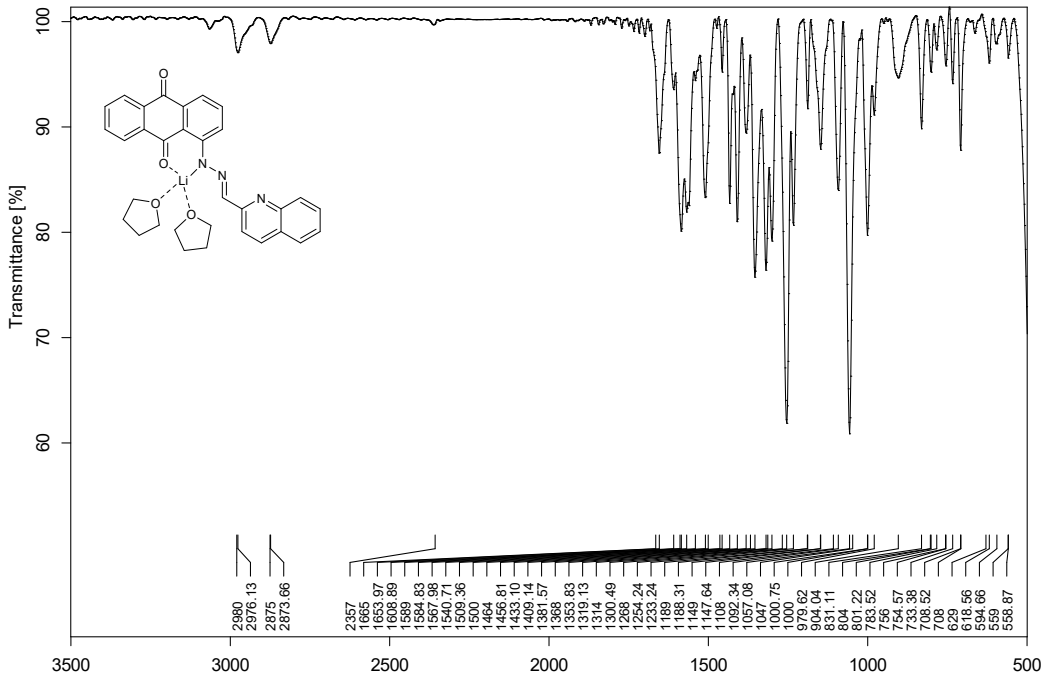

Figure S74. IR (THF solution) spectrum of **2b**.

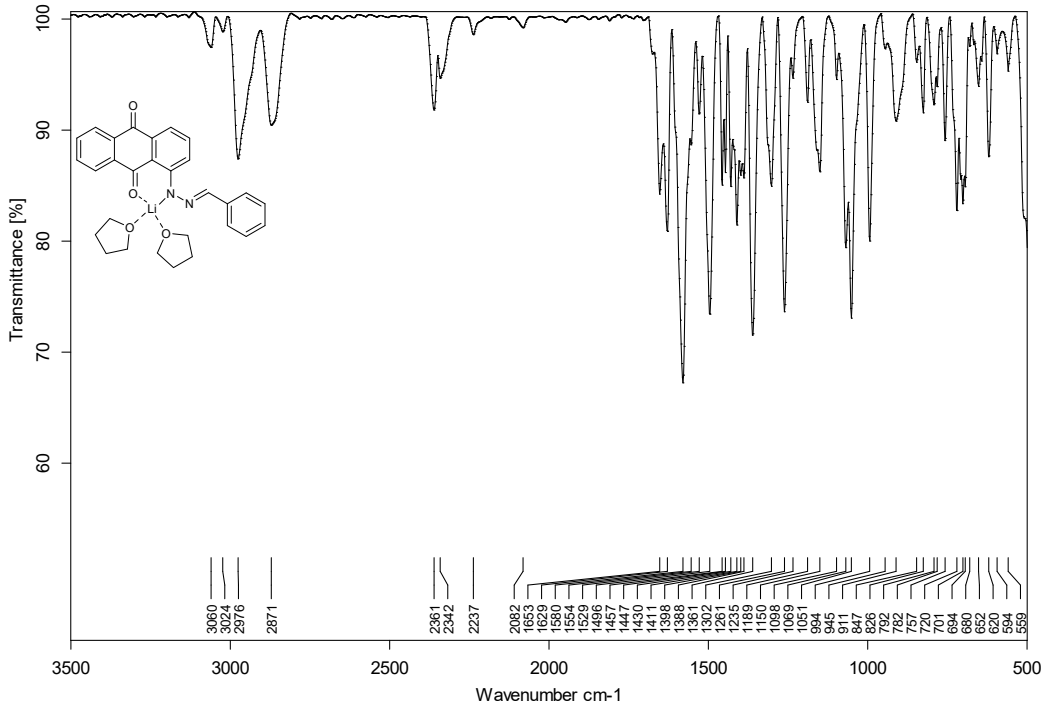

Figure S75. IR (THF solution) spectrum of **2c**.

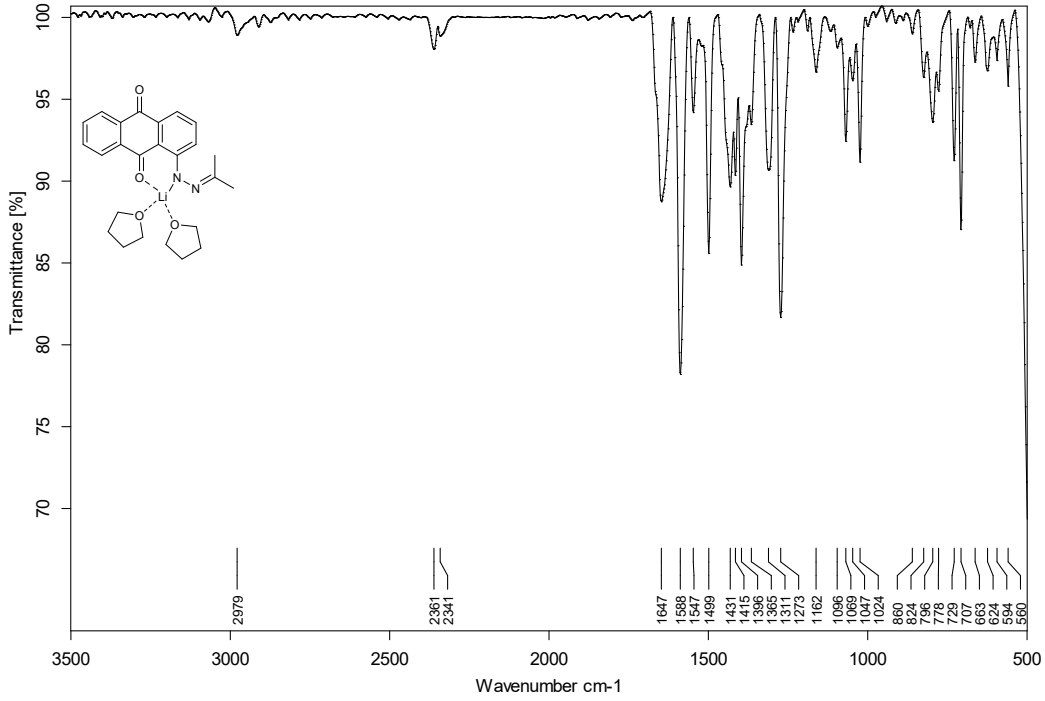

Figure S76. IR (THF solution) spectrum of **2d**.

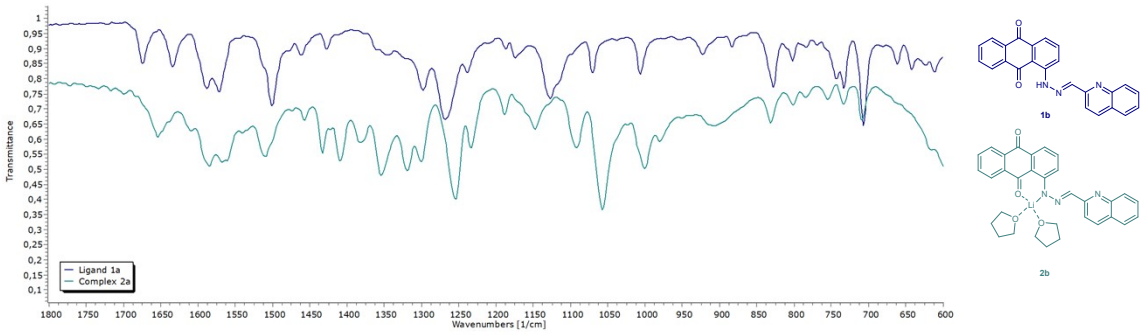

Figure S77. IR spectra comparation between ligand **1b** and Lithium complex **2b**.

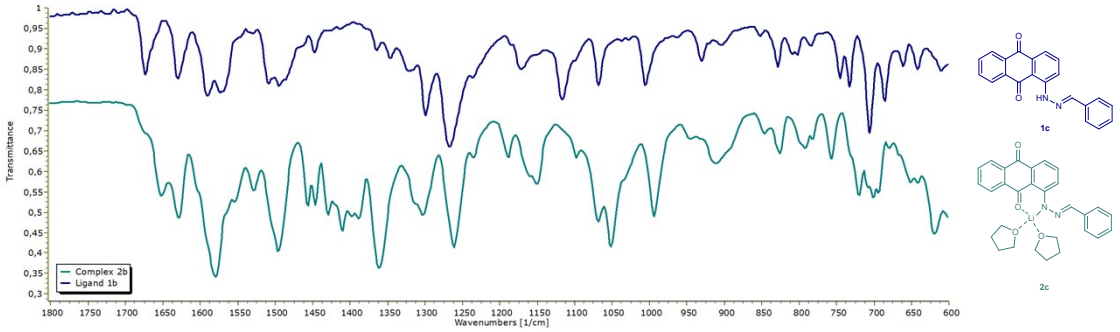

Figure S78. IR spectra comparation between ligand **1c** and Lithium complex **2c**.

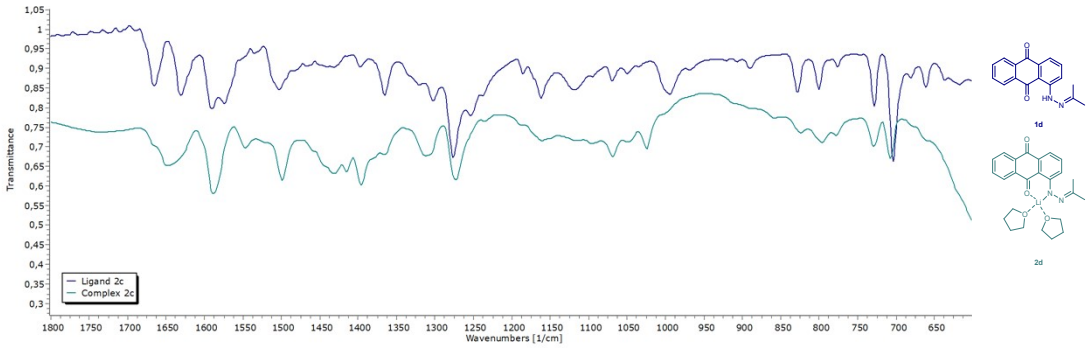

Figure S79. IR spectra comparation between ligand **1d** and Lithium complex **2d**.

10. ESI-MS data

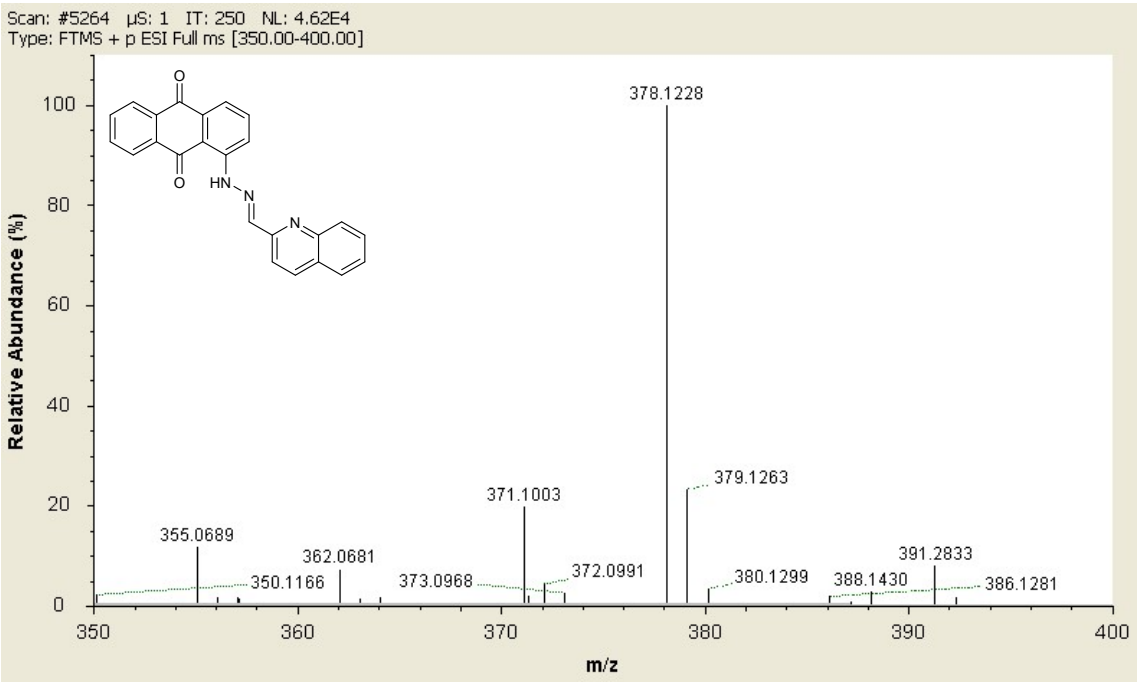

Figure S80. ESI-MS spectrum obtained for compound **1b**.

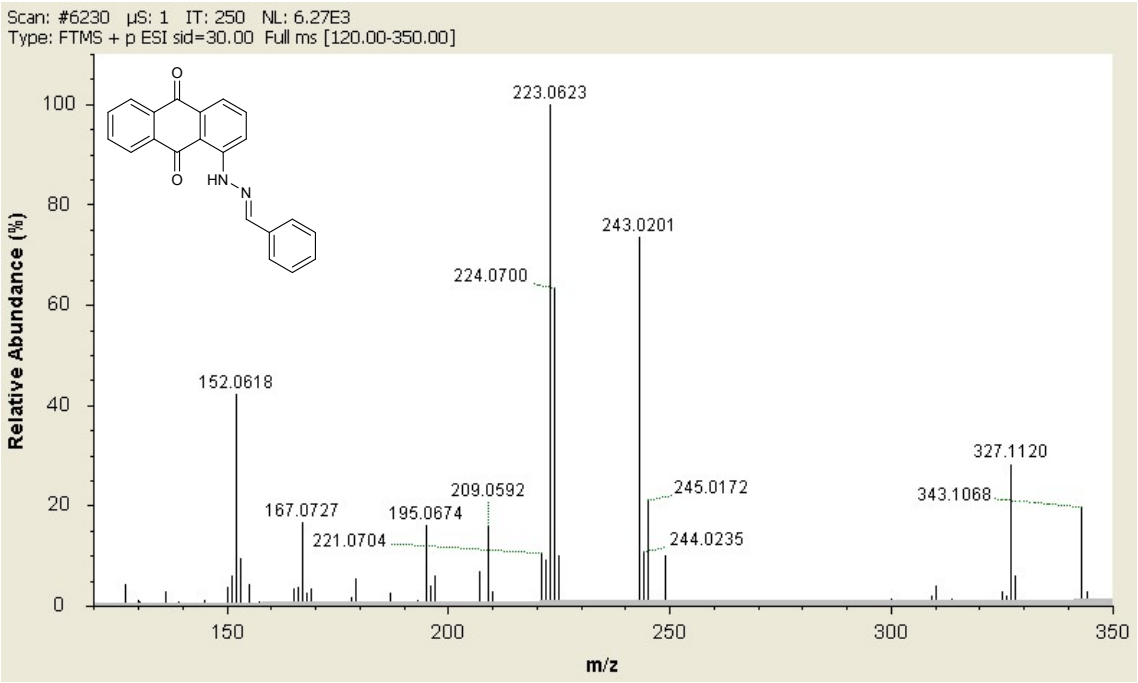

Figure S81. ESI-MS spectrum obtained for compound **1c**.

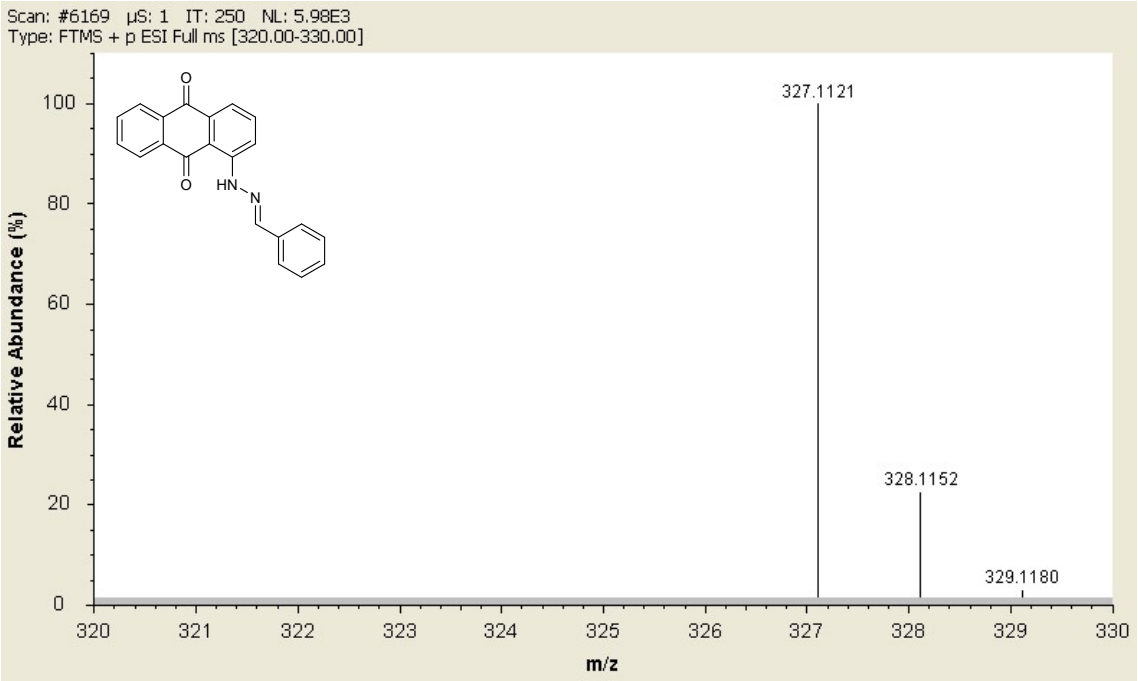

Figure S82. Expanded ESI-MS spectrum obtained for compound **1c**.

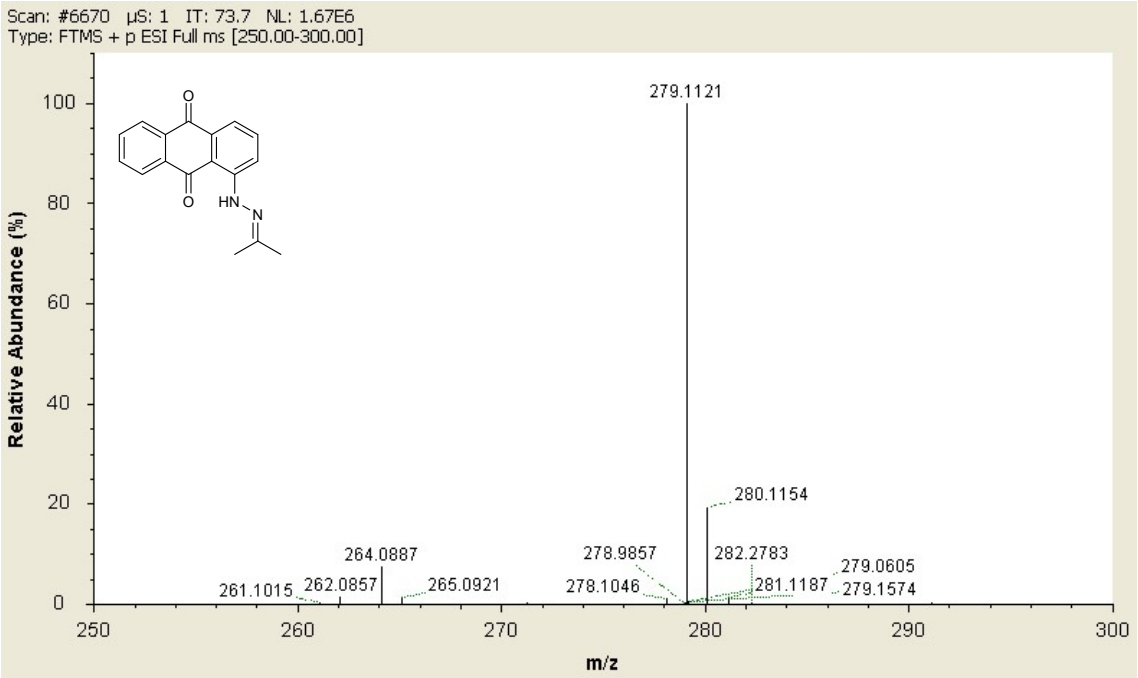

Figure S83. ESI-MS spectrum obtained for compound **1d**.

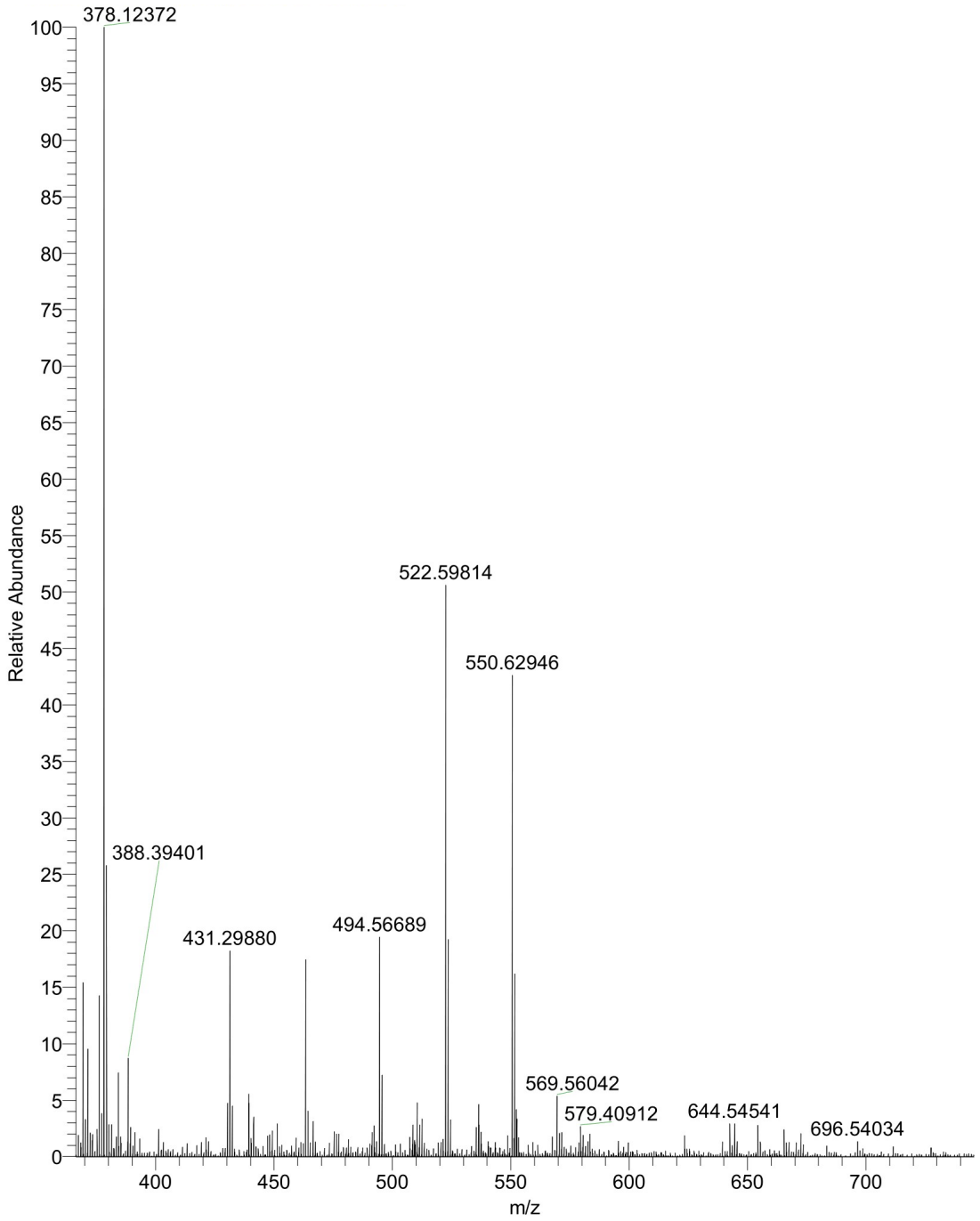

Figure S84. ESI-MS spectrum obtained for compound **2b**. Due to the presence of humidity during the introduction of the sample into the ionizer, the spectrum presents lower abundance of the parent peak compared to the adducts.

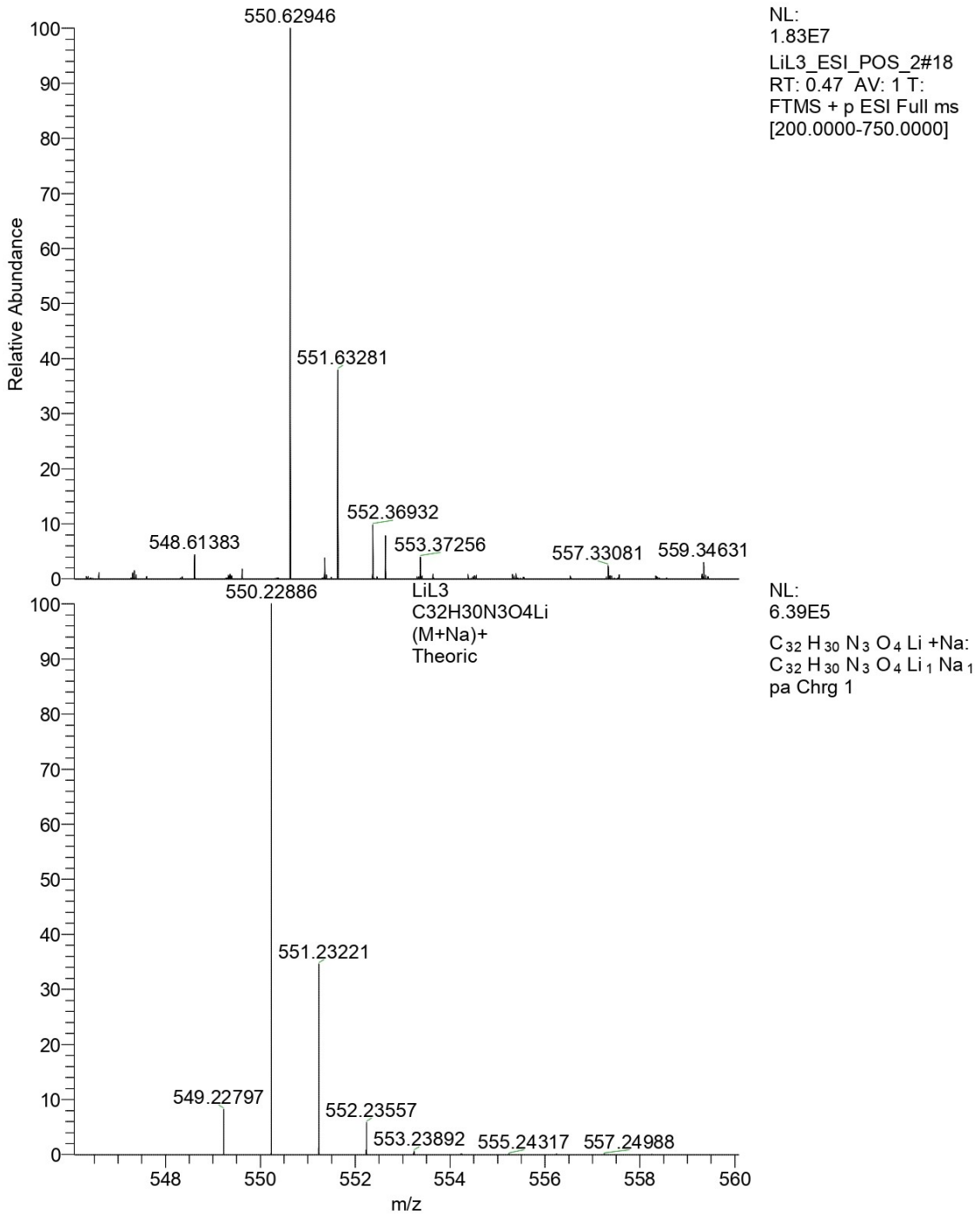

Figure S85. Expanded ESI-MS spectrum obtained for compound **2b** and theoretical $(M+Na)^+$ adduct.

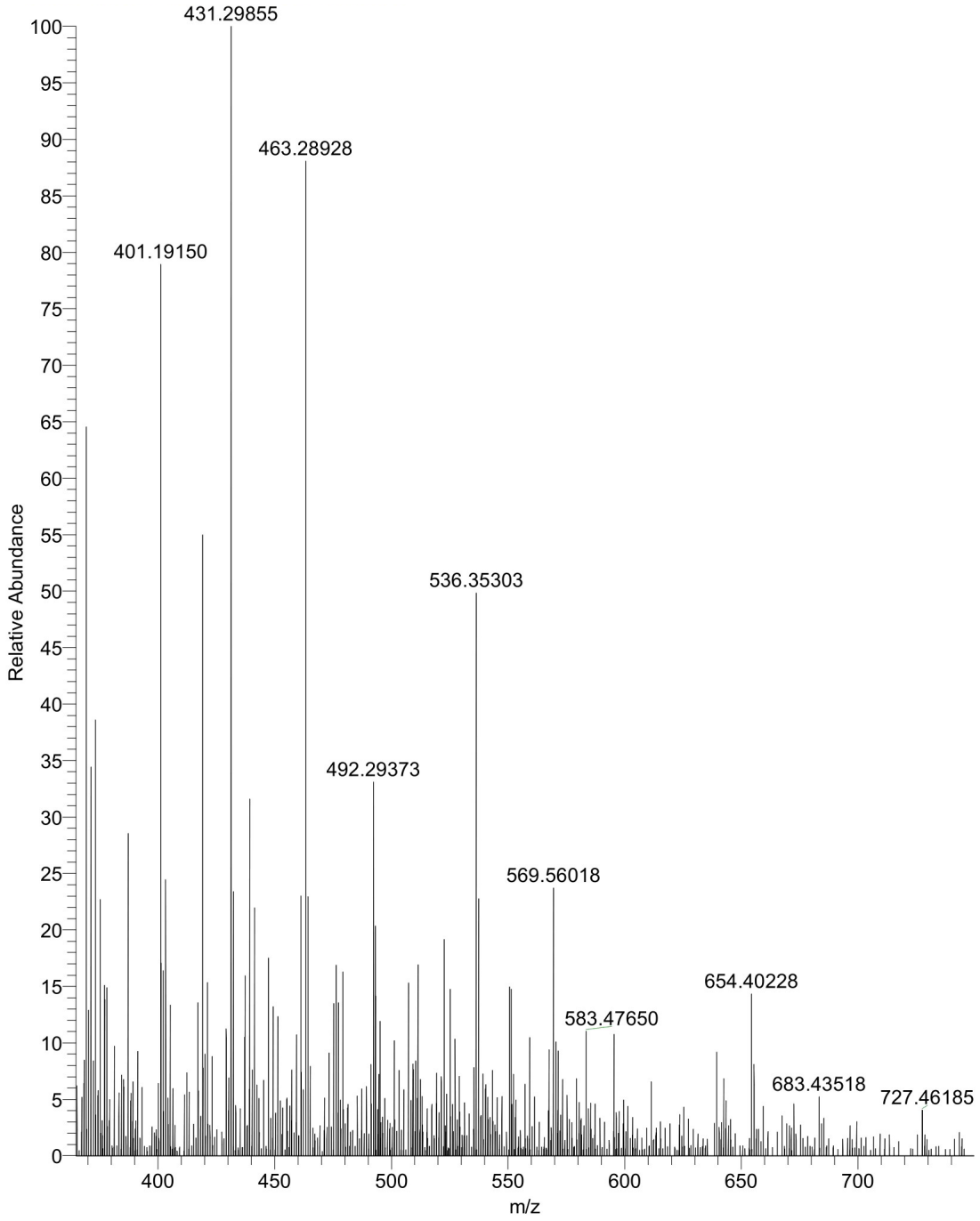

Figure S86. ESI-MS spectrum obtained for compound **2c**. Due to the presence of humidity during the introduction of the sample into the ionizer, the spectrum presents lower abundance of the parent peak compared to the adducts.

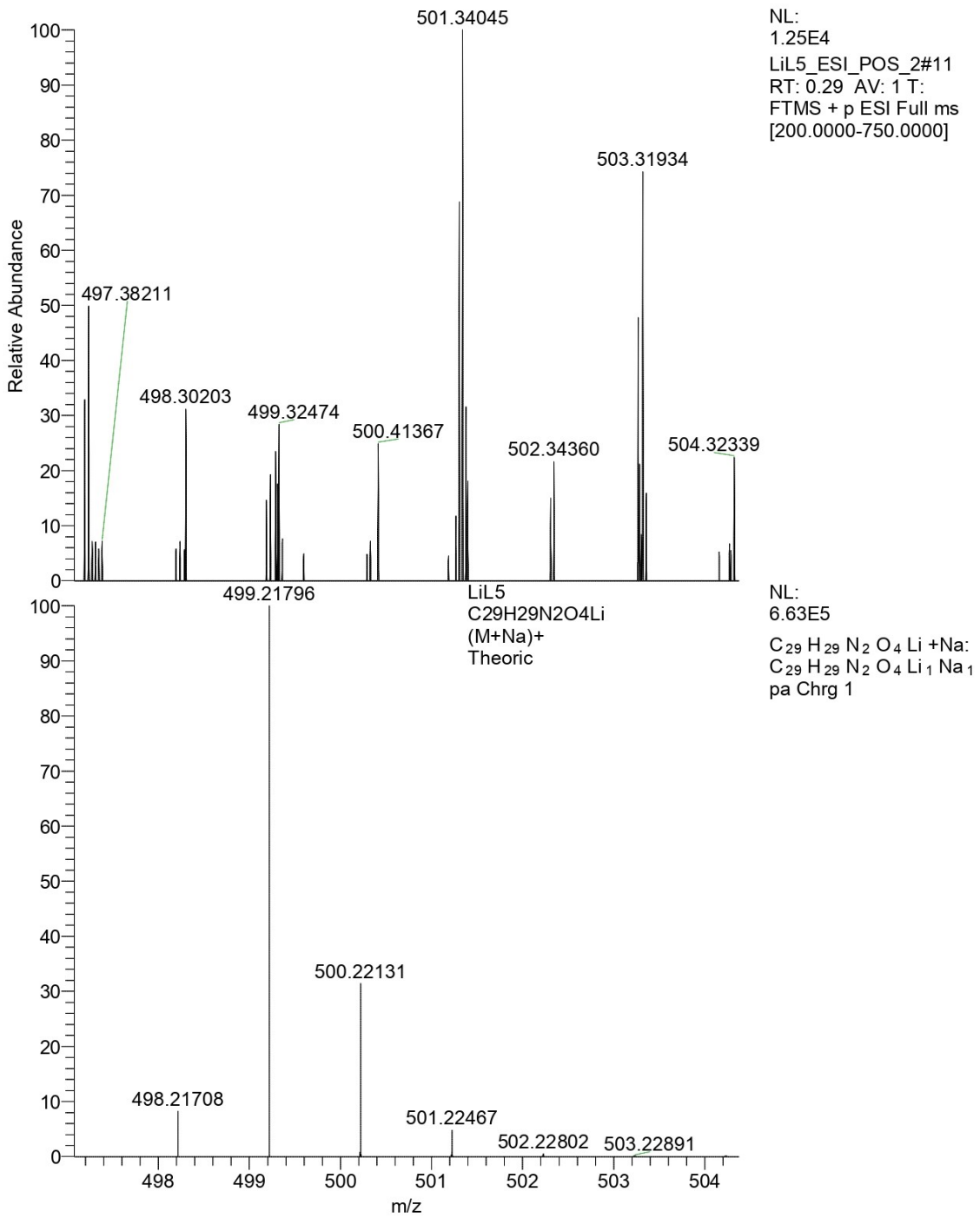

Figure S87..Expanded ESI-MS spectrum obtained for compound **2c** and theoretical $(M+Na)^+$ adduct.

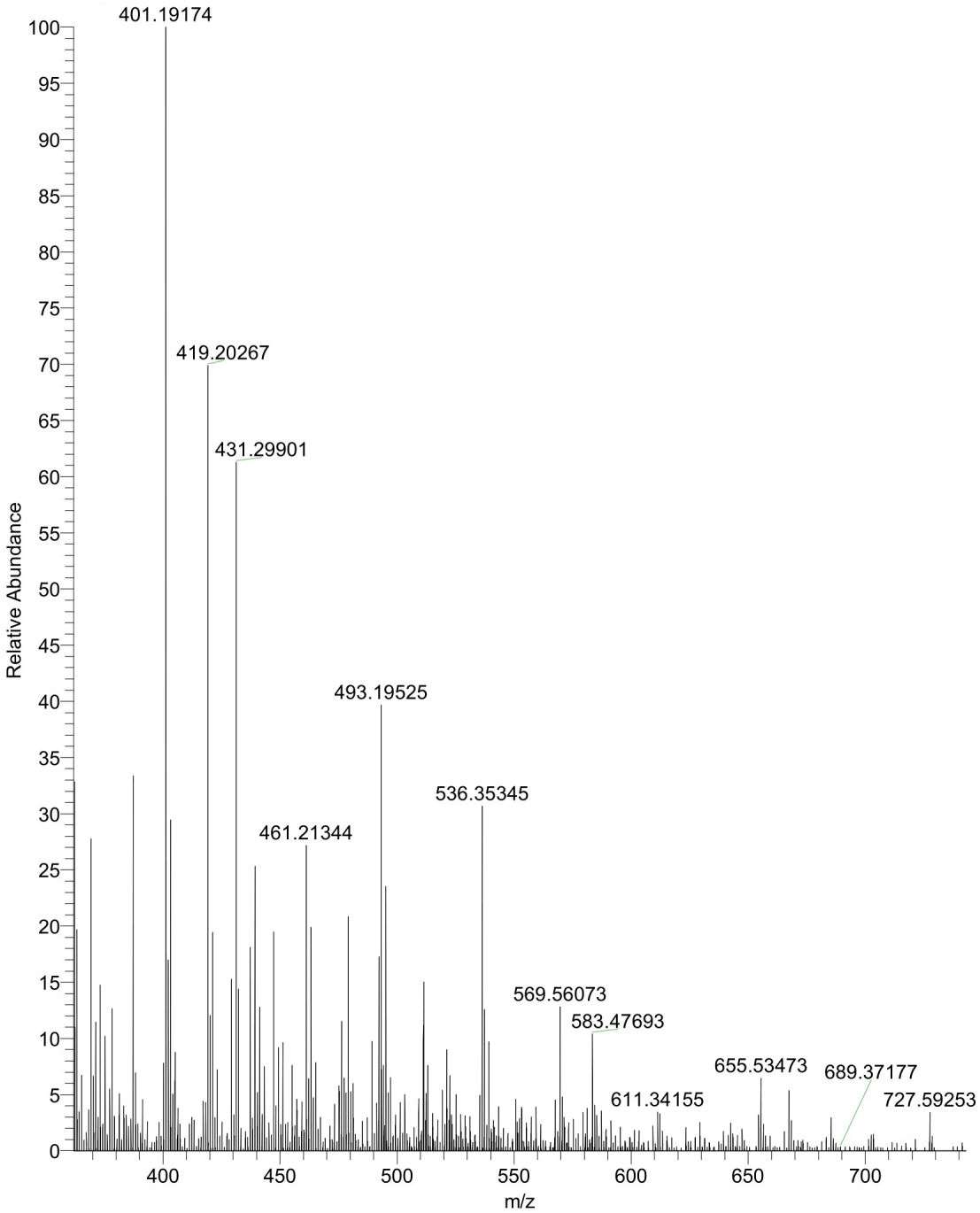

Figure S88. ESI-MS spectrum obtained for compound **2d**. Due to the presence of humidity during the introduction of the sample into the ionizer, the spectrum presents lower abundance of the parent peak compared to the adducts.

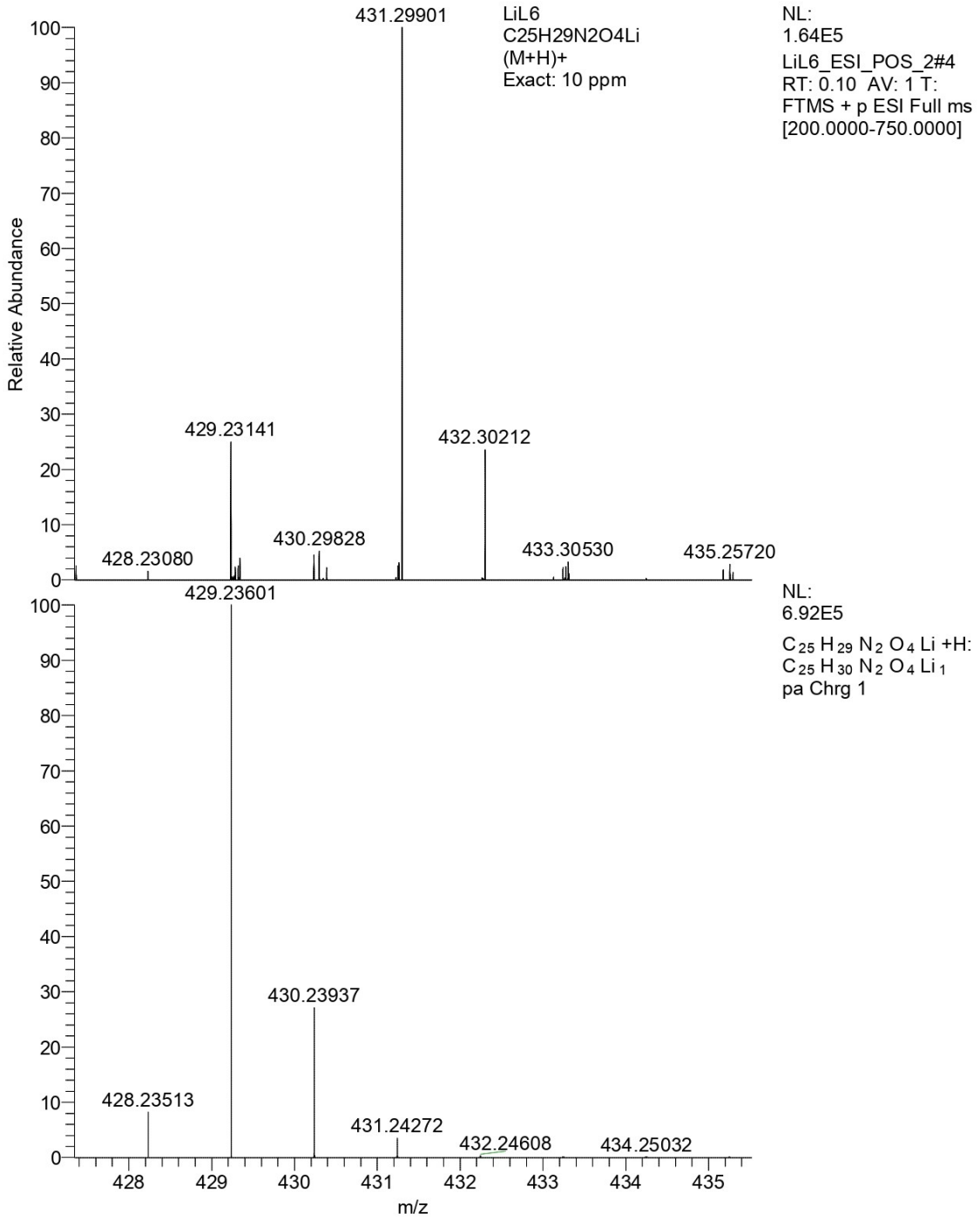

Figure S89. Expanded ESI-MS spectrum obtained for compound **2d** and theoretical $(M+H)^+$ adduct.

11. Results of polymerization reactions

Table S6. ^{1}H and ^{13}C NMR intensities (%) of tetrad fractions calculated via signal deconvolution of the methine signal ([M]/[Cat] ratio of 50:1 in **DCM**).

	rmr *(sis)*	***rmm*** *(sii)*	***mmr*** *(iis)*	***mmm*** *(iii)* ***rrr*** *(sss)* ***rrm*** *(ssi)* ***mrr*** *(iss)*	***mrm*** *(isi)*	P_m
Tacticity[a]	ht	sb it	sb it	it	ht	
δ_H *(ppm)*	5.23	5.22	5.18	5.17	5.16	
*L-/**LiHMDS***	-	-	-	100	-	0.0
*L-/**2a***	-	-	-	100	-	0.0
*L-/**2b***	-	-	-	100	-	0.0
*L-/**2c***	-	-	-	100	-	0.0
*L-/**2d***	-	-	-	100	-	0.0
*rac-/**LiHMDS***	17.0	13.1	11.8	27.3	30.8	**0.27**
*rac-/**2a***	12.2	16.1	12.2	29.7	29.9	**0.30**
rac-/***2b***	15.4	14.3	10.2	27.0	33.2	**0.27**
rac-/***2c***	13.1	15.0	10.7	29.2	32.1	**0.29**
rac-/***2d***	13.0	15.4	10.2	28.3	33.1	**0.28**

	mrr *(iss)*	***rrr*** *(sss)*	***mrm*** *(isi)*	***rrm*** *(ssi)*	***mmm*** *(iii)* ***rmm*** *(sii)* ***mmr*** *(iis)* ***rmr*** *(sis)*
δ_C *(ppm)*	69.4	69.3	69.2	69.1	69.0
*L-/**LiHMDS***					
*L-/**2a***					
*L-/**2b***	-	-	-	-	100
*L-/**2c***	-	-	-	-	100
*L-/**2d***	-	-	-	-	100
*rac-/**LiHMDS***	6.5	1.8	23.2	3.4	65.1
*rac-/**2a***	6.7	1.9	20.8	3.9	66.7
rac-/***2b***	7.2	9.3	22.9	4.5	63.0
rac-/***2c***	7.9	1.8	20.0	4.5	65.8
rac-/***2d***	7.9	1.8	20.5	4.7	65.1

[a] ht = heterotactic; sb it = stereoblock isotactic; it = isotactic.

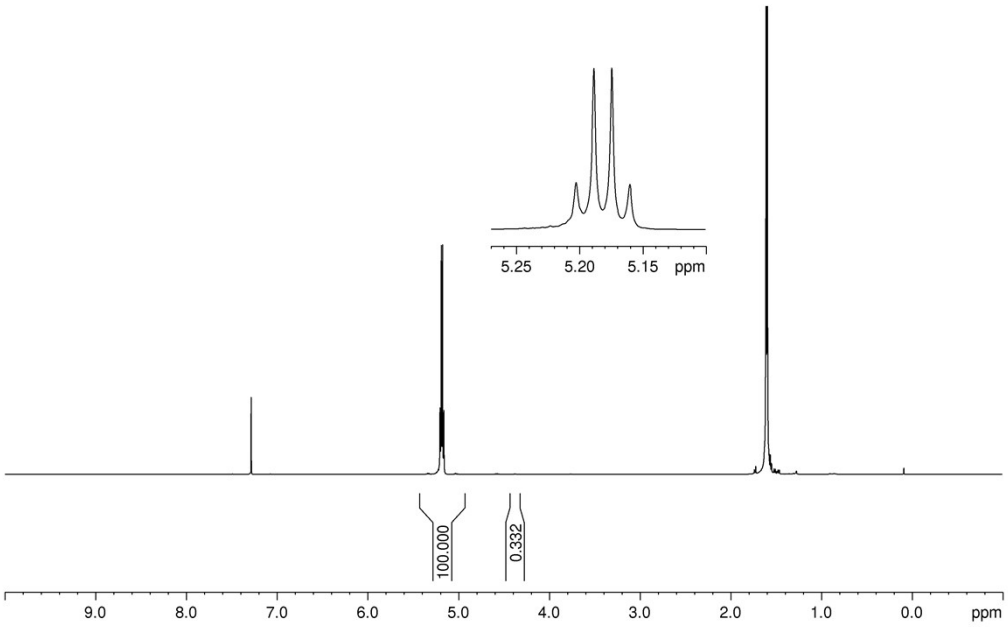

Figure S90. ^{1}H NMR spectrum (500.13 MHz, $CDCl_3$) of cyclic *L*-PLA obtained with **2b** at 50:1 $[LA]_0/[Cat]$ ratio in DCM at room temperature.

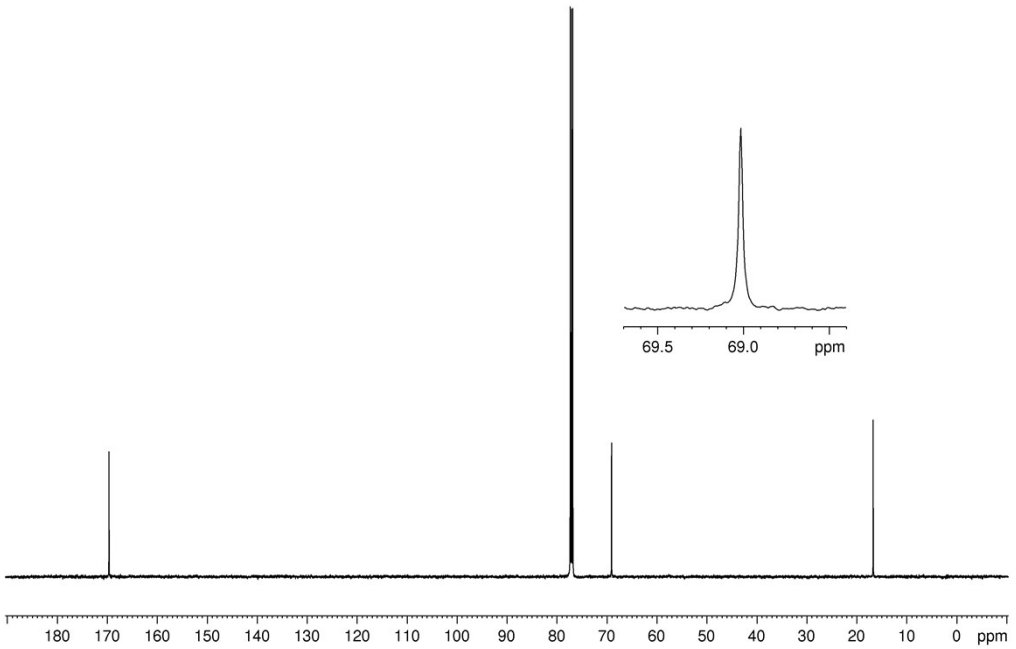

Figure S91. Inverse-gated $^{13}C\{^{1}H\}$ spectrum (125.76 MHz, $CDCl_3$) of cyclic *L*-PLA obtained with **2b** at 50:1 $[LA]_0/[Cat]$ ratio in DCM at room temperature.

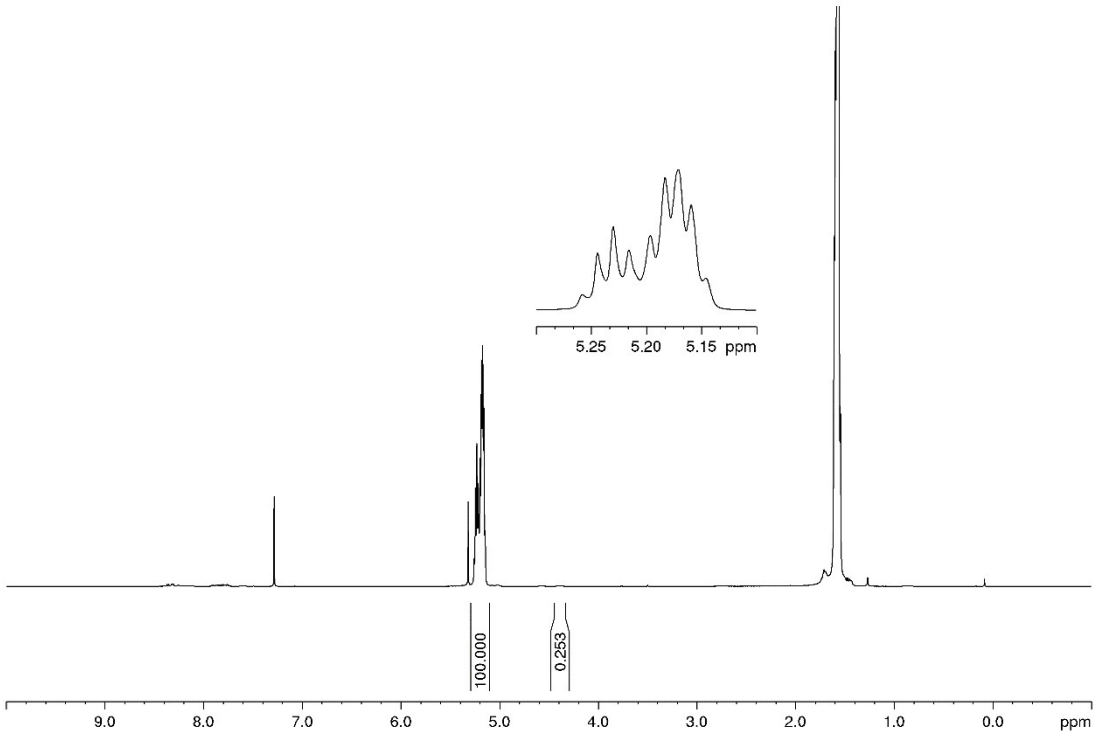

Figure S92. ^{1}H NMR spectrum (500.13 MHz, $CDCl_3$) of cyclic rac-PLA obtained with **2b** at 50:1 $[LA]_0$/[Cat] ratio in DCM at room temperature.

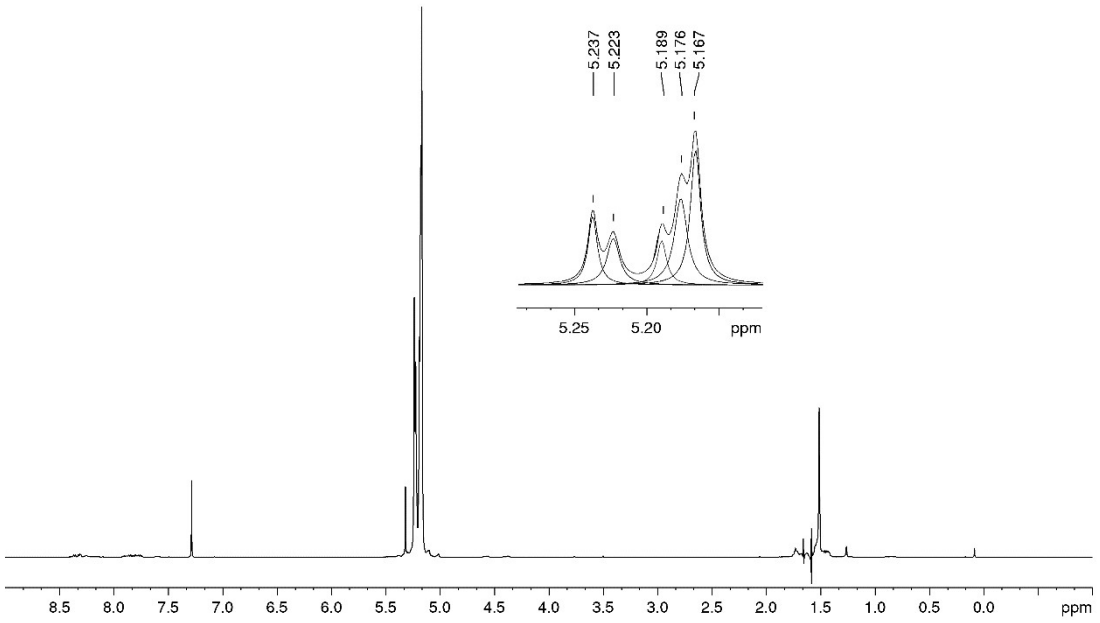

Figure S93. Homodecoupling^{1}H NMR spectrum (500.13 MHz, $CDCl_3$) of cyclic rac-PLA obtained with **2b** at 50:1 $[LA]_0$/[Cat] ratio in DCM at room temperature.

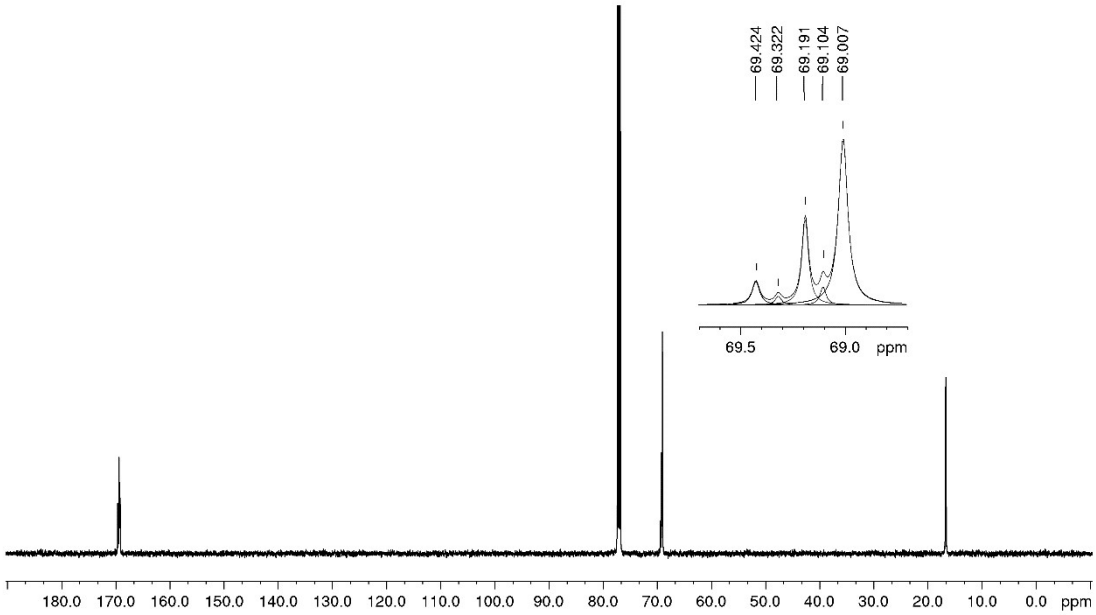

Figure S94. Inverse-gated $^{13}C\{^{1}H\}$ spectrum (125.76 MHz, $CDCl_3$) of cyclic rac-PLA obtained with **2b** at 50:1 $[LA]_0$/[Cat] ratio in DCM at room temperature.

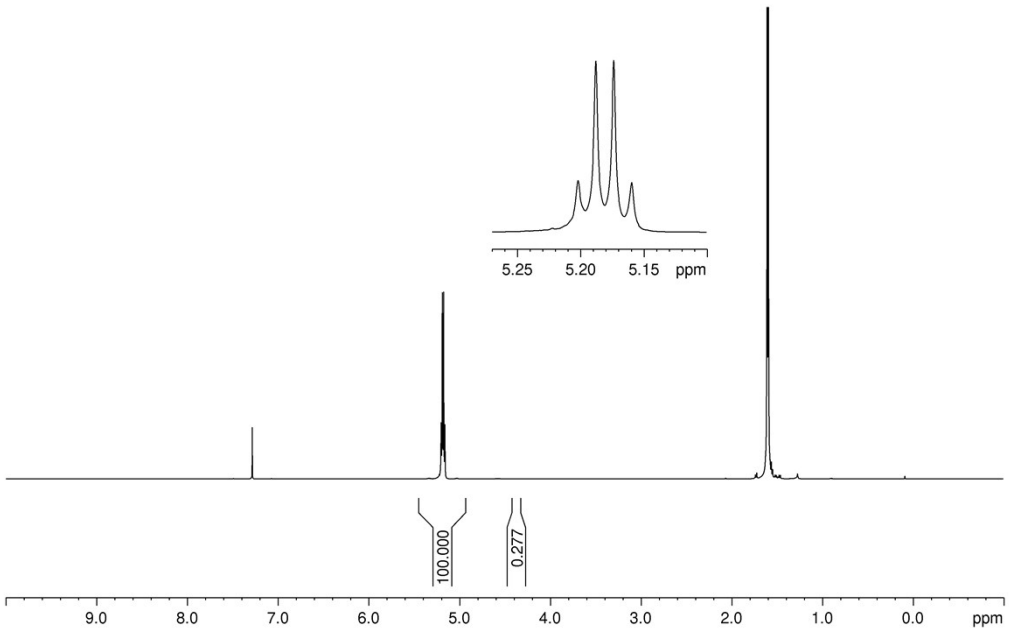

Figure S95. ^{1}H NMR spectrum (500.13 MHz, $CDCl_3$) of cyclic *L*-PLA obtained with **2c** at 50:1 $[LA]_0$/[Cat] ratio in DCM at room temperature.

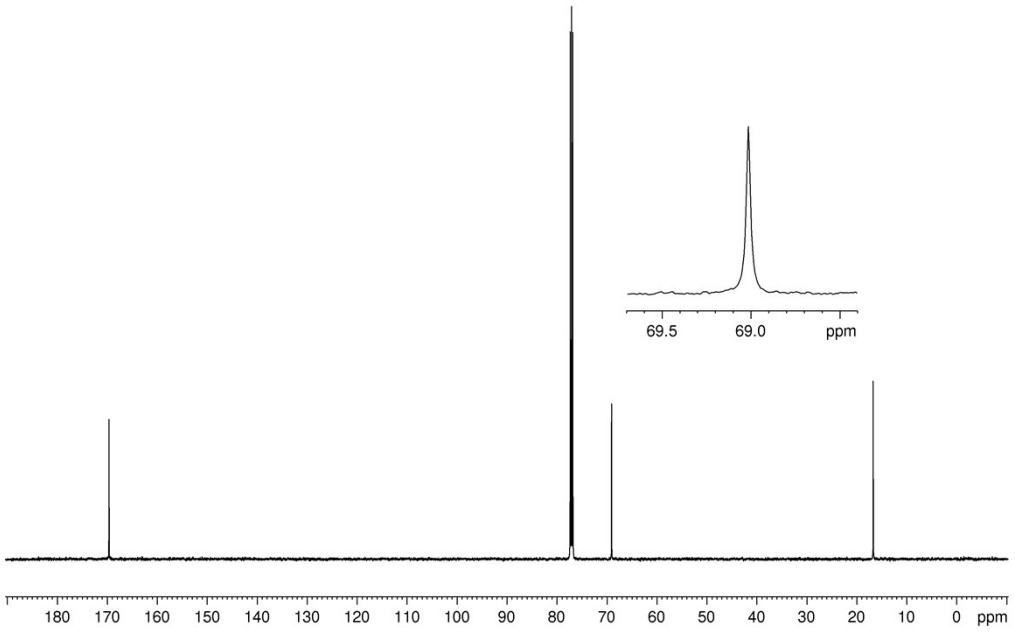

Figure S96. Inverse-gated $^{13}C\{^{1}H\}$ spectrum (125.76 MHz, $CDCl_3$) of cyclic *L*-PLA obtained with **2c** at 50:1 $[LA]_0$/[Cat] ratio in DCM at room temperature.

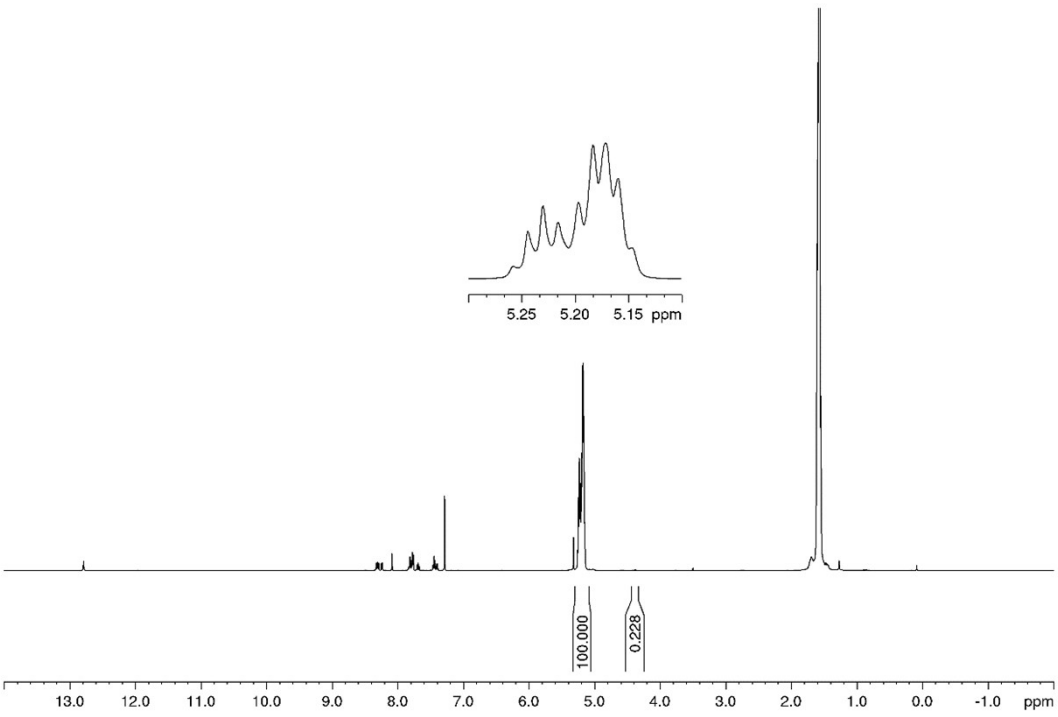

Figure S97. ^{1}H NMR spectrum (500.13 MHz, $CDCl_3$) of cyclic *rac*-PLA obtained with **2c** at 50:1 $[LA]_0$/[Cat] ratio in DCM at room temperature.

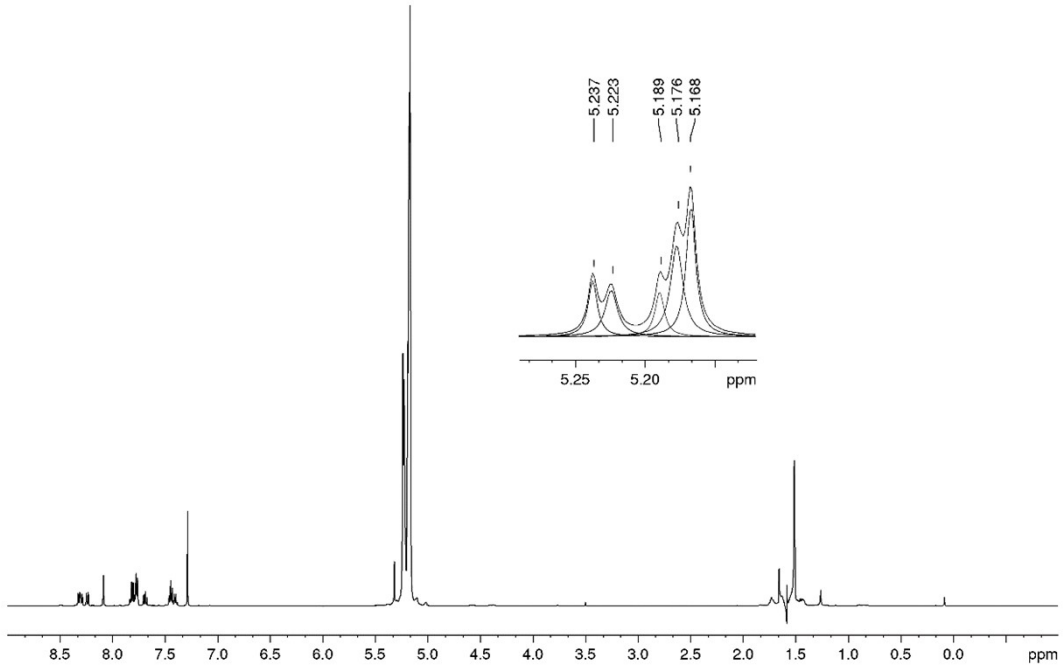

Figure S98. Homodecoupling ^{1}H NMR spectrum (500.13 MHz, $CDCl_3$) of cyclic *rac*-PLA obtained with **2c** at 50:1 $[LA]_0$/[Cat] ratio in DCM at room temperature.

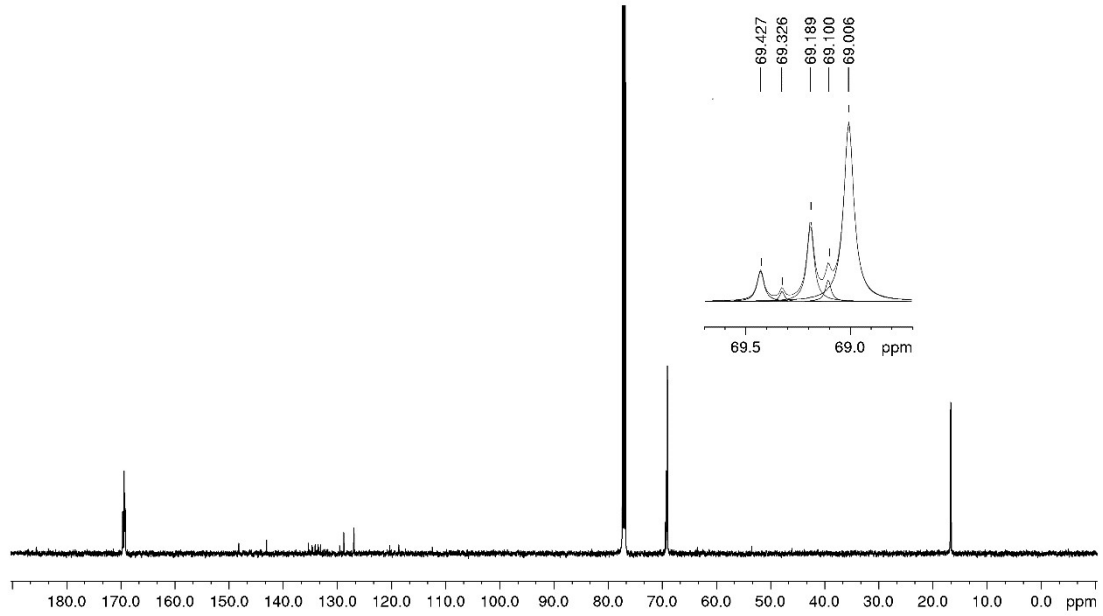

Figure S99. Inverse-gated $^{13}C\{^{1}H\}$ spectrum (125.76 MHz, $CDCl_3$) of cyclic *rac*-PLA obtained with **2c** at 50:1 $[LA]_0$/[Cat] ratio in DCM at room temperature.

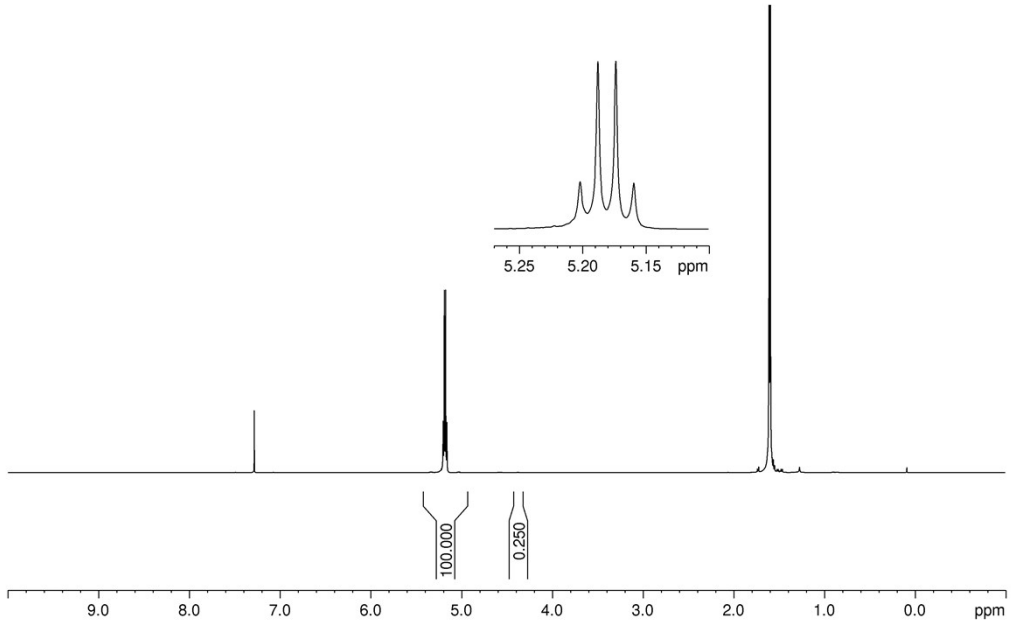

Figure S100. ^{1}H NMR spectrum (500.13 MHz, $CDCl_3$) of cyclic *L*-PLA obtained with **2d** at 50:1 $[LA]_0$/[Cat] ratio in DCM at room temperature.

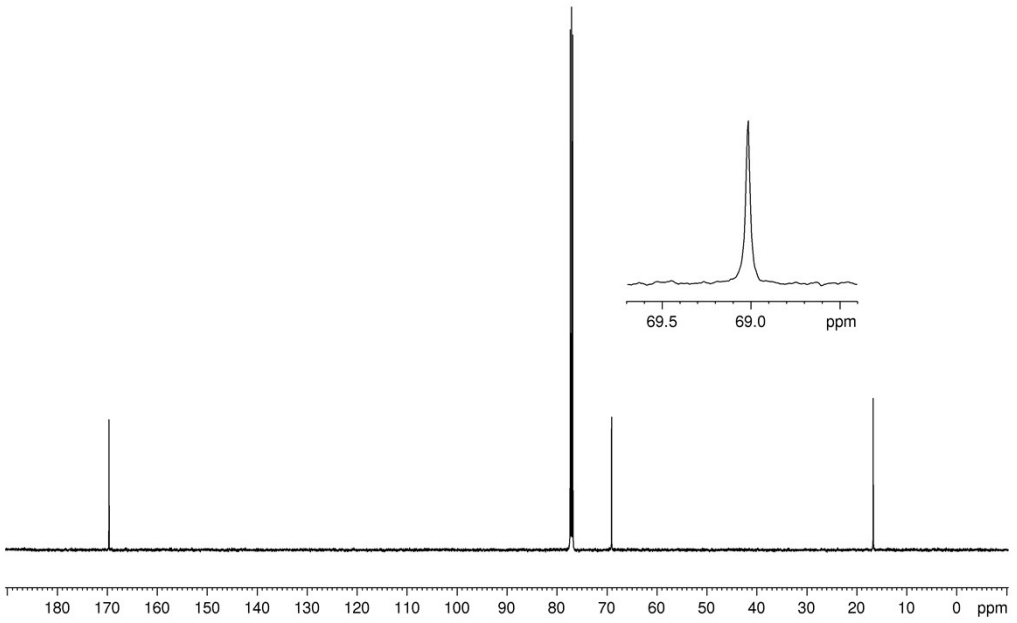

Figure S101. Inverse-gated $^{13}C\{^{1}H\}$ spectrum (125.76 MHz, $CDCl_3$) of cyclic *L*-PLA obtained with **2d** at 50:1 $[LA]_0$/[Cat] ratio in DCM at room temperature.

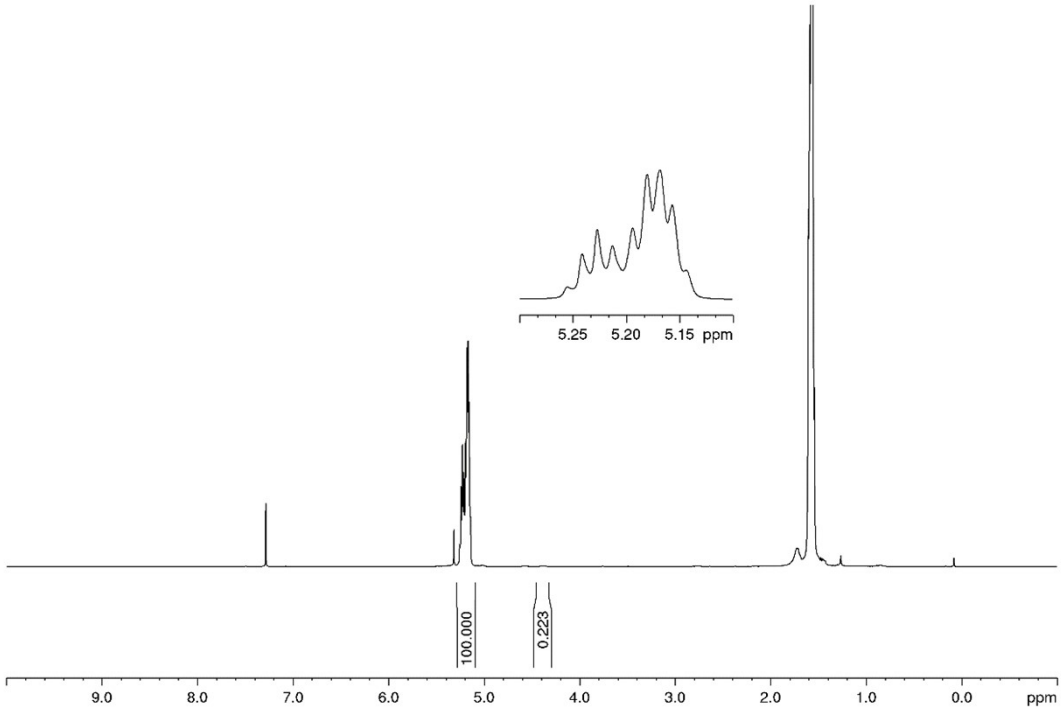

Figure S102. ^{1}H NMR spectrum (500.13 MHz, $CDCl_3$) of cyclic *rac*-PLA obtained with **2d** at 50:1 $[LA]_0$/[Cat] ratio in DCM at room temperature.

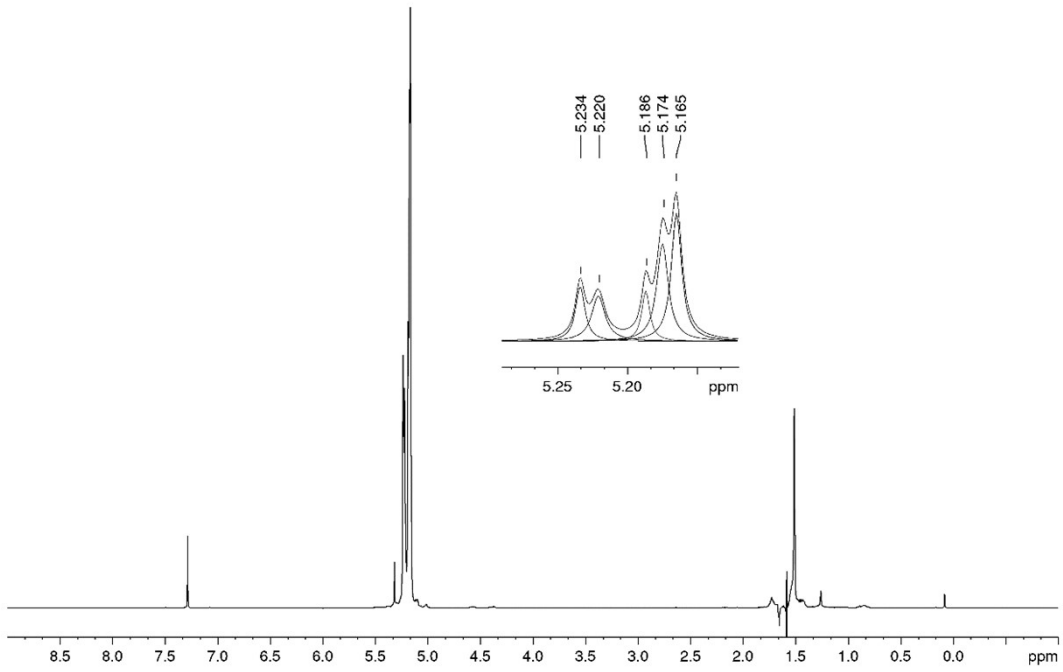

Figure S103. Homodecoupling ^{1}H NMR spectrum (500.13 MHz, $CDCl_3$) of cyclic *rac*-PLA obtained with **2d** at 50:1 $[LA]_0$/[Cat] ratio in DCM at room temperature.

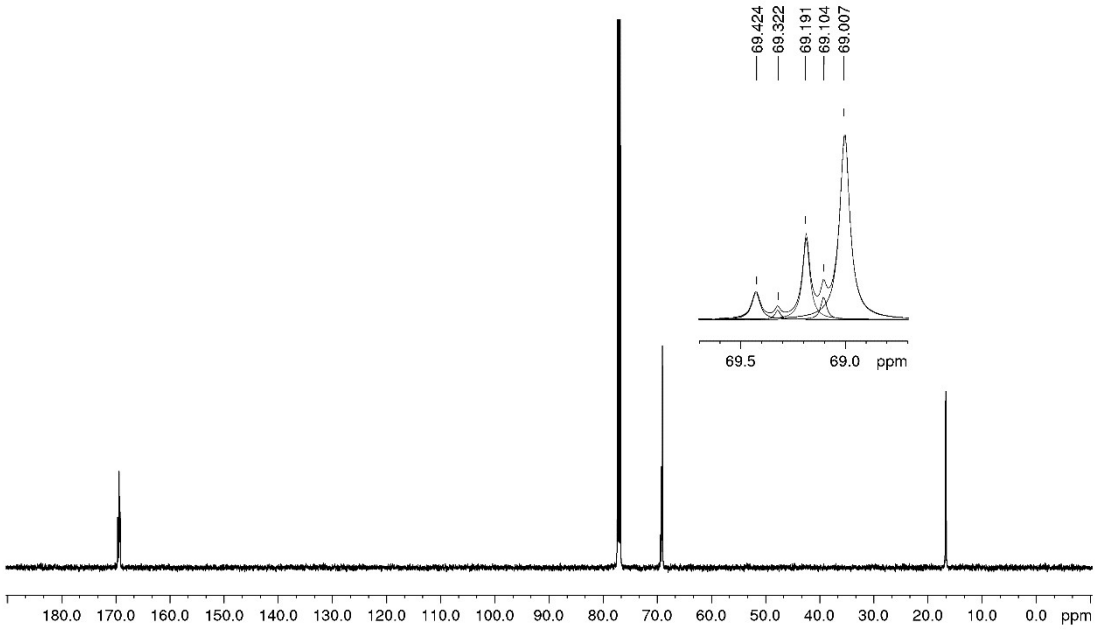

Figure S104. Inverse-gated $^{13}C\{^{1}H\}$ spectrum (125.76 MHz, $CDCl_3$) of cyclic *rac*-PLA obtained with **2d** at 50:1 $[LA]_0/[Cat]$ ratio in DCM at room temperature.

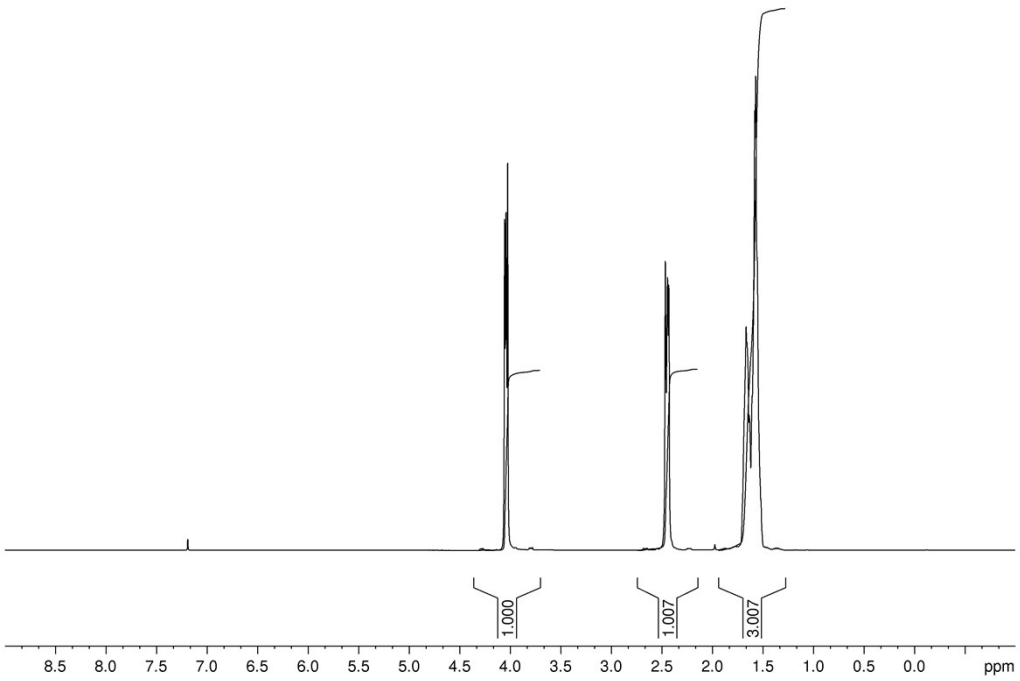

Figure S105. ^{1}H NMR spectrum (500.13 MHz, $CDCl_3$) of ε-Caprolactone.

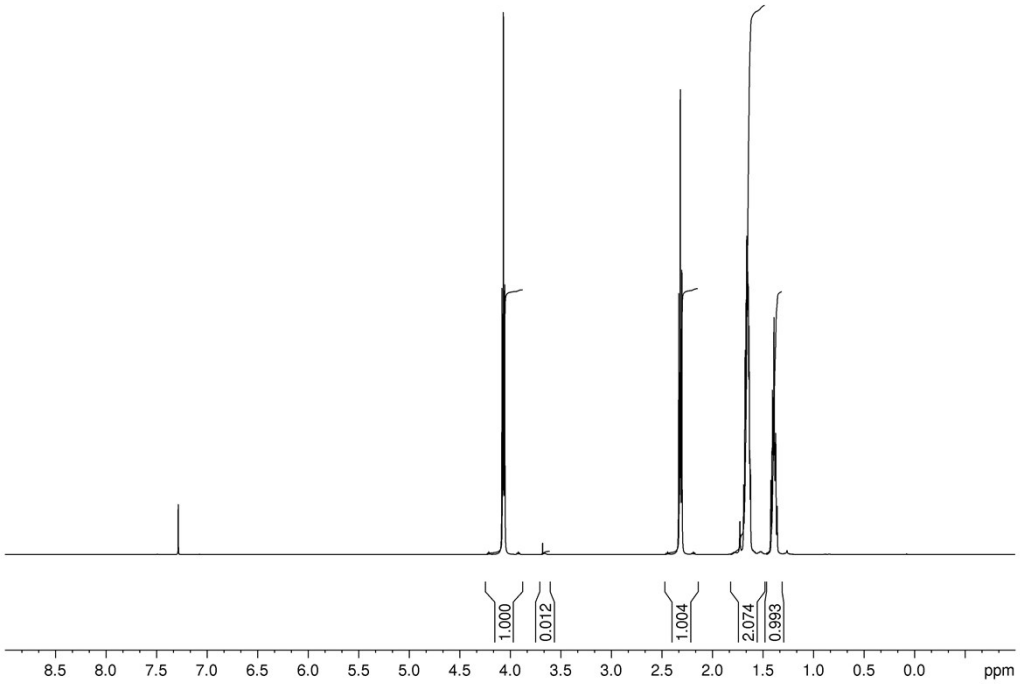

Figure S106. ^{1}H NMR spectrum (500.13 MHz, $CDCl_3$) of cyclic PCL obtained with **2a** at 50:1 $[CL]_0/[Cat]$ ratio in DCM at room temperature.

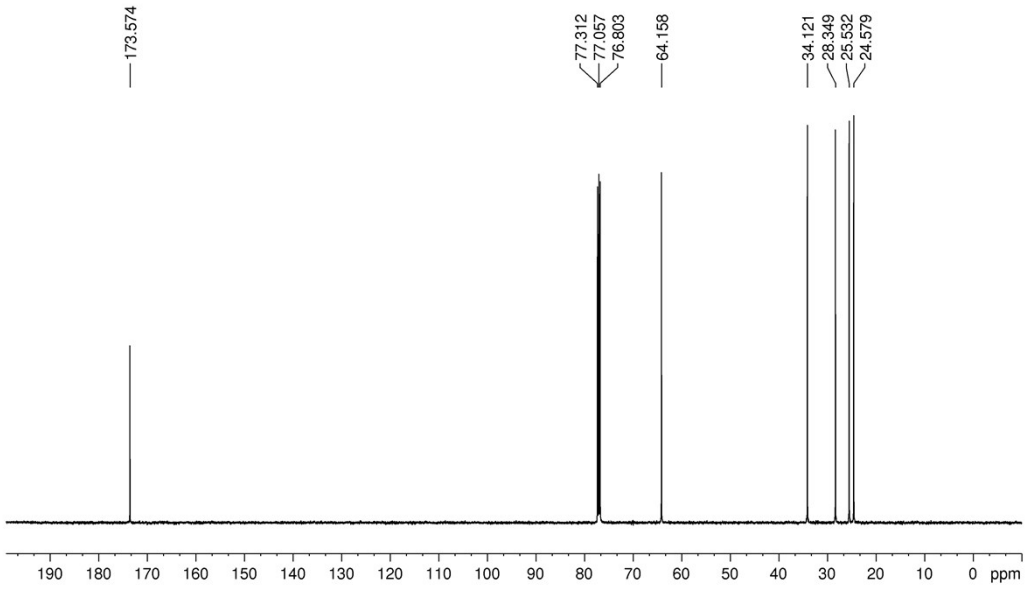

Figure S107. ^{13}C NMR (125.76 MHz, $CDCl_3$) of cyclic PCL obtained with **2a** at 50:1 $[CL]_0/[Cat]$ ratio in DCM at room temperature.

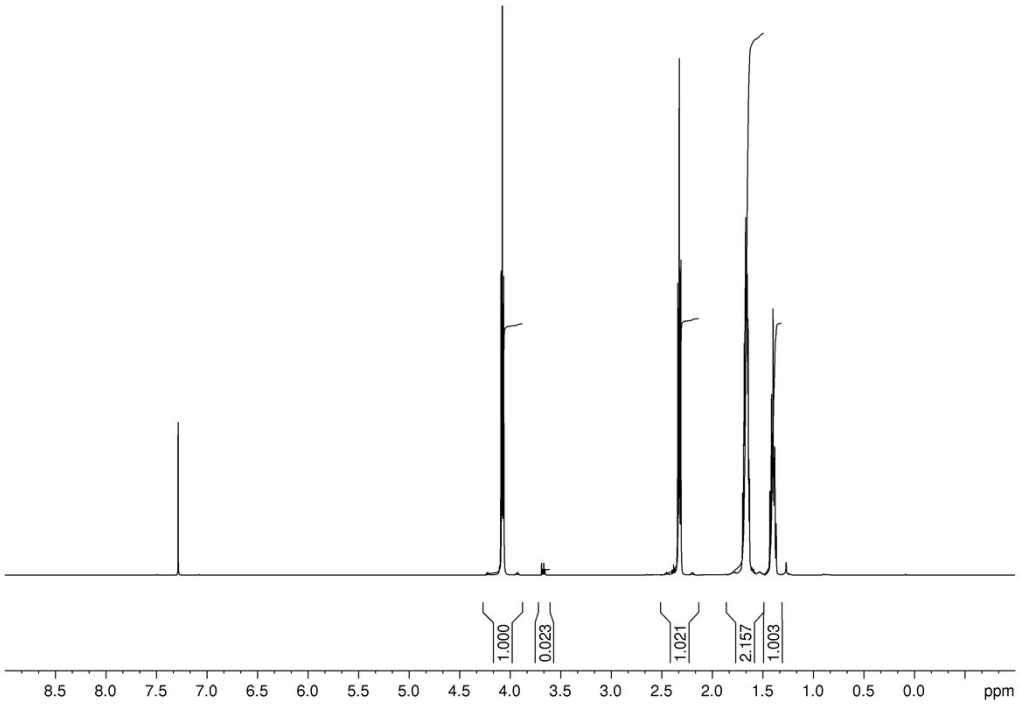

Figure S108. ^{1}H NMR spectrum (500.13 MHz, $CDCl_3$) of cyclic PCL obtained with **2a** at 50:1 $[CL]_0$/[Cat] ratio in THF at room temperature.

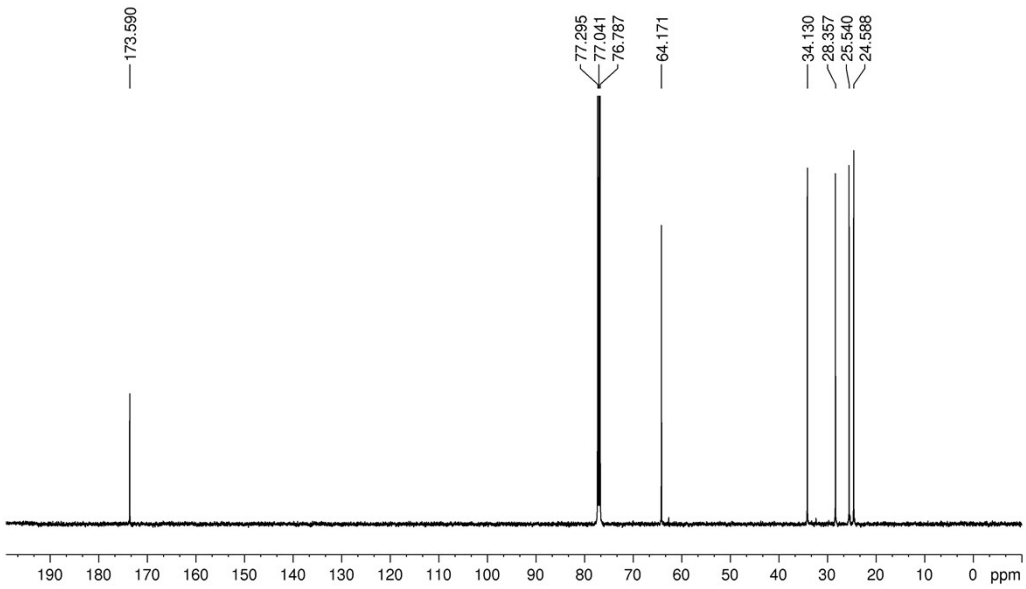

Figure S109. ^{13}C spectrum (125.76 MHz, $CDCl_3$) of cyclic PCL obtained with **2a** at 50:1 $[CL]_0$/[Cat] ratio in THF at room temperature.

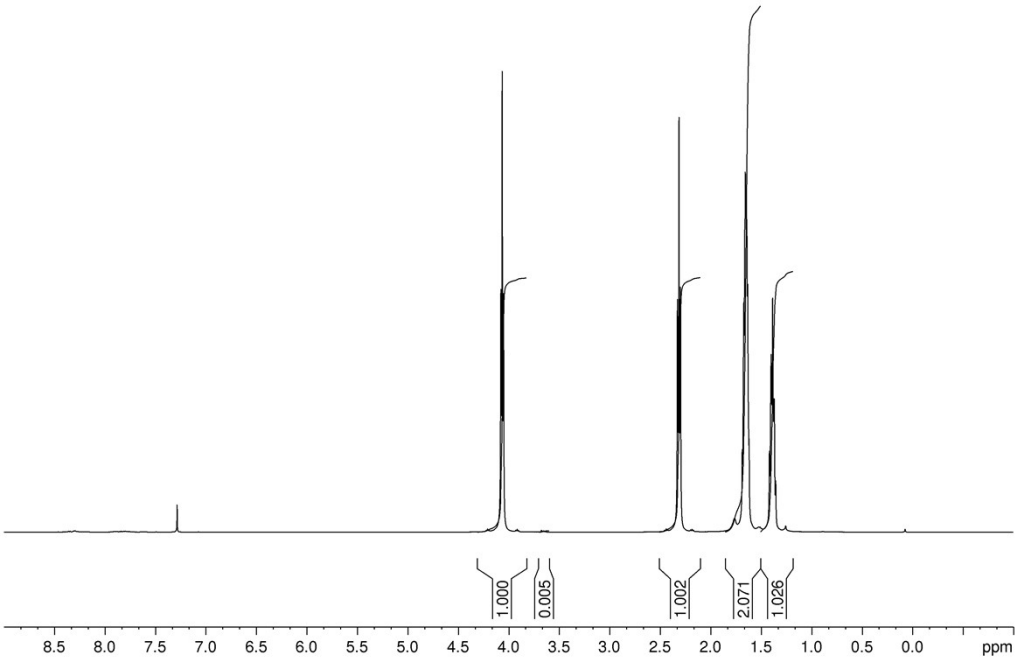

Figure S110. ^{1}H NMR spectrum (500.13 MHz, $CDCl_3$) of cyclic PCL obtained with 2b at 50:1 $[CL]_0/[Cat]$ ratio in DCM at room temperature.

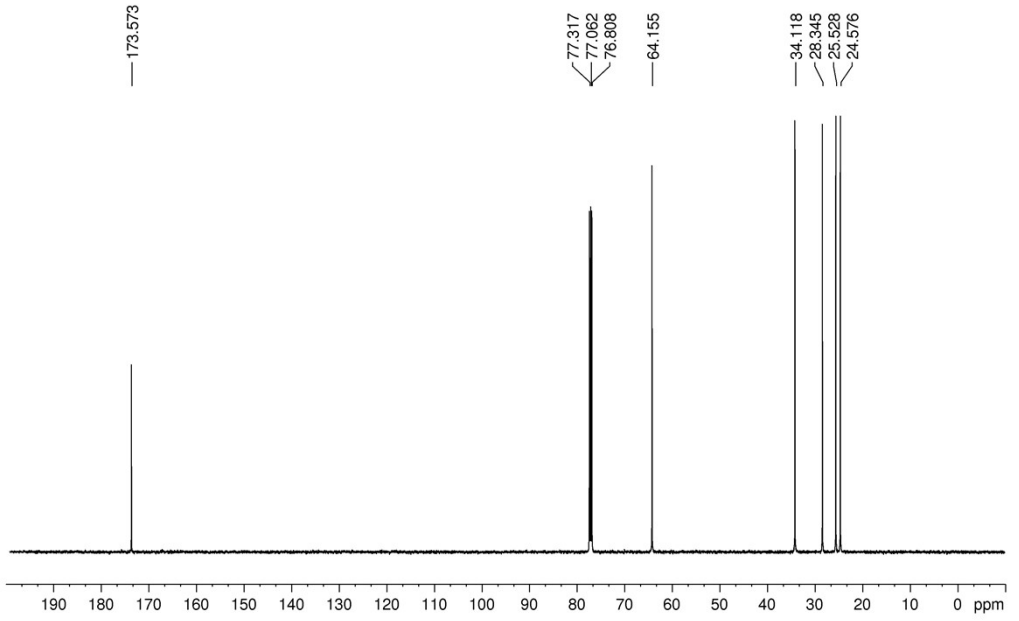

Figure S111. ^{13}C NMR (125.76 MHz, $CDCl_3$) of cyclic PCL obtained with **2b** at 50:1 $[CL]_0/[Cat]$ ratio in DCM at room temperature.

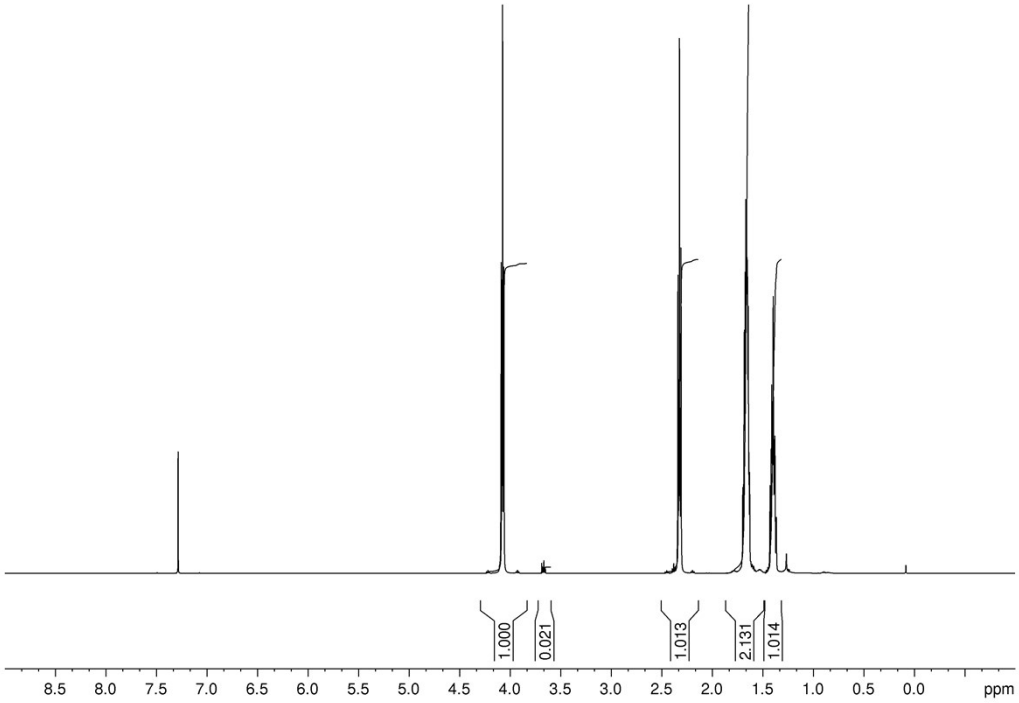

Figure S112. ^{1}H NMR spectrum (500.13 MHz, $CDCl_3$) of cyclic PCL obtained with **2b** at 50:1 $[CL]_0/[Cat]$ ratio in THF at room temperature.

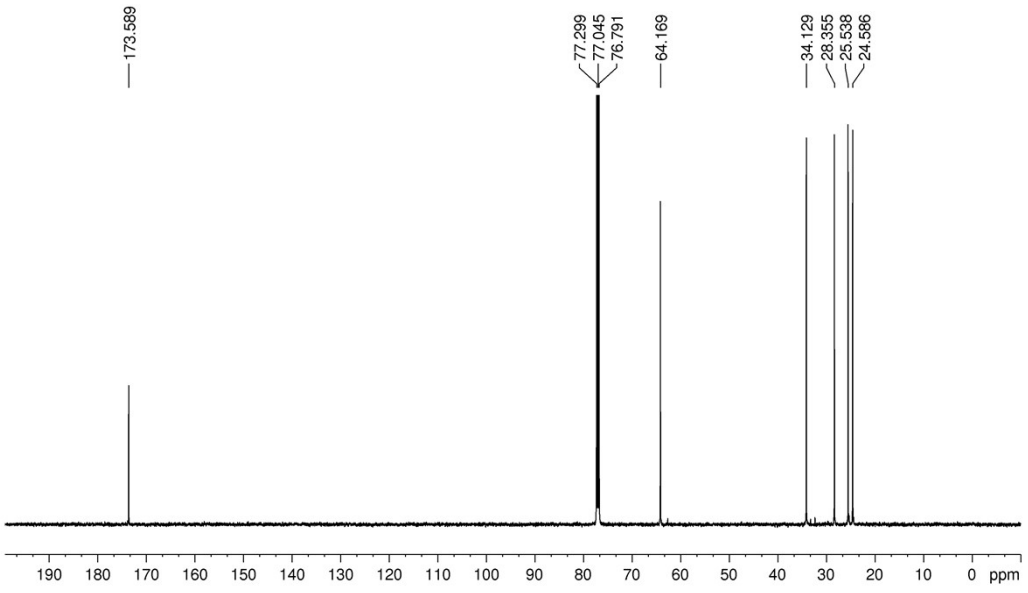

Figure S113. ^{13}C spectrum (125.76 MHz, $CDCl_3$) of cyclic PCL obtained with **2b** at 50:1 $[CL]_0/[Cat]$ ratio in THF at room temperature.

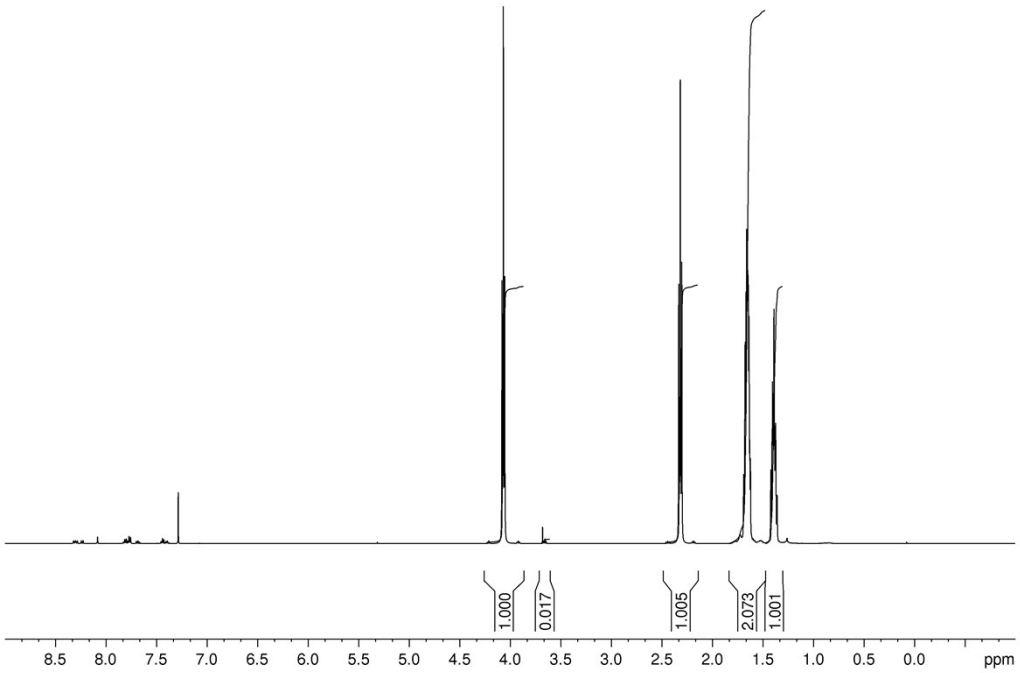

Figure S114. ^{1}H NMR spectrum (500.13 MHz, $CDCl_3$) of cyclic PCL obtained with **2c** at 50:1 $[CL]_0$/[Cat] ratio in DCM at room temperature.

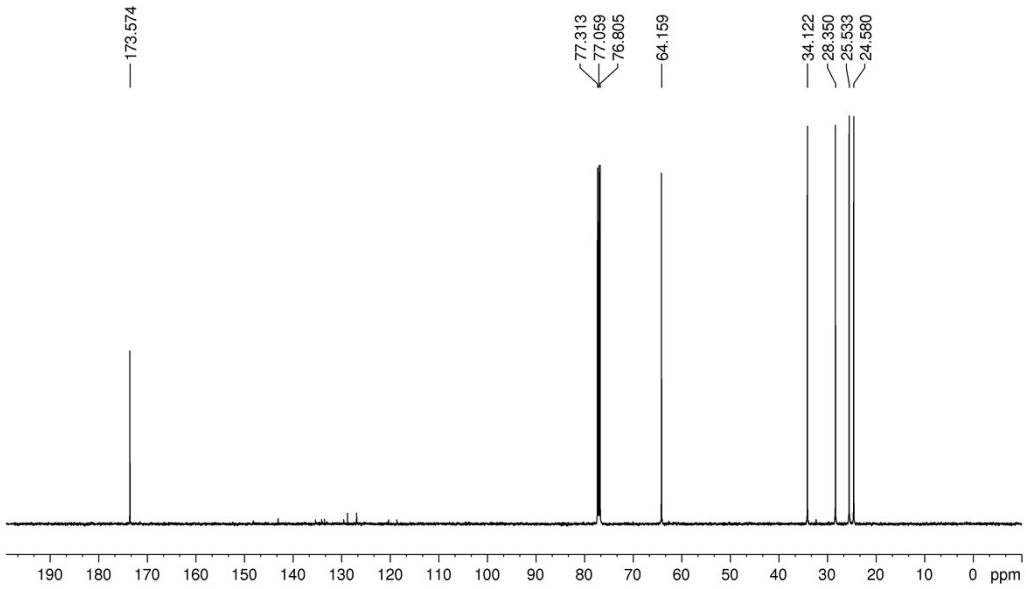

Figure S115. ^{13}C spectrum (125.76 MHz, $CDCl_3$) of cyclic PCL obtained with **2c** at 50:1 $[CL]_0$/[Cat] ratio in DCM at room temperature.

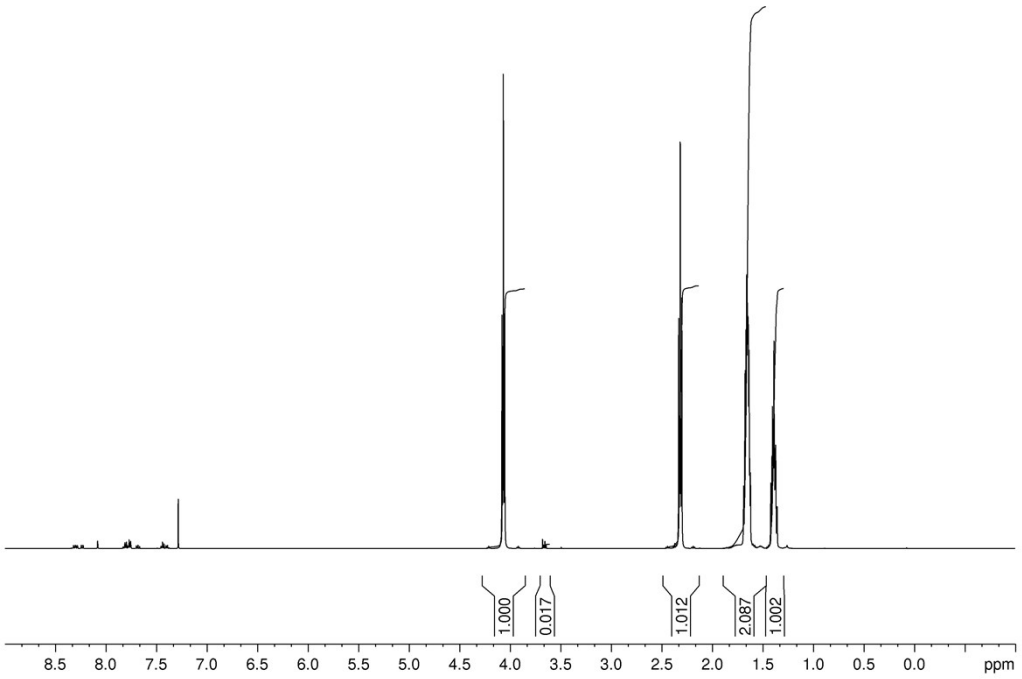

Figure S116. ^{1}H NMR spectrum (500.13 MHz, $CDCl_3$) of cyclic PCL obtained with **2c** at 50:1 $[CL]_0/[Cat]$ ratio in THF at room temperature.

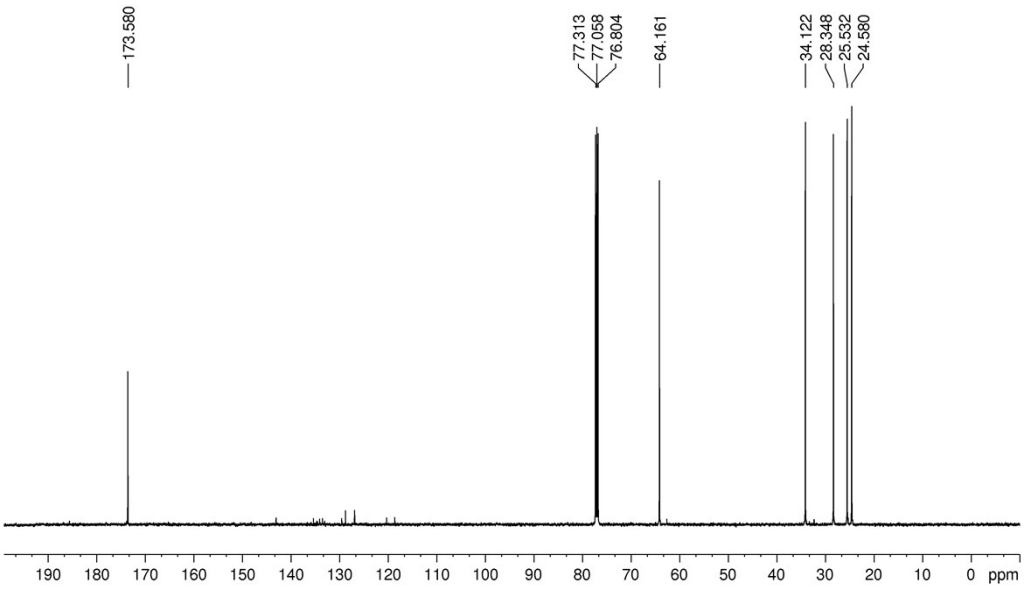

Figure S117. ^{13}C spectrum (125.76 MHz, $CDCl_3$) of cyclic PCL obtained with **2c** at 50:1 $[CL]_0/[Cat]$ ratio in THF at room temperature.

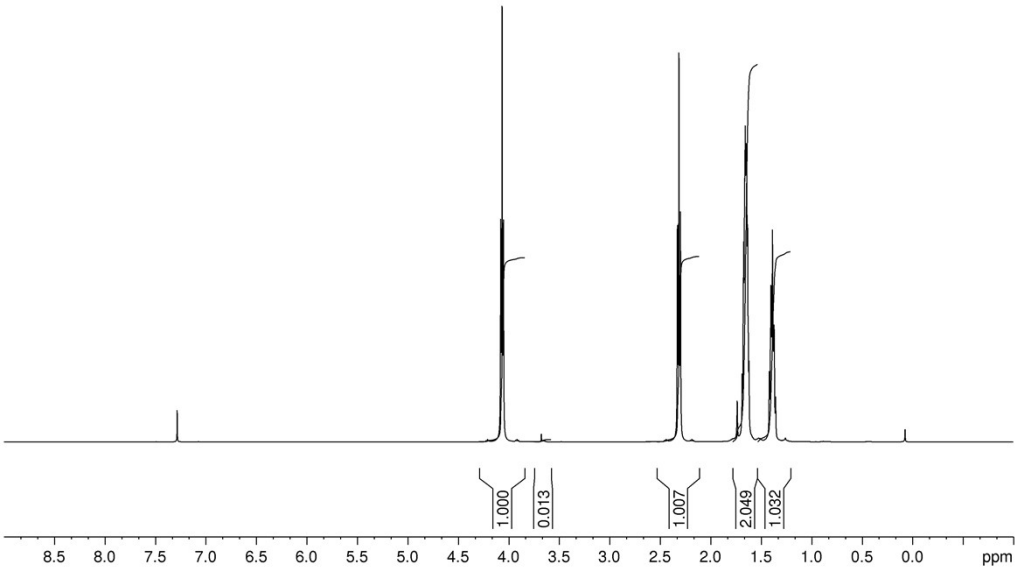

Figure S118. ^{1}H NMR spectrum (500.13 MHz, $CDCl_3$) of cyclic PCL obtained with **2d** at 50:1 $[CL]_0$/[Cat] ratio in DCM at room temperature.

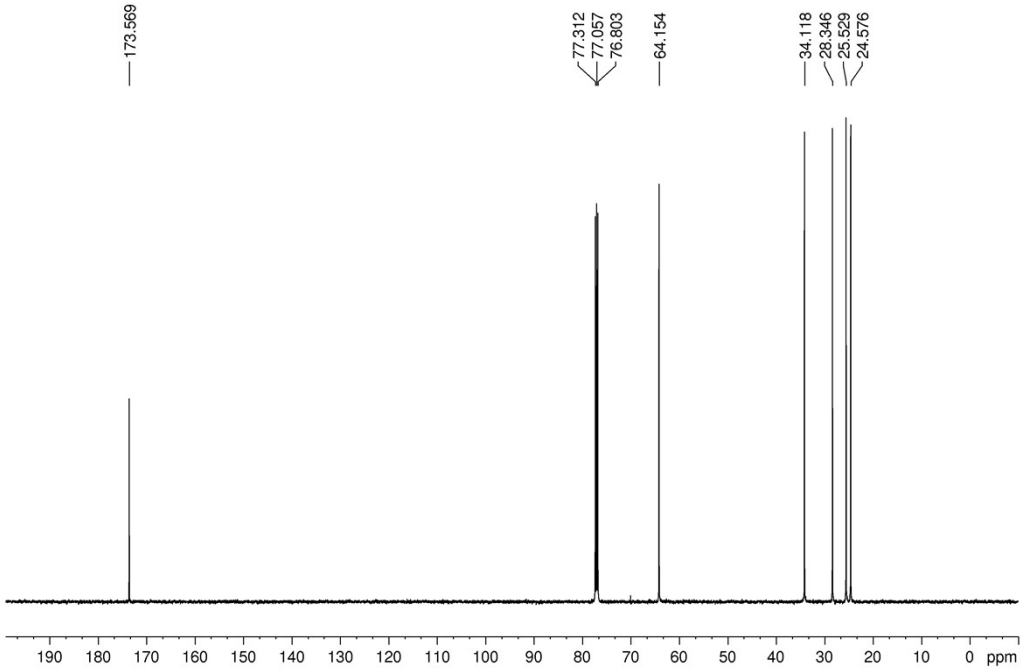

Figure S119.^{13}C NMR (125.76 MHz, $CDCl_3$) of cyclic PCL obtained with **2d** at 50:1 $[CL]_0$/[Cat] ratio in DCM at room temperature.

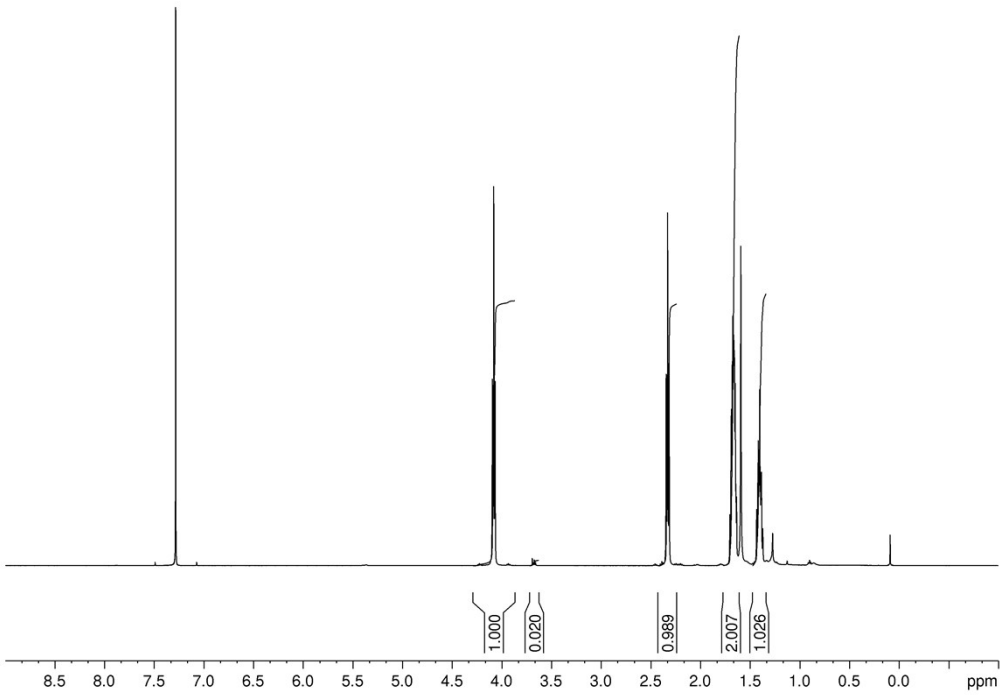

Figure S120. ^{1}H NMR spectrum (500.13 MHz, $CDCl_3$) of cyclic PCL obtained with **2d** at 50:1 $[CL]_0/[Cat]$ ratio in THF at room temperature.

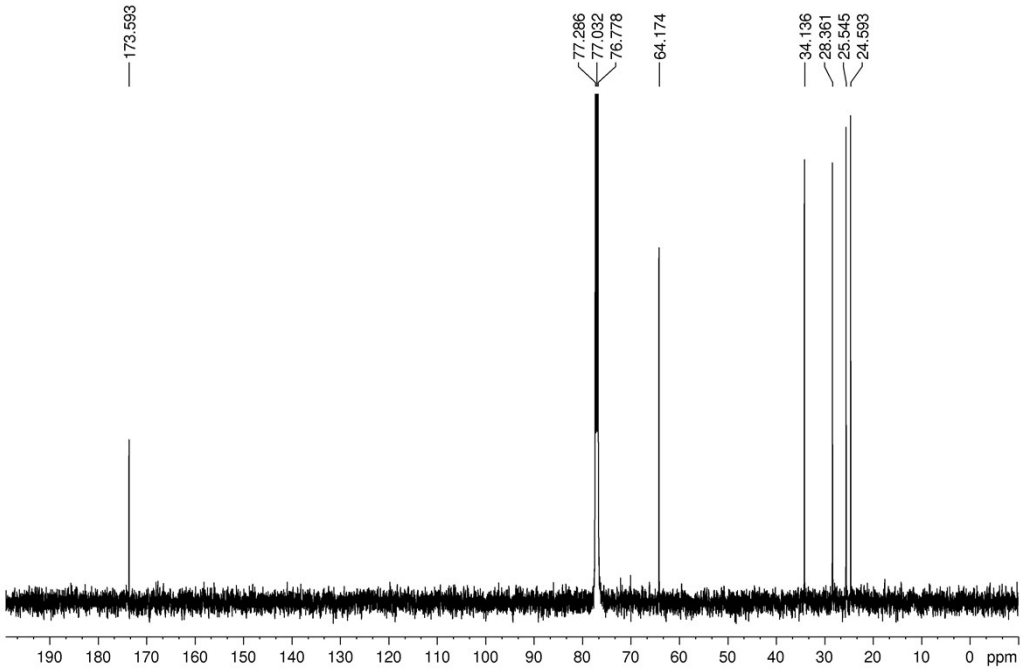

Figure S121. ^{13}C NMR (125.76 MHz, $CDCl_3$) of cyclic PCL obtained with **2d** at 50:1 $[CL]_0/[Cat]$ ratio in THF at room temperature.

12. MALDI-TOF.

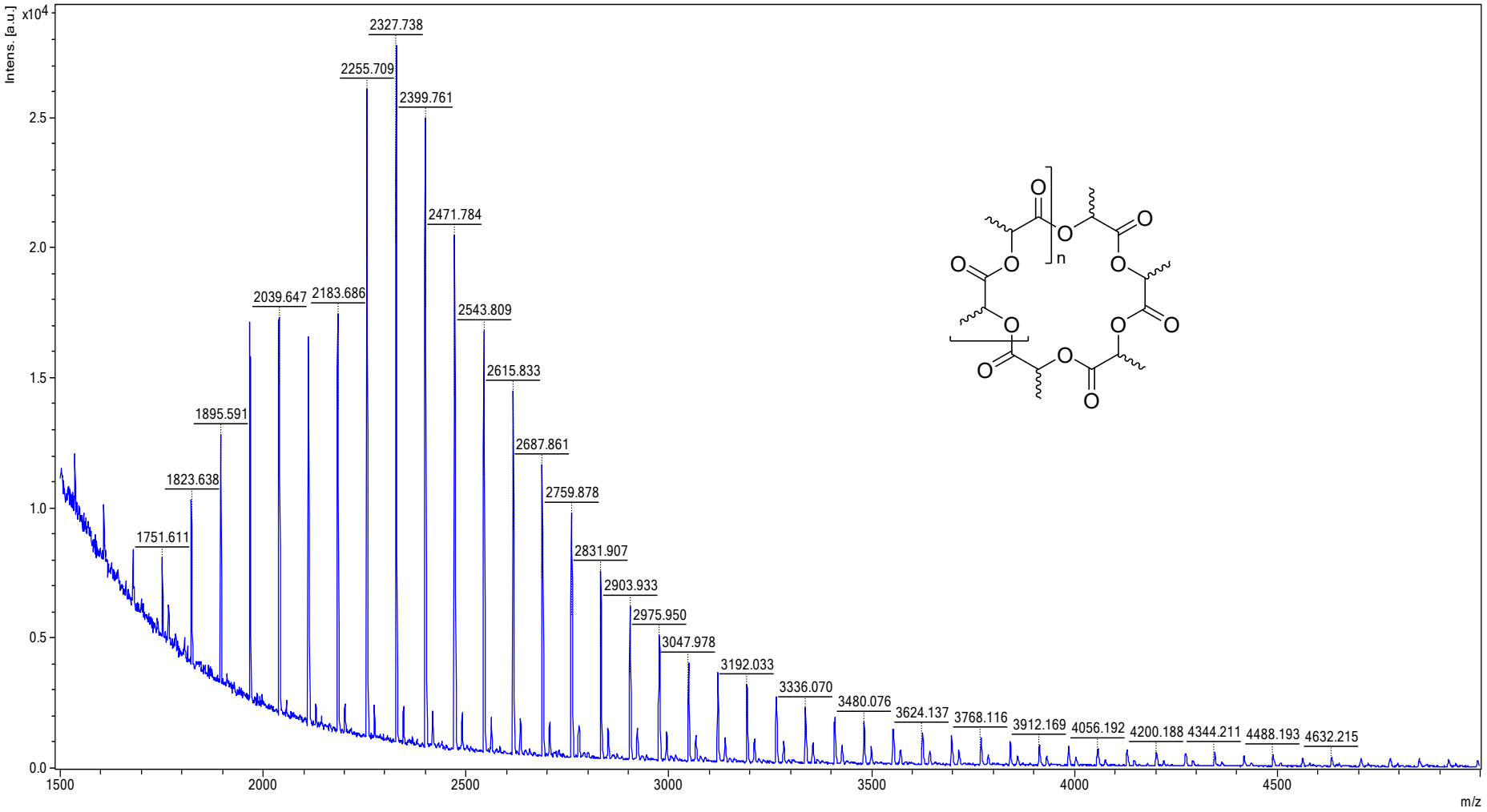

Figure S122. MALDI-TOF spectra of cyclic *L*-PLA obtained using **2b** as catalyst in DCM at a 50:1 $[LA]_0$/[Cat] ratio.

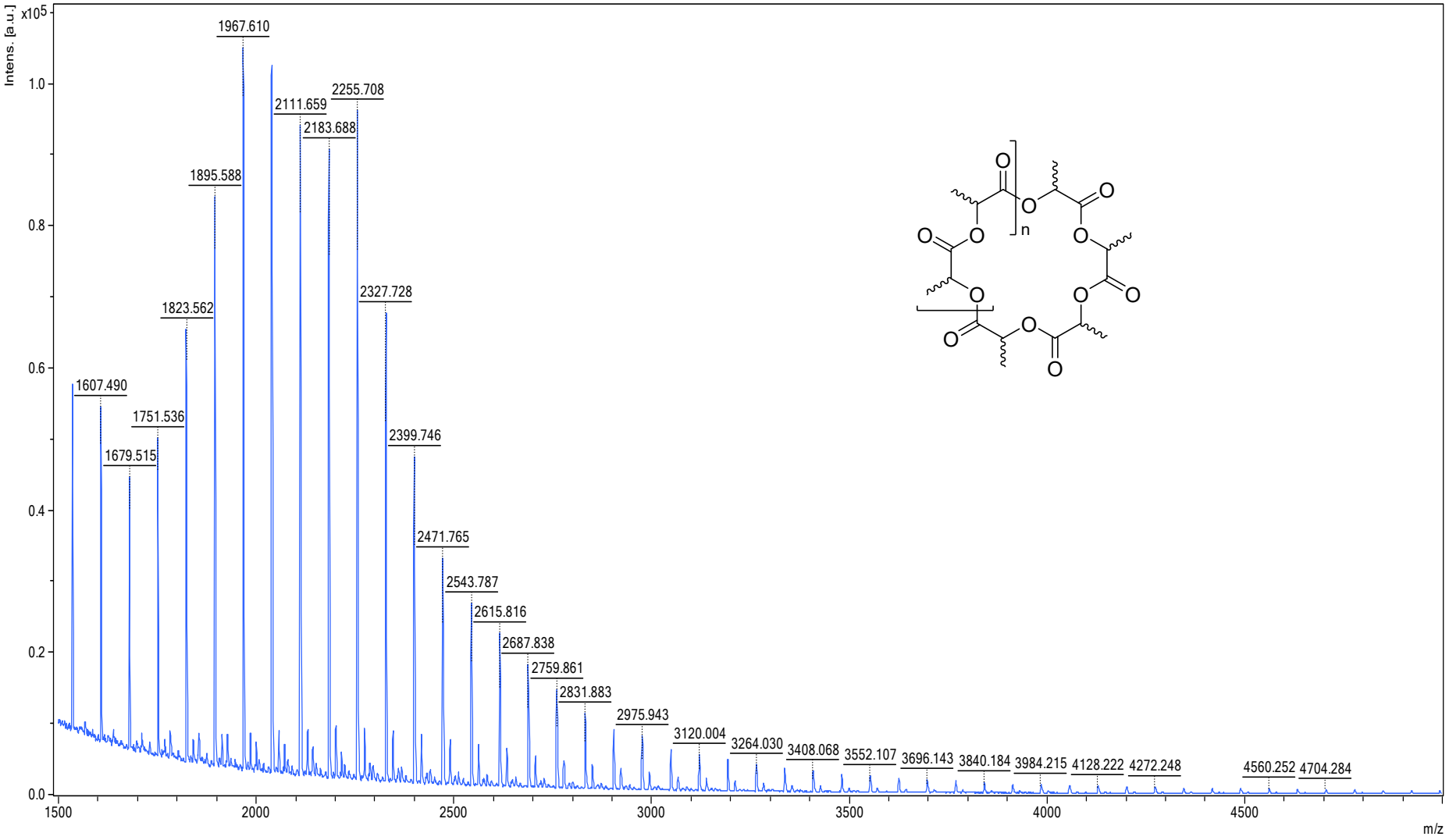

Figure S123. MALDI-TOF spectra of cyclic L-PLA obtained using **2c** as catalyst in DCM at a 50:1 $[LA]_0/[Cat]$ ratio.

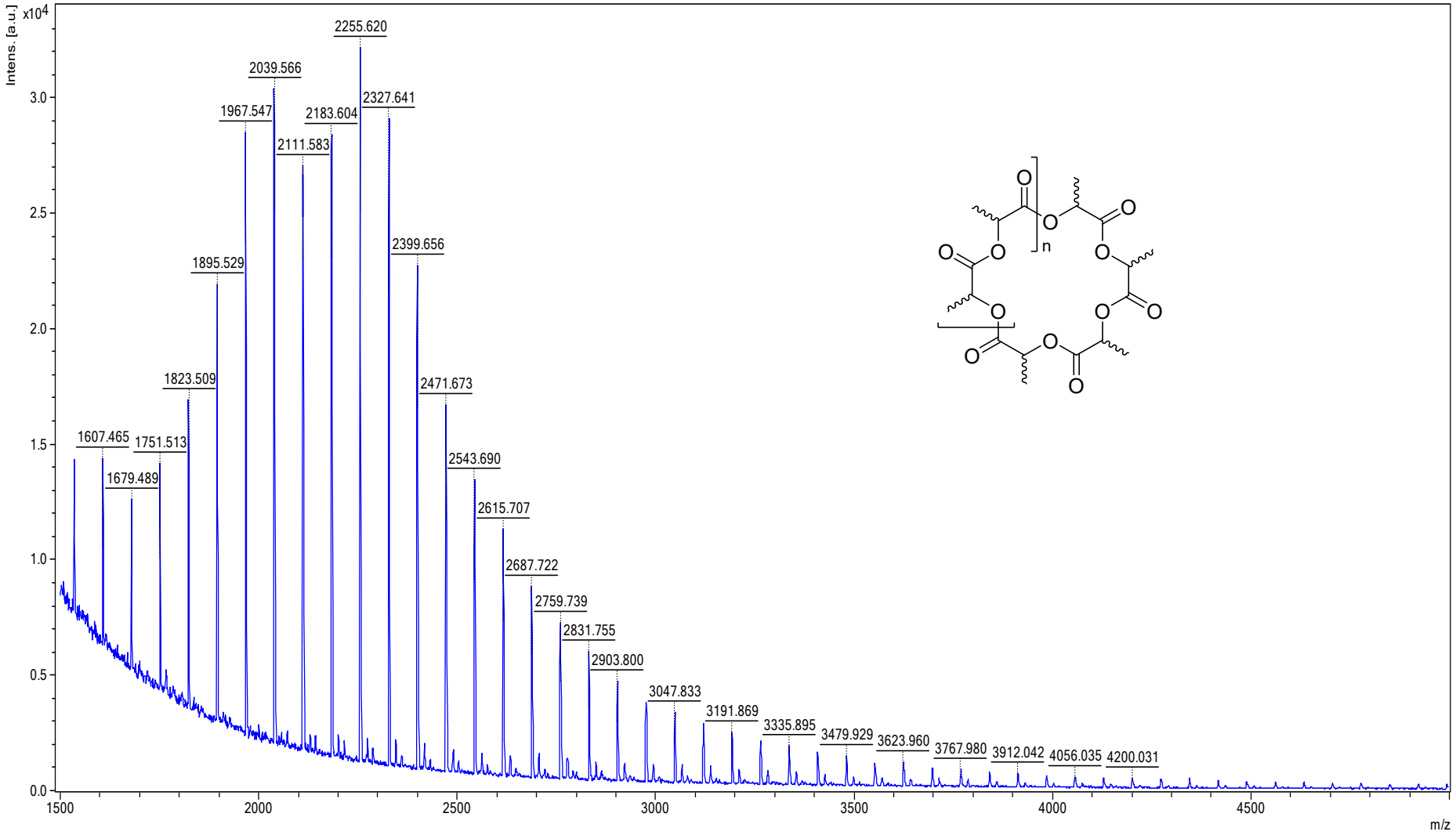

Figure S124. MALDI-TOF spectra of cyclic L-PLA obtained using **2d** as catalyst in DCM at a 50:1 $[LA]_0$/[Cat] ratio.

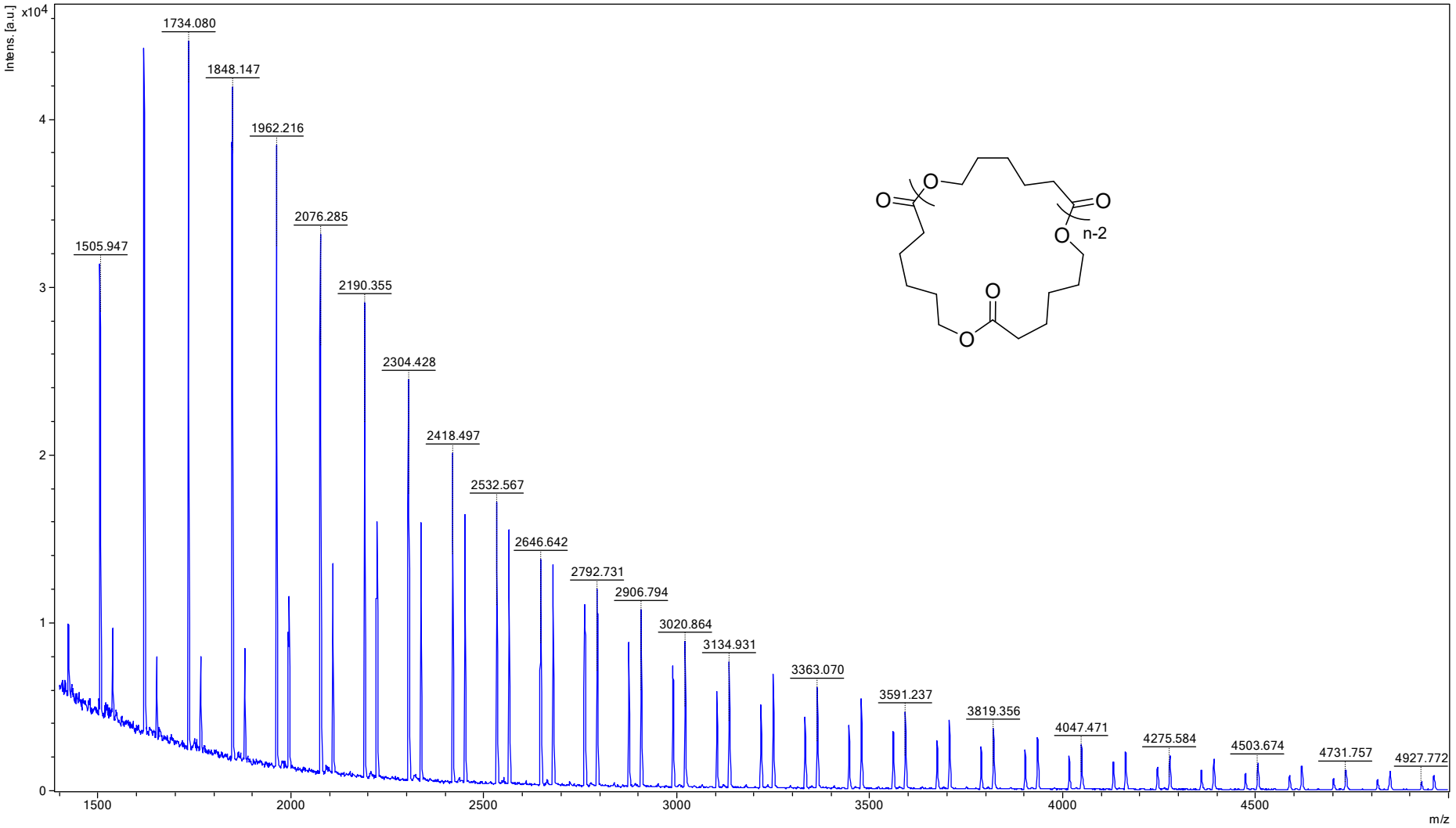

Figure S125. MALDI-TOF spectra of cyclic PCL obtained using **2a** as catalyst in DCM at a 50:1 $[LA]_0/[Cat]$ ratio.

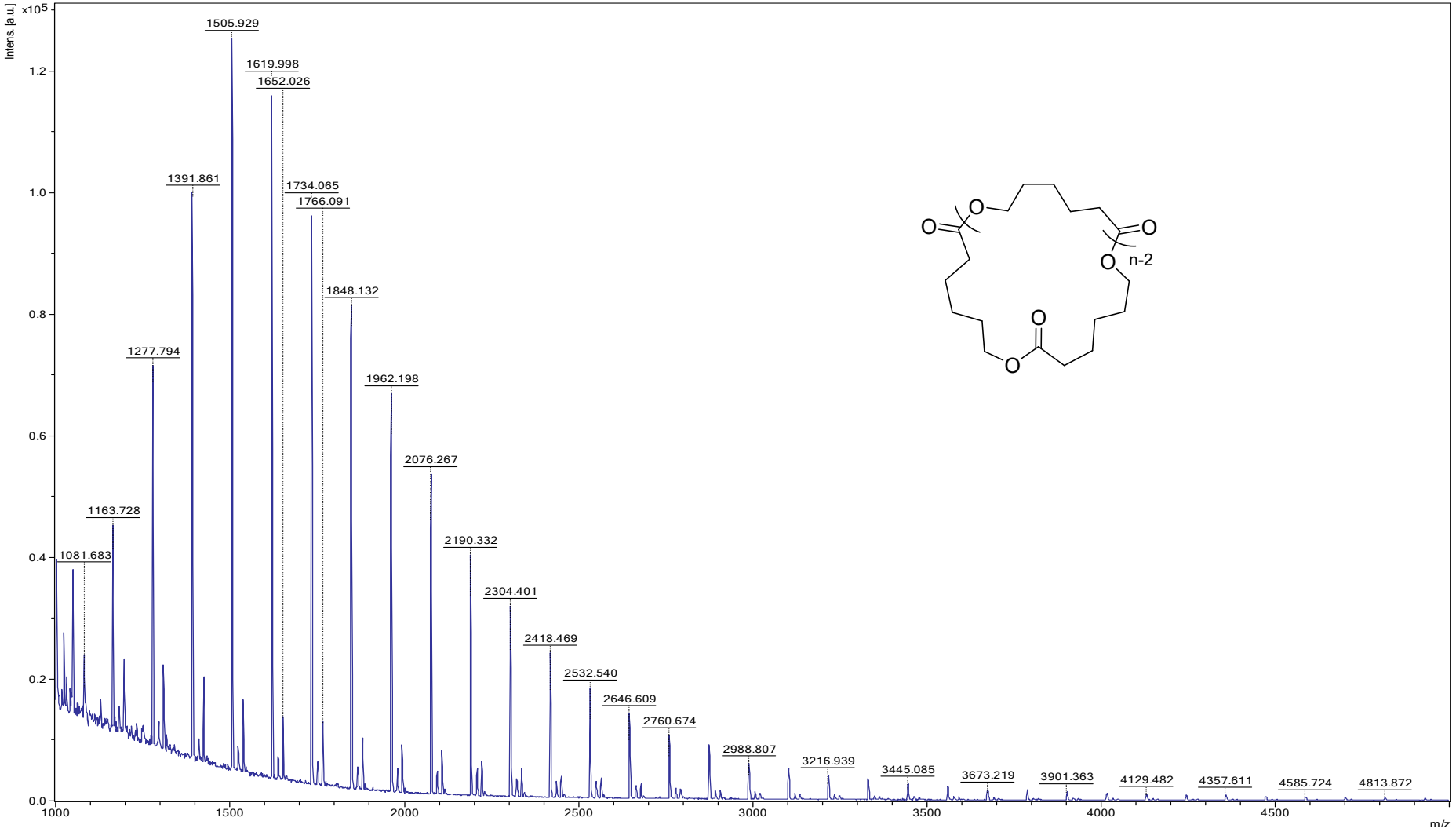

Figure S126. MALDI-TOF spectra of cyclic PCL obtained using **2b** as catalyst in DCM at a 50:1 $[LA]_0$/[Cat] ratio.

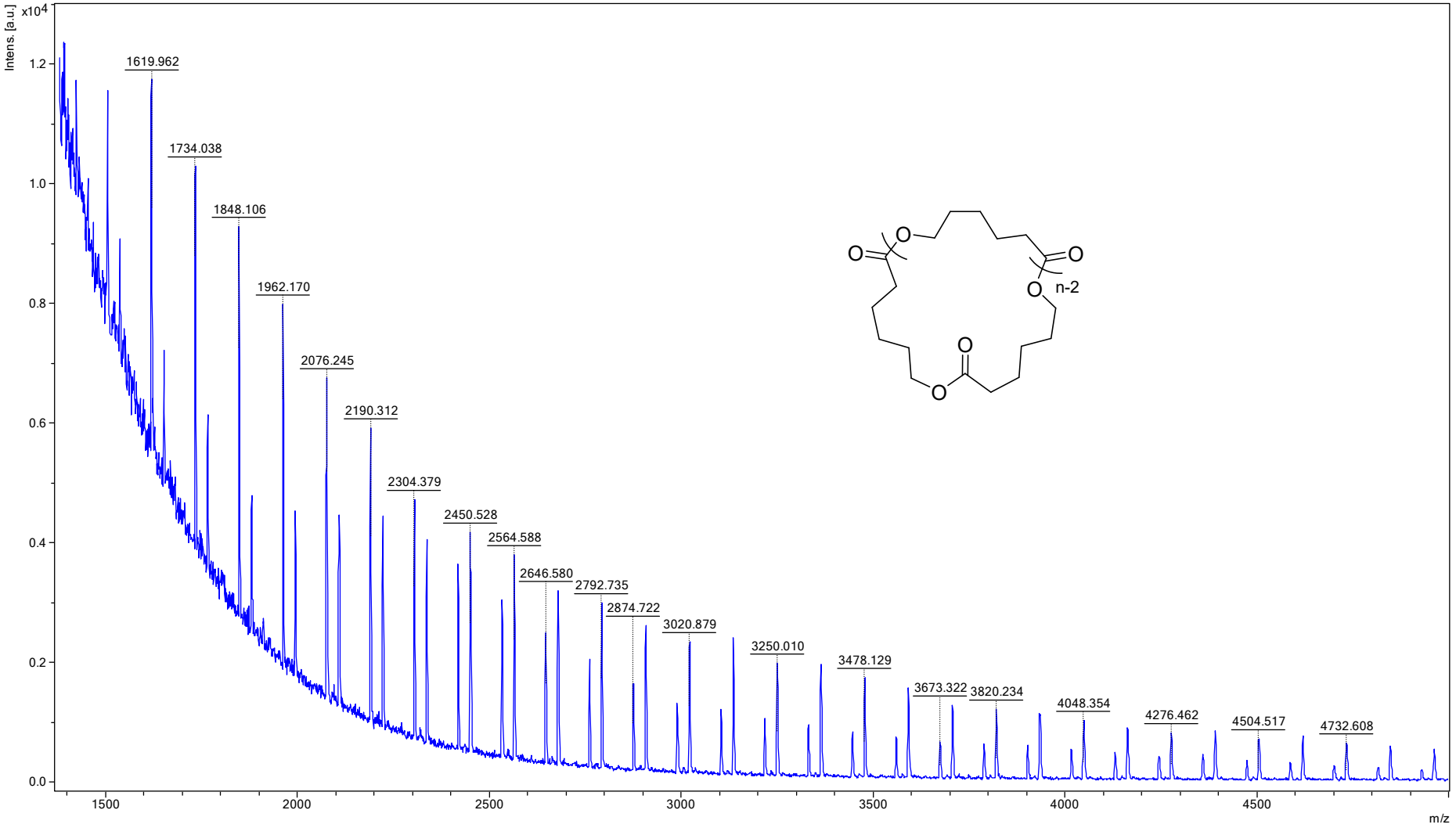

Figure S127. MALDI-TOF spectra of cyclic PCL obtained using **2c** as catalyst in DCM at a 50:1 $[LA]_0/[Cat]$ ratio.

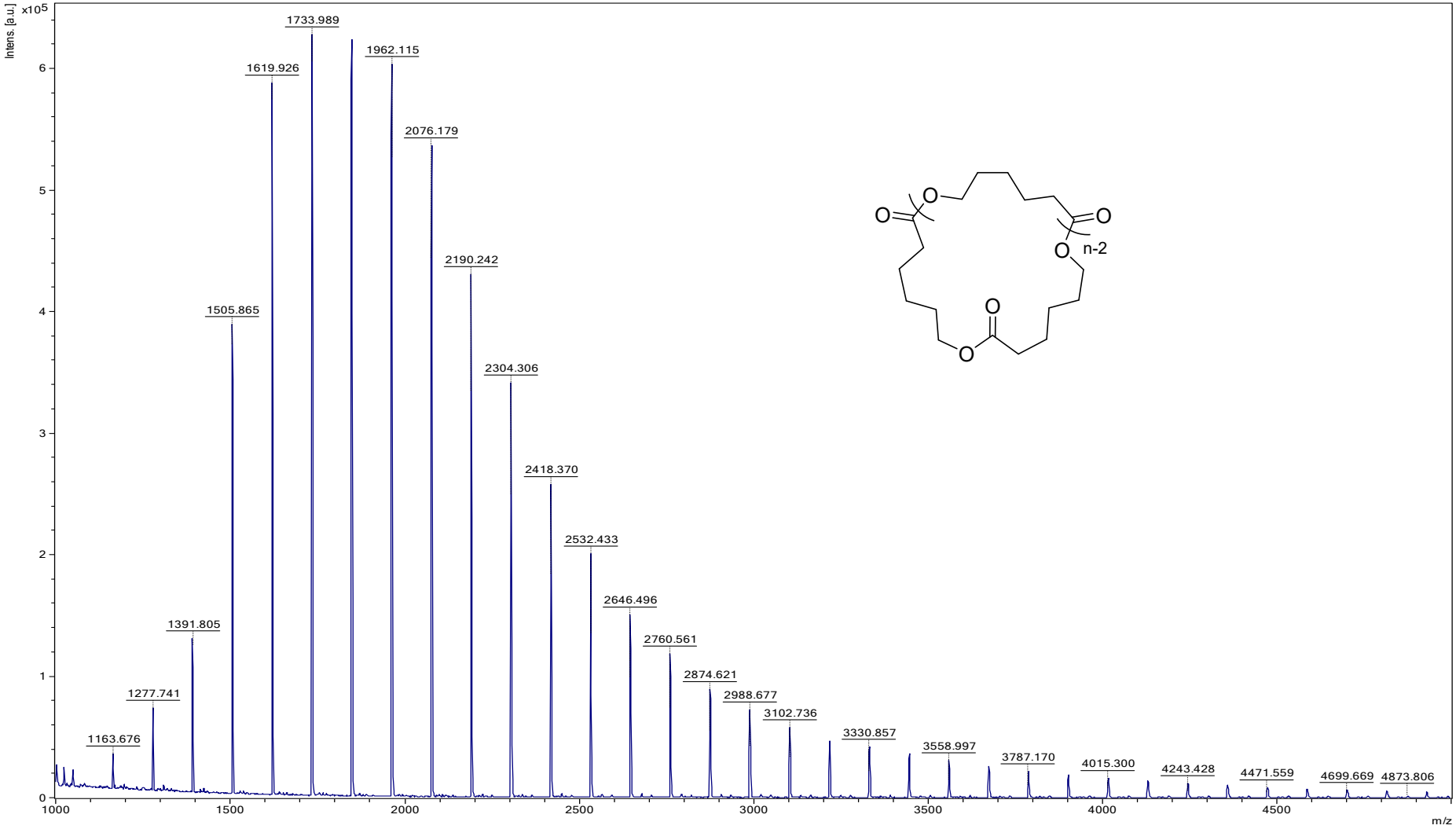

Figure S128. MALDI-TOF spectra of cyclic PCL obtained using **2d** as catalyst in DCM at a 50:1 $[LA]_0$/[Cat] ratio.

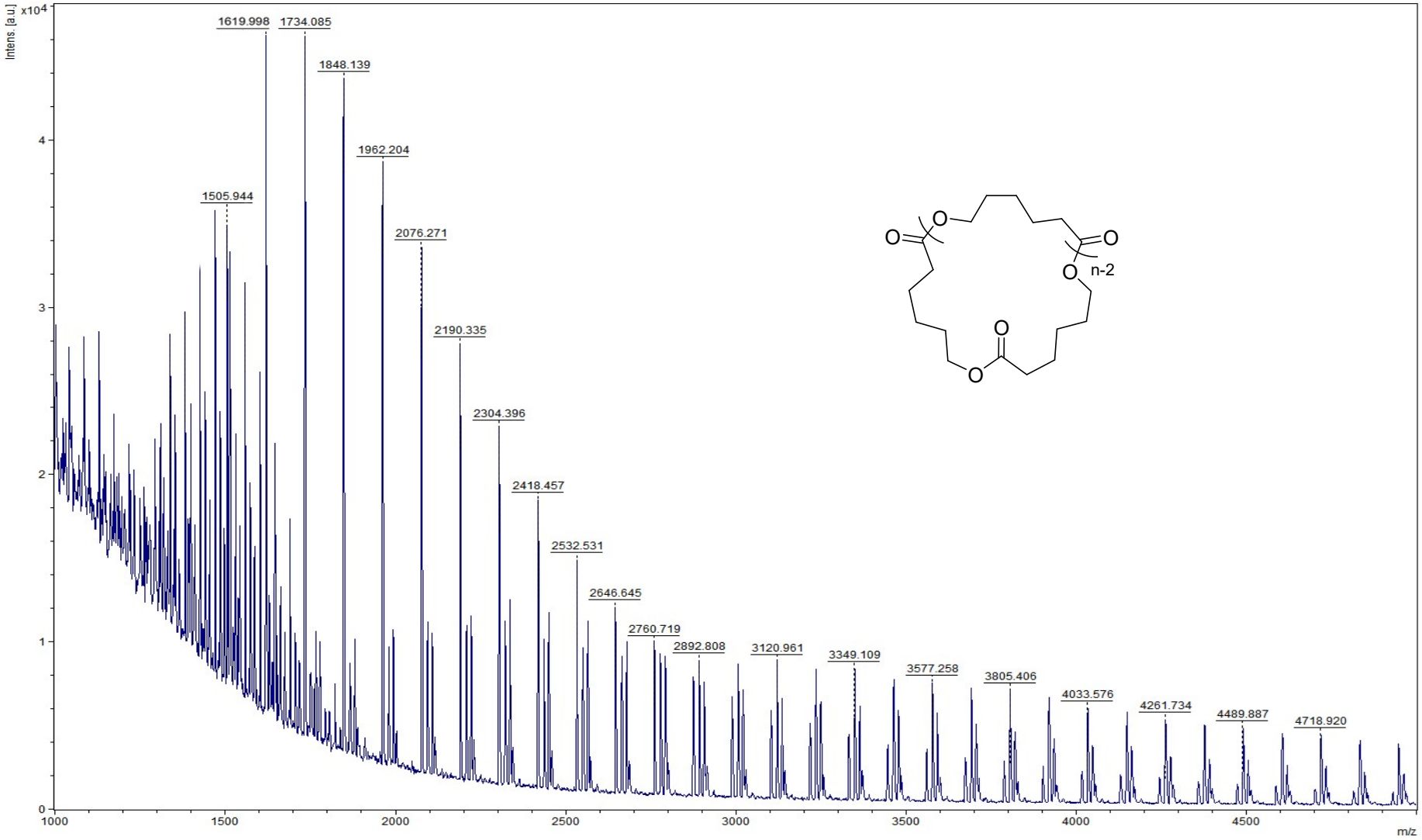

Figure S129.MALDI-TOF spectra of cyclic PCL obtained using **2a** as catalyst in THF at a 50:1 $[LA]_0/[Cat]$ ratio.

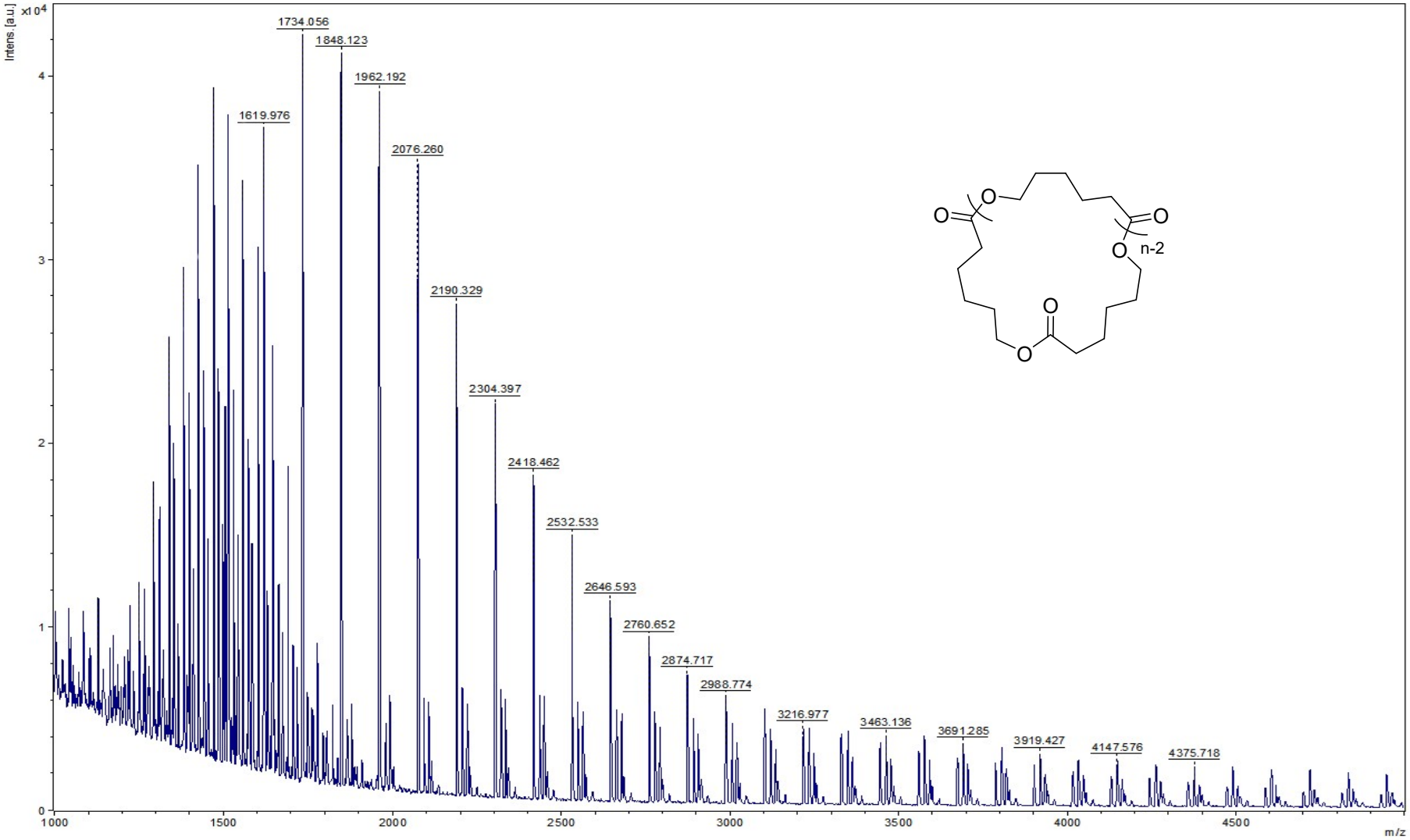

Figure S130. MALDI-TOF spectra of cyclic PCL obtained using **2b** as catalyst in THF at a 50:1 $[LA]_0/[Cat]$ ratio.

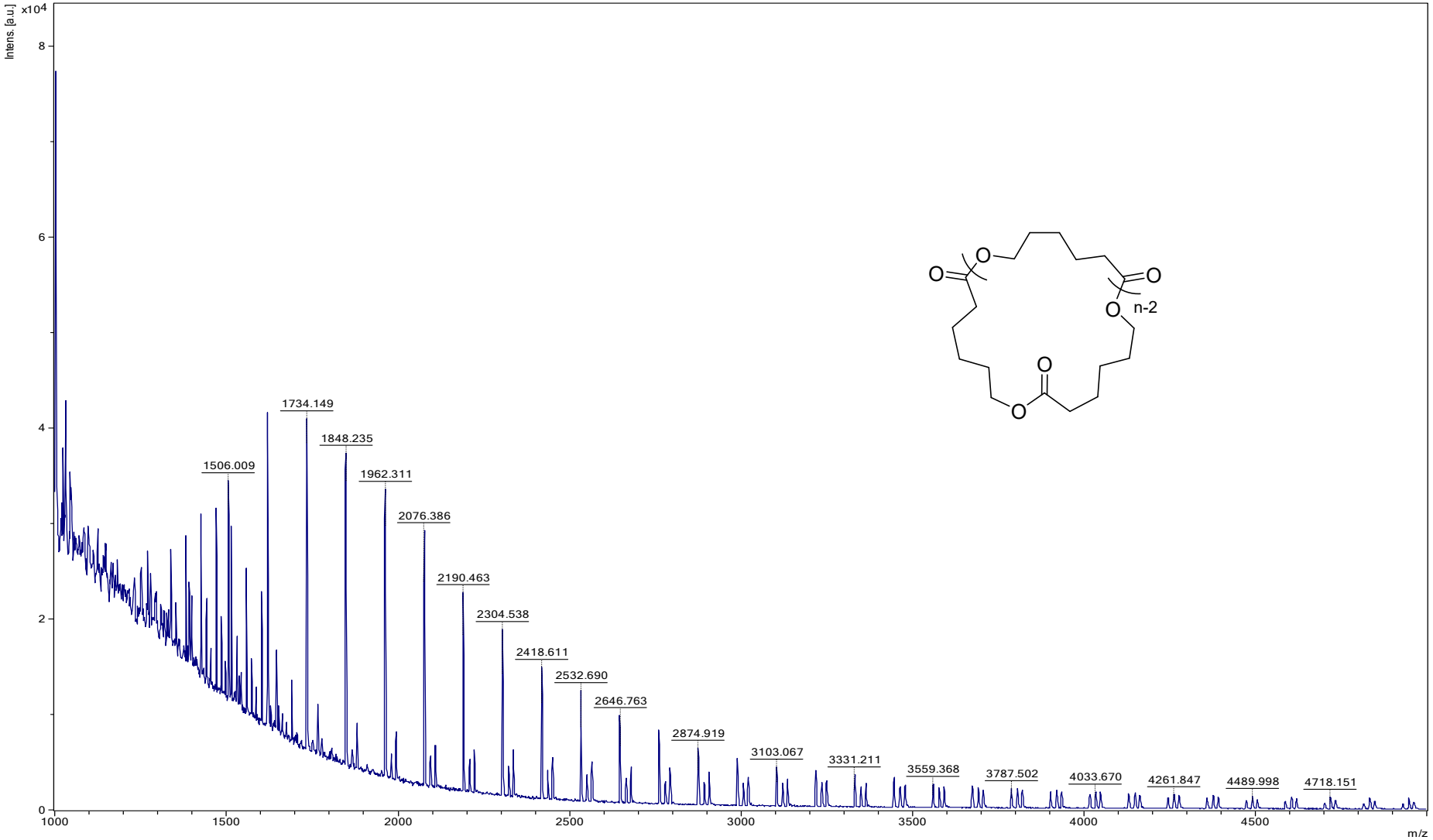

Figure S131. MALDI-TOF spectra of cyclic PCL obtained using **2c** as catalyst in THF at a 50:1 $[LA]_0$/[Cat] ratio.

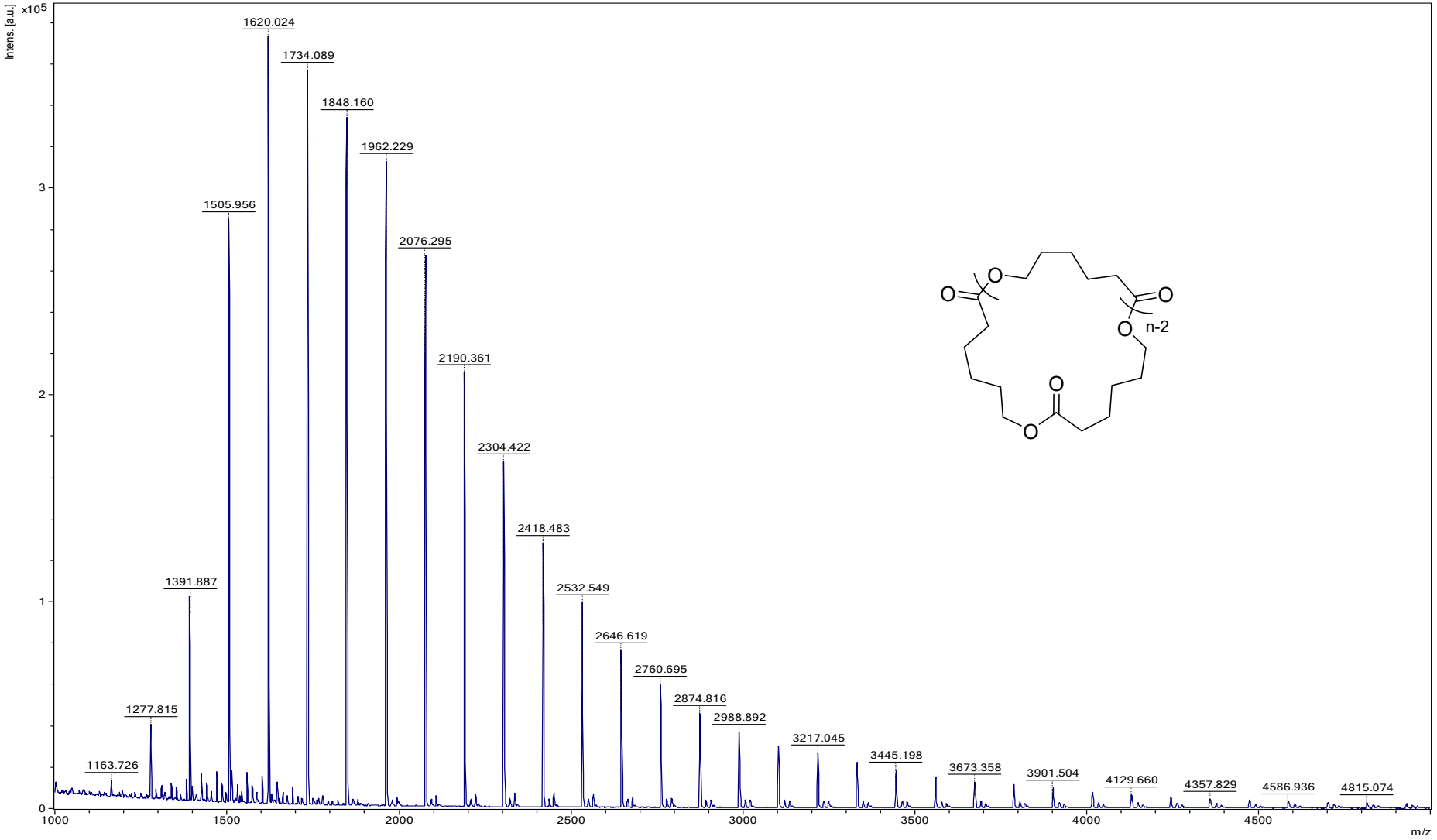

Figure S132. MALDI-TOF spectra of cyclic PCL obtained using **2d** as catalyst in THF at a 50:1 $[LA]_0$/[Cat] ratio.

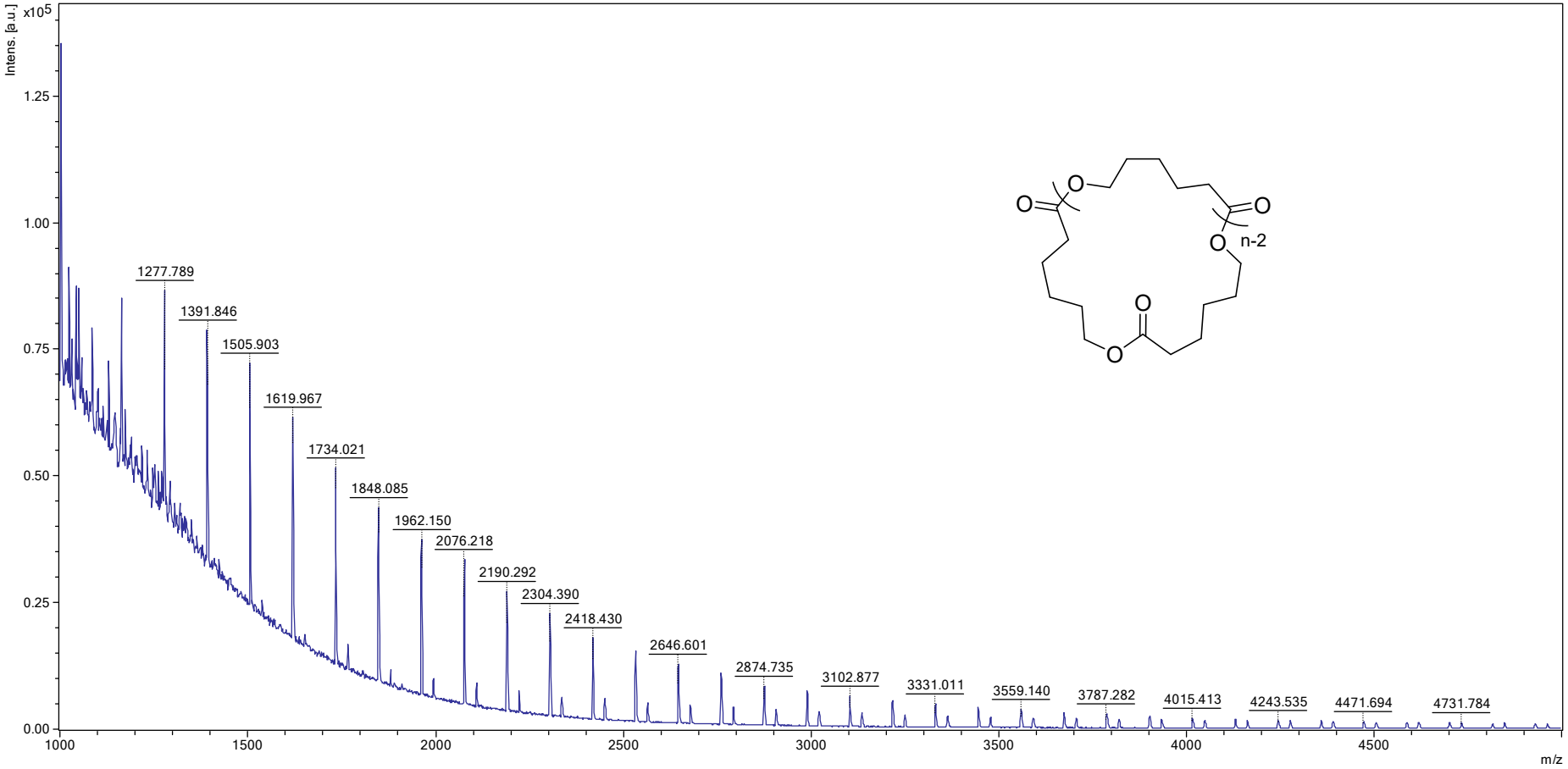

Figure S133. MALDI-TOF spectra of cyclic PCL obtained using **2d** as catalyst in DCM at a 75:1 $[LA]_0$/[Cat] ratio.

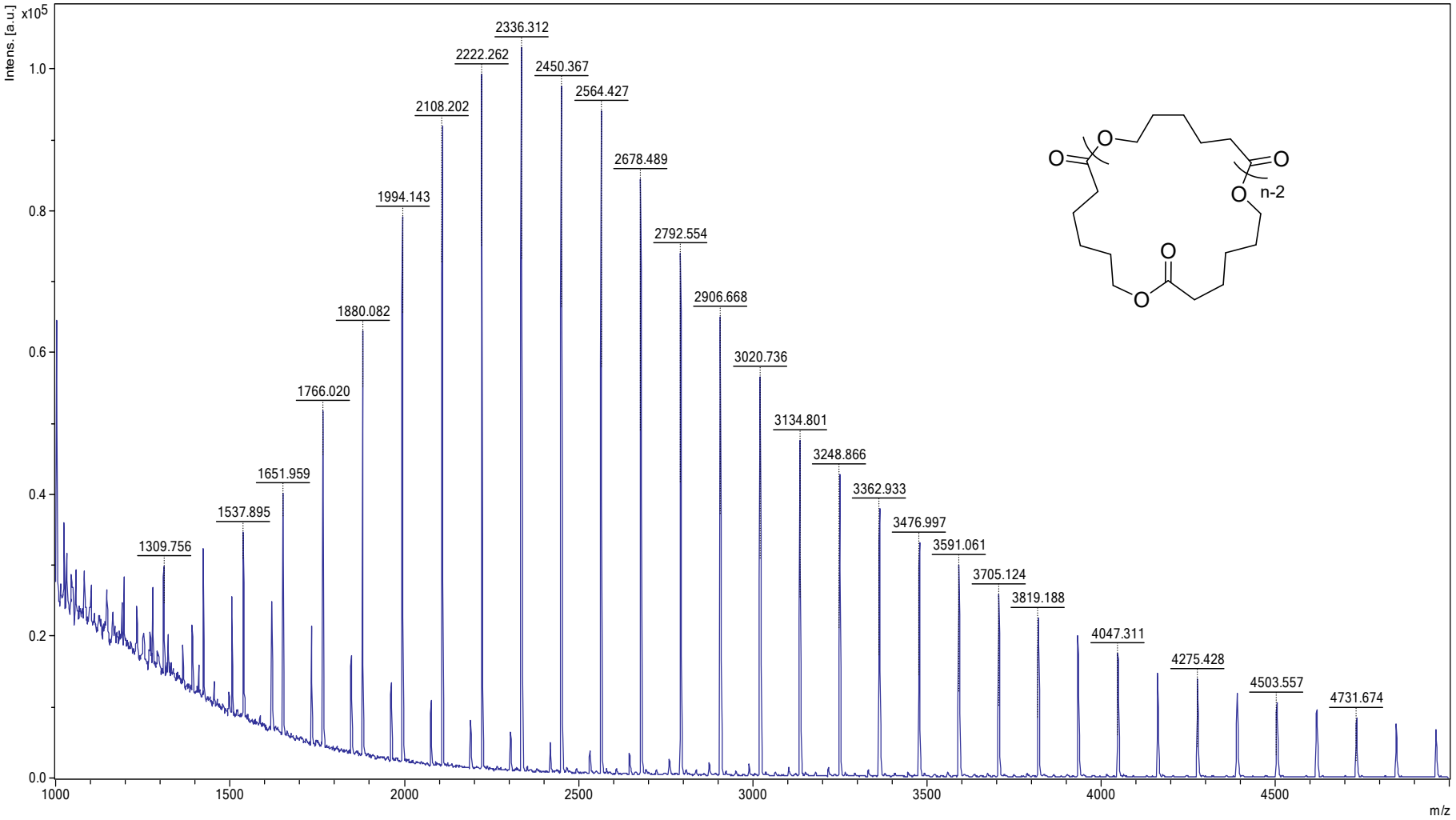

Figure S134. MALDI-TOF spectra of cyclic PCL obtained using **2d** as catalyst in DCM at a 100:1 $[LA]_0$/[Cat] ratio.

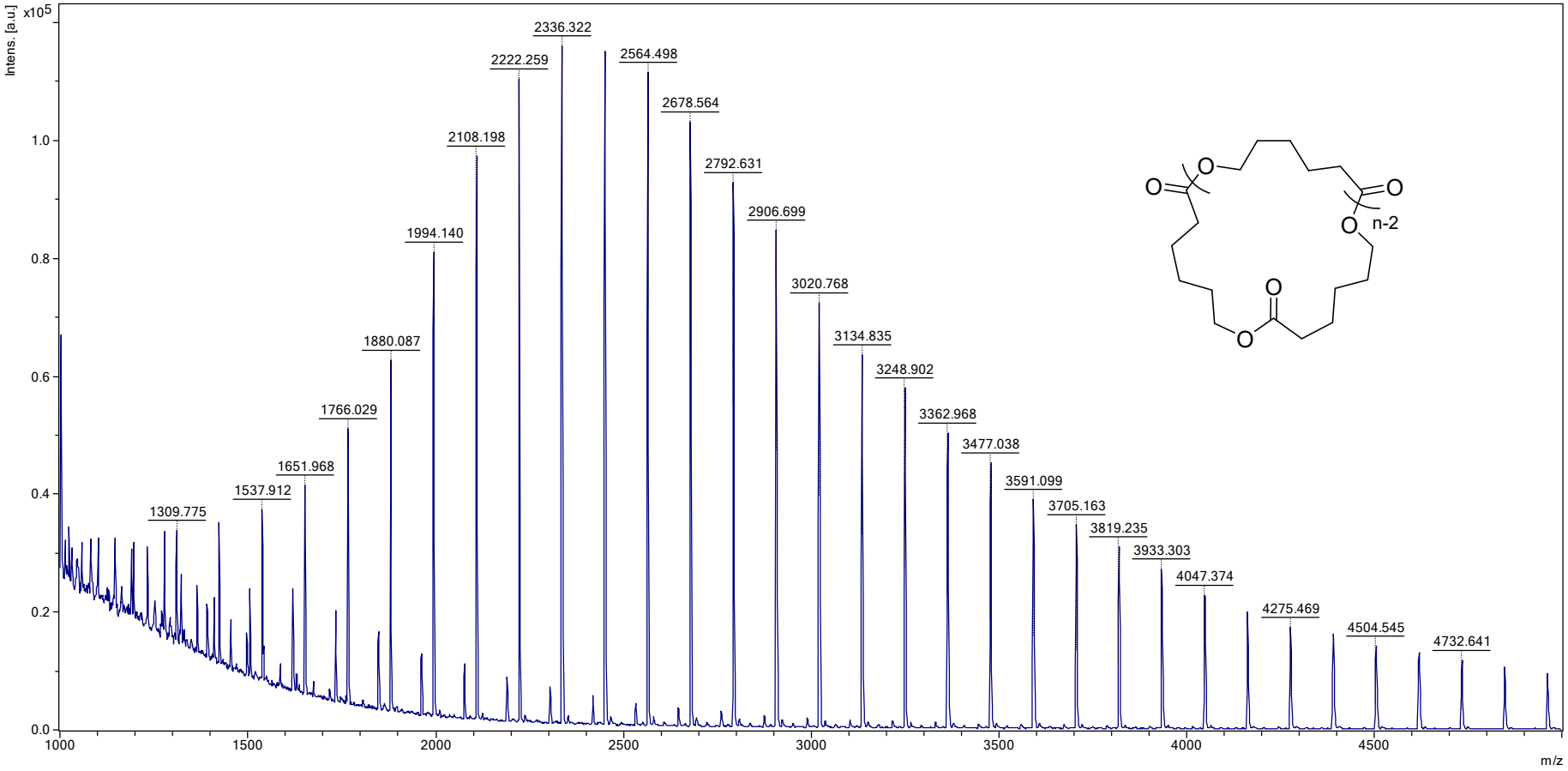

Figure S135. MALDI-TOF spectra of cyclic PCL obtained using **2d** as catalyst in DCM at a 150:1 $[LA]_0$/[Cat] ratio.

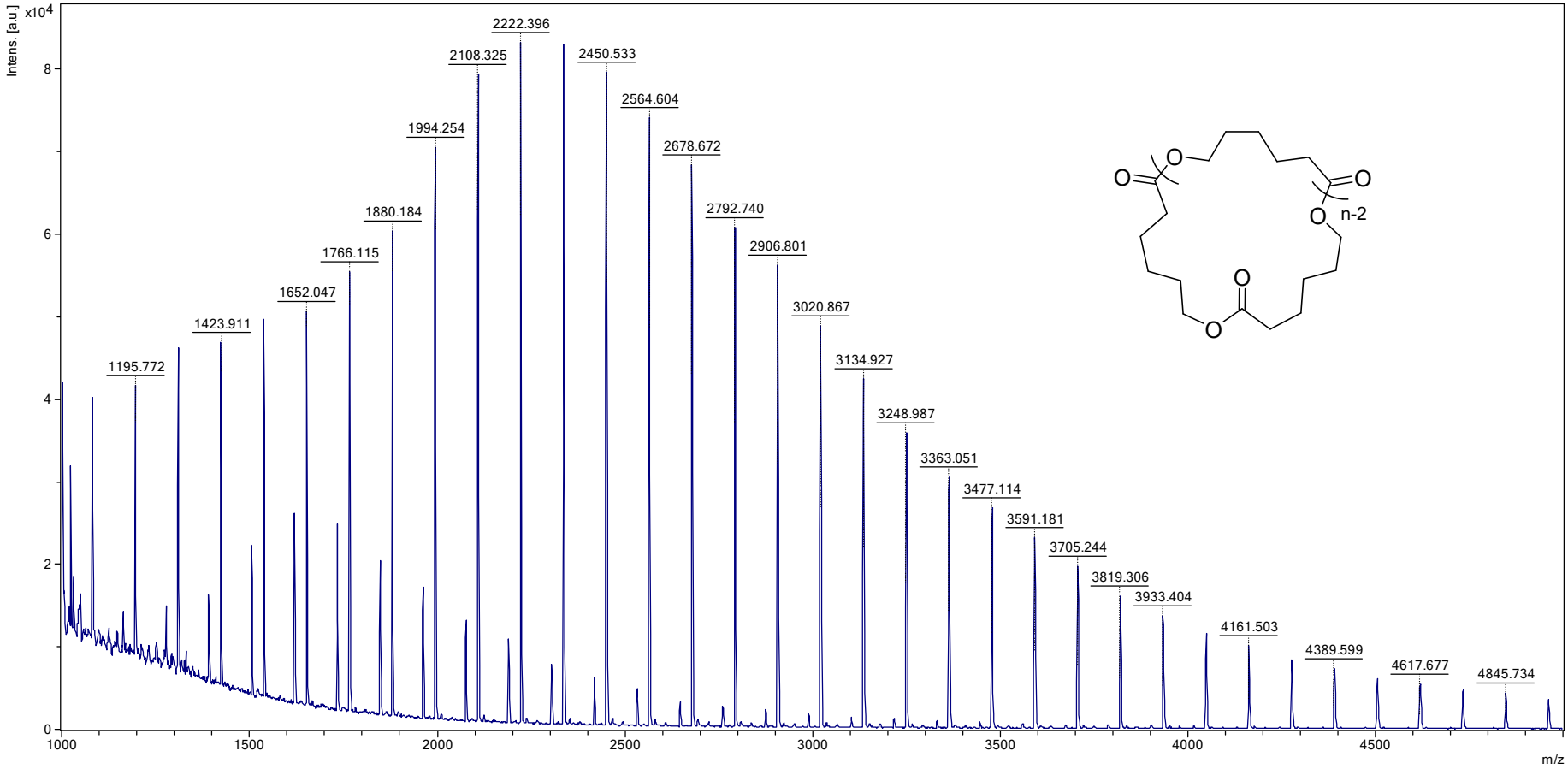

Figure S136. MALDI-TOF spectra of cyclic PCL obtained using **2d** as catalyst in DCM at a 300:1 $[LA]_0/[Cat]$ ratio.

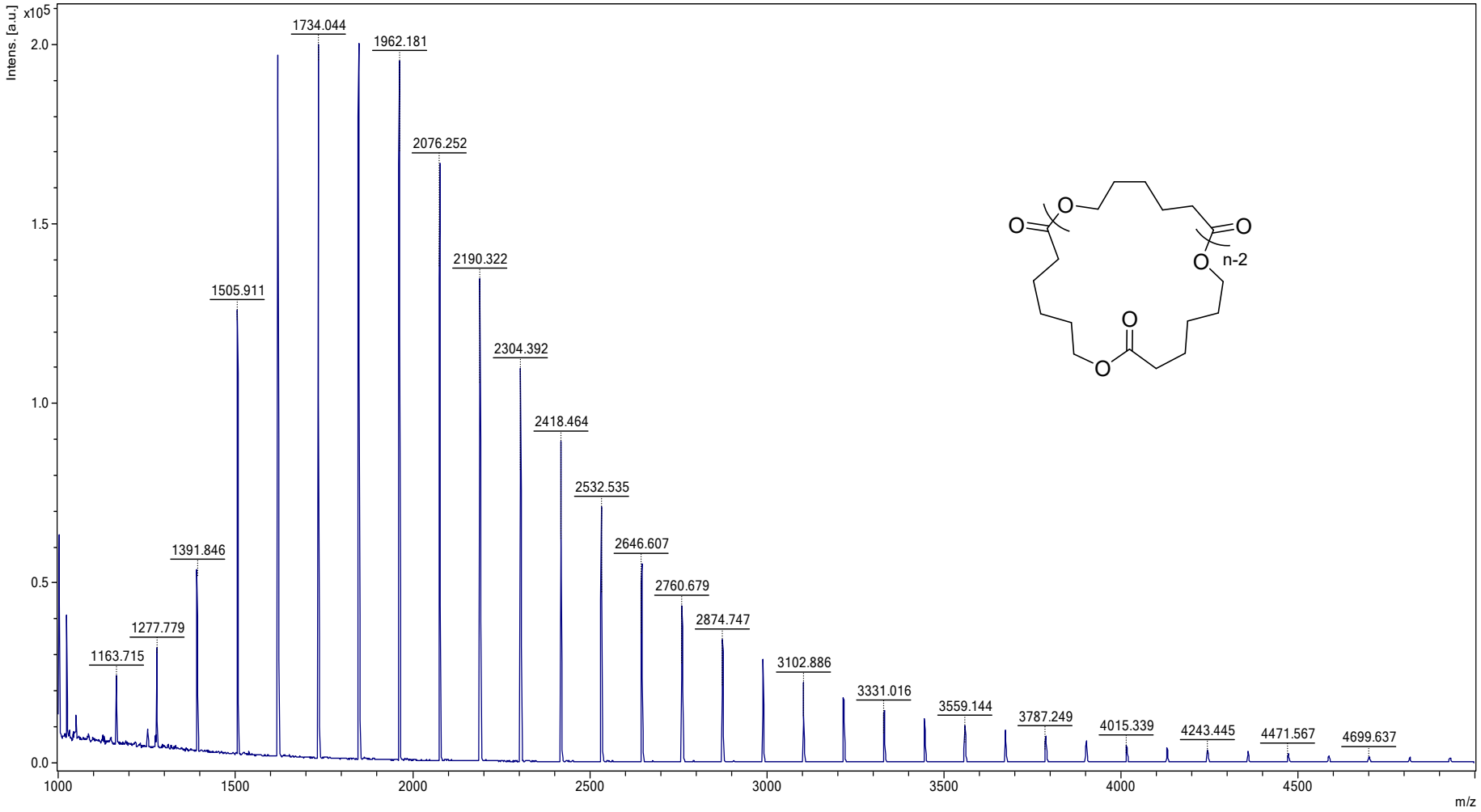

Figure S137. MALDI-TOF spectra of cyclic PCL obtained using **2d** as catalyst in THF at a 100:1 $[LA]_0/[Cat]$ ratio.

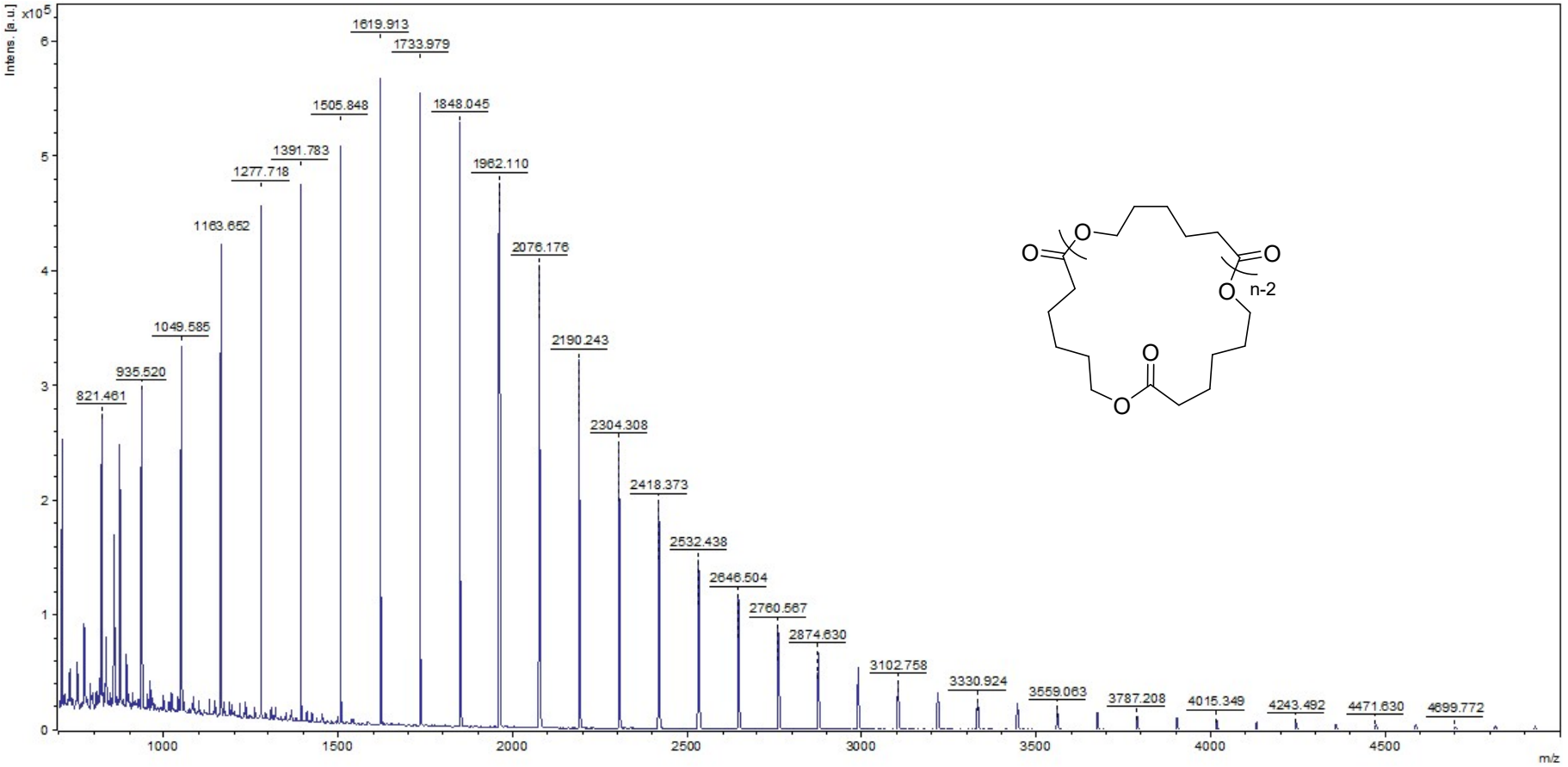

Figure S138. MALDI-TOF spectra of cyclic PCL obtained using **2d** as catalyst in THF at a 150:1 $[LA]_0$/[Cat] ratio.

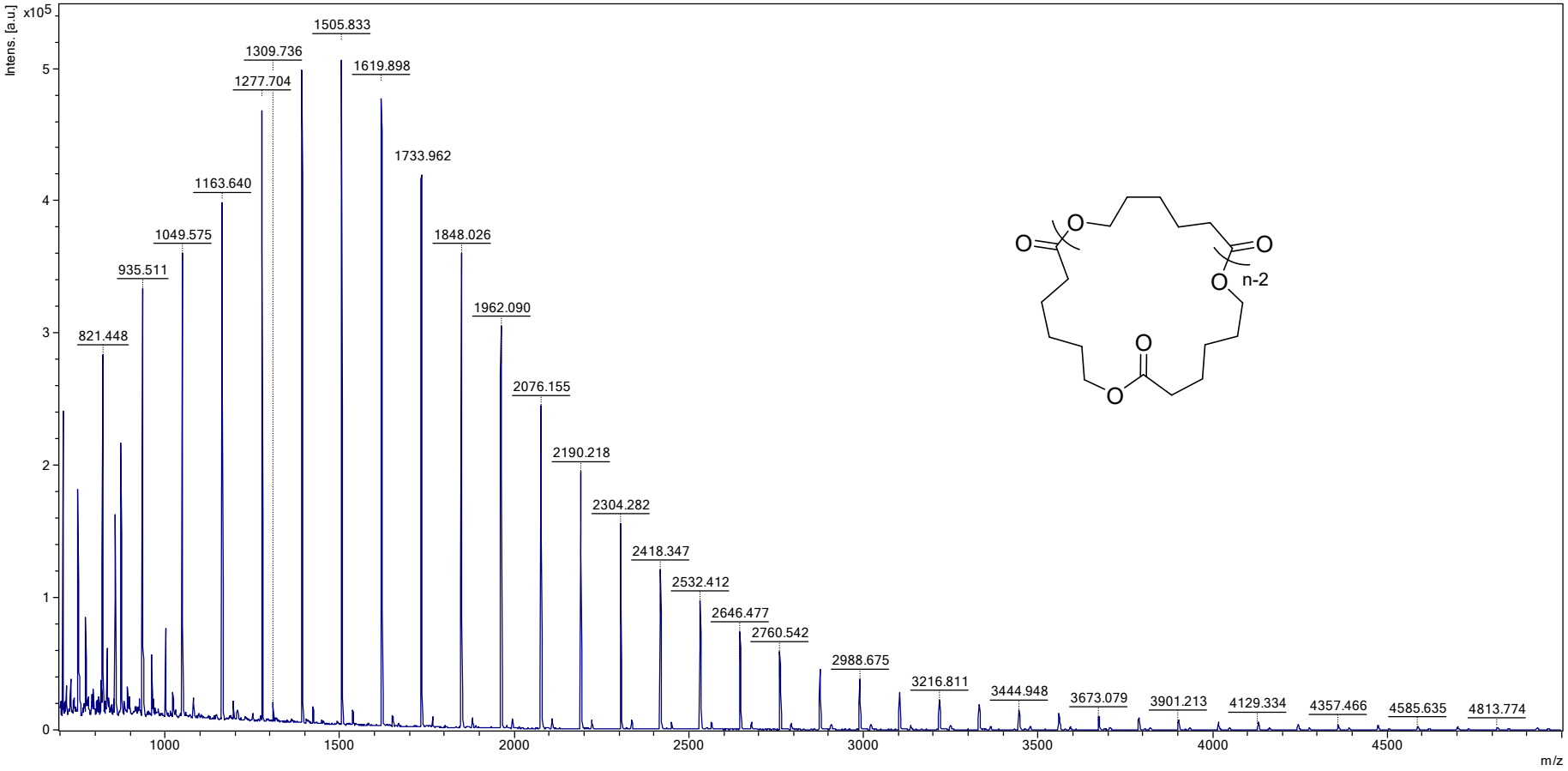

Figure S139. MALDI-TOF spectra of cyclic PCL obtained using **2d** as catalyst in THF at a 300:1 $[LA]_0/[Cat]$ ratio.

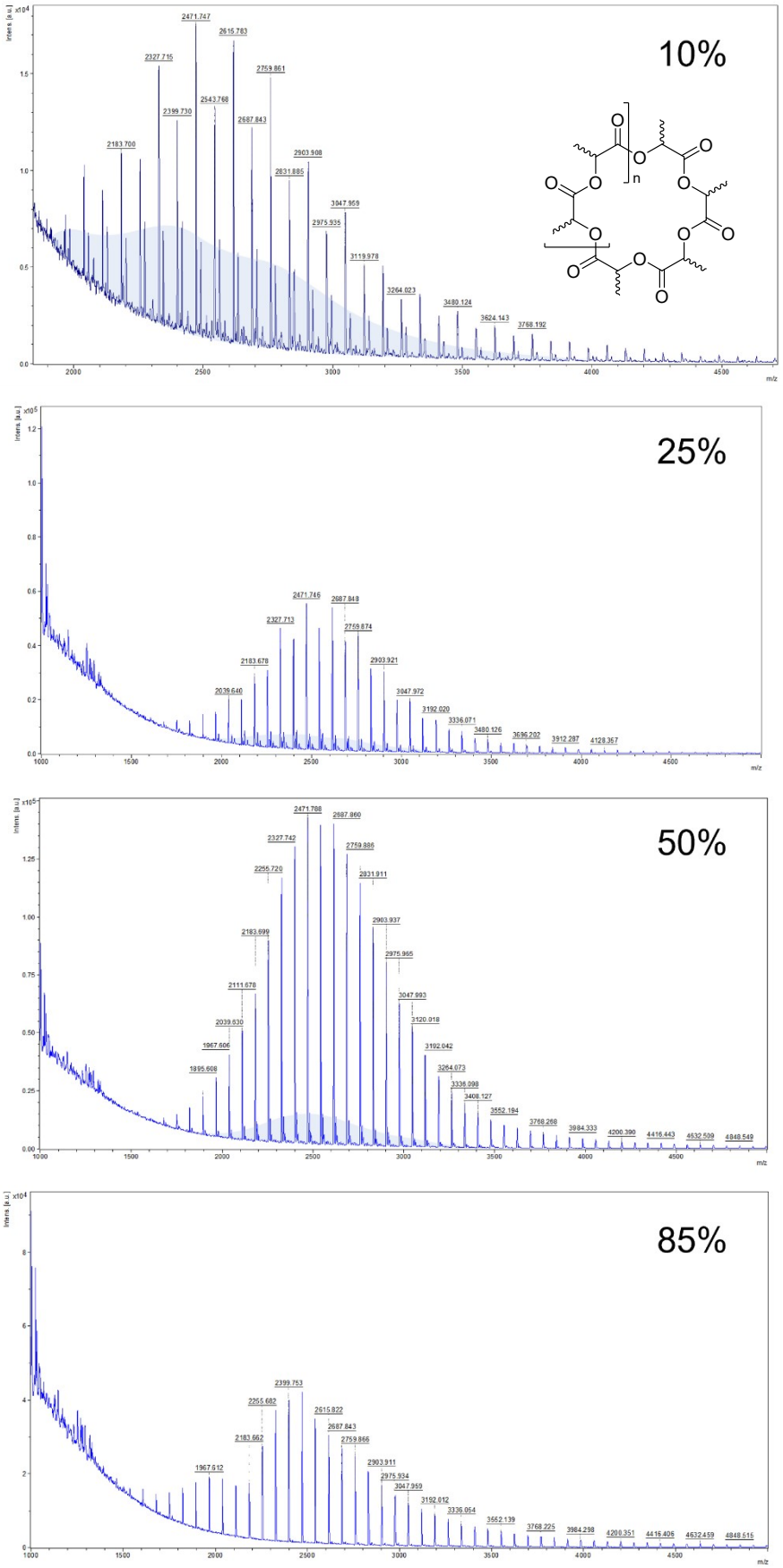

Figure S140. MALDI-TOF spectra of cyclic PLA samples at increasing conversions during polymerization using **2d** as catalyst in DCM at a 50:1 $[LA]_0/[Cat]$ ratio. Blue area indicates linear population.

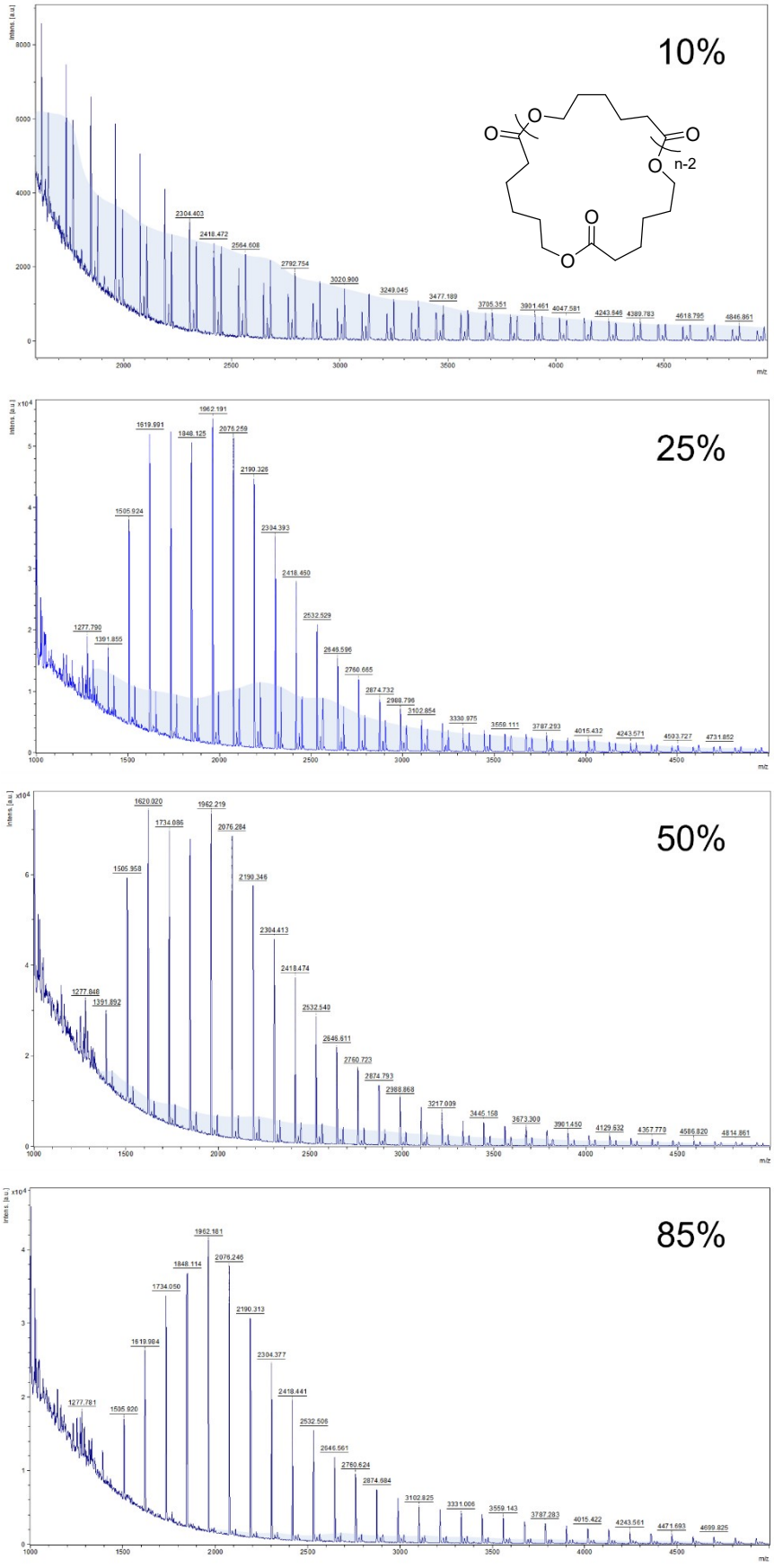

Figure S141. MALDI-TOF spectra of cyclic PCL samples at increasing conversions during polymerization using **2d** as catalyst in THF at a 50:1 $[LA]_0/[Cat]$ ratio. Blue area indicates linear population.

13. Turnover Frequency (TOF) in DCM

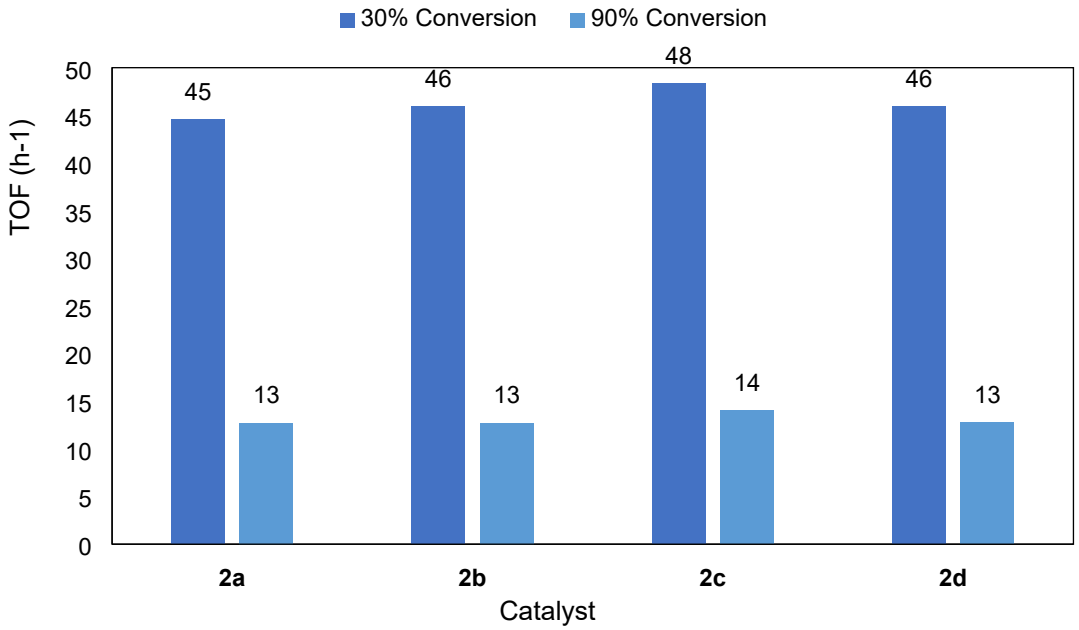

Figure S142. TOF obtained with different complexes (**2a**-**2d**) at conversions of 30 and 90% using *L*-LA in DCM.

14. Molecular weight vs $[M]_0/[2d]$ ratio

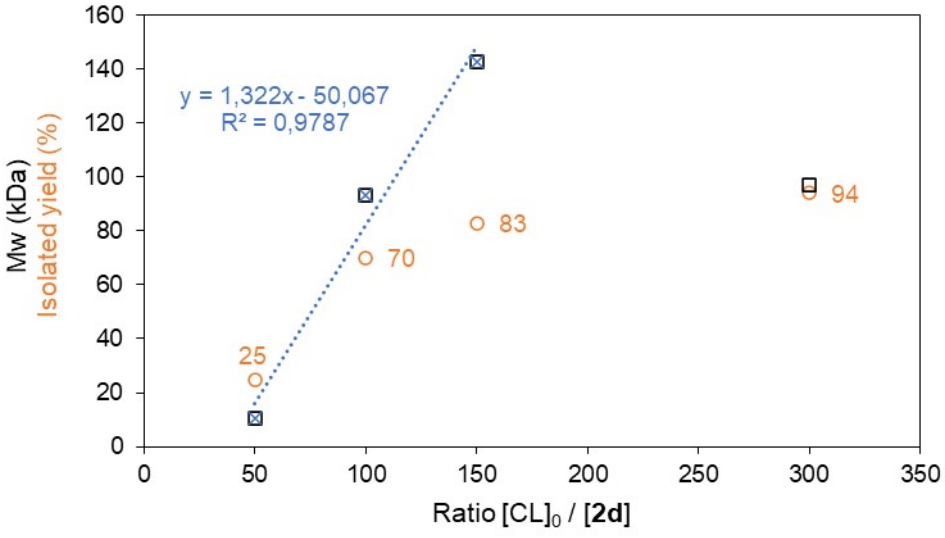

Figure S143. Polymerization of ε-CL catalyzed by **2d** in THF at 25 ºC. The relationship between Mw of the polymer and the initial monomer-to-catalyst ratio is shown. Black squares circles correspond to weight-average molecular weight whereas orange circles correspond to isolated yield.

15. References

1. F. M. Arrabal-Campos, L. M. Aguilera-Sáez and I. Fernández, *J. Phys. Chem. A* 2019, **123** (4), 943–950.
2. K. Xu and S. Zhang, *Anal. Chem.* 2014, **86** (1), 592–599.
3. I. Fernández and F. M. Arrabal-Campos, DiffAtOnce®, University of Almería, 2013.
4. Y. Zhao and D. G. Truhlar, *Theor. Chem. Acc.* 2008, **120**, 215.
5. M. J. Frisch et al.,GAUSSIAN 3 (Revision C.01), Gaussian Inc., Wallingford, CT, 2016.
6. A. V. Marenich, C. J. Cramer and D. G. Truhlar, *J. Phys.* Chem. B 2009, **113**, 6378.
7. a) W. J. Hehre, K. Ditchfield and J. A. People, *J. Chem. Phys.* 1972, **56**, 2257. b) M. M. Francl, W. J. Pietro, W. J. Hehre, J. S. Binkley, M. S. Gordon, D. J. DeFrees and J, A. People, *J. Chem. Phys.* 1982, **77**, 3654.
8. T. Clark, J. Chandrasekhar, G. W. Spitznagel and P. V. R. Schleyer, *J. Comput. Chem.* 1983, **4**, 294.
9. S. Grimme, *Chem. Eur. J.* 2012, **18**, 9955.
10. G. Luchini, J. V. Alegre-Requena, Y. Guan, I. Funes-Ardoiz and R. S. Paton, GoodVibes: 3.0.1, 2019, https://zenodo.org/record/6977304, (accessed November 2022).
11. R. Ditchfield, *Mol. Phys.* 1974, **27**, 789.
12. C. Adamo and V. Barone. J. Chem. Phys, 1998, **108**, 664.
13. R. Krishnan, J. S. Binkley, R. Seeger and J. A. People, *J. Chem. Phys.* 1980, **72**, 650.
14. P. Gao, X. Wang and H. Yu, *Adv. Theory Simul.* 2019, **2**, 1800148.
15. I. Fernández, E. Martínez-Viviente and P. S. Pregosin, *Inorg. Chem.*, 2005, **44**, 5509–5513
16. M. Álvarez-Moreno, C. De Graaf, N. López, F. Maseras, J. M. Poblet and C. Bo, *J. Chem. Inf. Model.* 2015, **55**, 95.
17. ioChem-BD, https://iochem-bd.bsc.es/browse/review-collection/100/216352/a367d0e55f70eade1c28cba8 (accessed November 2022)